

2006

A five-year spectroscopic and photometric campaign on the supergiant star Deneb

Noel Douglas Richardson
The University of Toledo

Follow this and additional works at: <http://utdr.utoledo.edu/theses-dissertations>

Recommended Citation

Richardson, Noel Douglas, "A five-year spectroscopic and photometric campaign on the supergiant star Deneb" (2006). *Theses and Dissertations*. Paper 1381.

This Thesis is brought to you for free and open access by The University of Toledo Digital Repository. It has been accepted for inclusion in Theses and Dissertations by an authorized administrator of The University of Toledo Digital Repository. For more information, please see the repository's [About page](#).

A Thesis
entitled
A Five-Year Spectroscopic and Photometric Campaign on the
Supergiant Star Deneb

by
Noel Douglas Richardson

As partial fulfillment of the requirements for the
Masters of Science Degree in Physics

Advisor: Dr. N. D. Morrison

Graduate School

The University of Toledo
August 2006

This thesis is dedicated to my wonderful fiancée Kristina Varner as well as to my ever supportive parents, Douglas and Julia Richardson.

An Abstract of
A Five-Year Spectroscopic and Photometric Campaign on the
Supergiant Star Deneb

Noel Douglas Richardson

Submitted in partial fulfillment
of the requirements for the
Masters of Science Degree in Physics

The University of Toledo
August 2006

Deneb is a type A2 supergiant, often thought of as the prototype A-type supergiant. A-type supergiants are some of the most luminous stars in the optical region of the spectrum, and could be potential extragalactic distance indicators. Unfortunately, the literature detailing the variability of these objects is sparse. We are analyzing 339 spectra in the $H\alpha$ wavelength region obtained at Ritter Observatory (University of Toledo) taken over the five year span from 1997 through 2001. We also obtained during the same time period, 370 Strömngren photometric measurements at the Four College Automated Photoelectric Telescope (Washington Camp, Arizona).

The $H\alpha$ profile of Deneb exhibits a characteristic P Cygni profile, consistent with mass-loss in Deneb. Dynamical spectra of the $H\alpha$ profile were constructed to visually search for cyclic variability in the wind of the star. No clear evidence was found for

this type of behavior.

Time-series analysis was performed to analyze the $H\alpha$ net equivalent widths, radial velocities, and photometry using the CLEAN algorithm, developed by Roberts et al. (1986). Correlations have been found between some radial velocity periods and photometry, consistent with the star having both radial and non-radial pulsations. No clear correlation has been found between the $H\alpha$ equivalent widths and the pulsational periods. Some of the periods seem to persist, while others are only present in one observing season. Lucy (1976) found some evidence that Deneb was a binary with a 750 or 850 day period. Noteworthy in our data set is the absence of this period.

Acknowledgments

I would like to thank a number of important people for their support through this project. This project would not have been as insightful without the excellent guidance of my advisor, Dr. Nancy Morrison. I would like to thank the following people for the spectroscopic observations of Deneb: Dr. Nancy Morrison, Dr. Karen Bjorkman, Dr. Anatoly Miroshnichenko, David Knauth, Chris Mulliss, Howard Ritter, Tracy Smith, Will Fischer, Patrick Ouellette, John Wisniewski, Josh Thomas, Amanda Gault, Lori Schmetzer, Denver Seeley, and Pat Sadowski. Chris Mulliss created the first dynamical spectrum of Deneb from Ritter spectra. I appreciate the help of Erin Allgaier, who assisted in the creation of the dynamical spectra through the NSF REU program under the supervision of Dr. Nancy Morrison and myself. I also would like to thank Robert Burmeister for his work as Ritter Observatory technician and keeping the telescope in excellent working condition. Furthermore, a thank you to Saul Adelman for taking photometric measurements during the coinciding time period.

This research has made use of the SIMBAD database, operated at CDS, Strasbourg, France.

Support for Ritter Observatory during the time of the observations was provided by the Fund for Astrophysical Research and the American Astronomical Society Small Grants Program.

Support for FCAPT during the time period came from NSF grant AST-0587381. Special thanks to Louis J. Boyd, George McCook, and Robert J. Dukes, Jr. for their help in keeping the FCAPT in good working order.

Contents

Abstract	ii
Acknowledgments	iv
Contents	vi
List of Figures	ix
List of Tables	xii
1 Introduction	1
2 Observations	17
2.1 Ritter Observatory	17
2.2 The Four College Automated Photoelectric Telescope	20
3 Reductions	24

3.1	H α Spectroscopic Reductions	24
3.2	H α Dynamical Spectra	29
3.3	The Equivalent Width of H α	30
3.4	Si II Radial Velocities	33
3.5	Strömgen Photometry	39
3.6	Photometric Colors	40
4	Results	42
4.1	The H α dynamical spectra	42
4.2	H α Equivalent Width Measurements	48
4.3	Radial Velocities	52
4.4	Light Curves	55
4.5	Photometric Colors	57
5	Time-Series Analysis	60
5.1	The Scargle Periodogram	60
5.2	The CLEAN algorithm	64
6	Discussion and Conclusions	72
6.1	Binarity	72
6.2	H α	73

6.3	Pulsations	78
6.4	Connections between pulsations and the wind?	81
6.5	Conclusions	81
	References	84
A	Ritter Observations of Deneb	89
B	Hα Measurements	99
C	Radial Velocities	106
D	Photometry	114

List of Figures

1-1	The formation of the P Cygni profile.	12
1-2	An H α spectrum of P Cygni	13
1-3	H α spectrum of Deneb	14
2-1	The Response functions of the Strömngren filters	21
3-1	Telluric lines in the spectrum	25
3-2	Gaussian fits of telluric (water) lines	26
3-3	Telluric Line Template	27
3-4	Telluric lines removed from the spectrum	28
3-5	The <i>sbands</i> window	31
3-6	Measuring the equivalent width of the emission component	32
3-7	The spectrum around the Si II doublet	36
3-8	Radial velocity Error	38

4-1	A dynamical spectrum for 1997	43
4-2	A dynamical spectrum for 1998	44
4-3	A dynamical spectrum for 1999	45
4-4	A dynamical spectrum for 2000	46
4-5	A dynamical spectrum for 2001	47
4-6	The <i>sbands</i> -derived net Equivalent Width of H α (1999)	49
4-7	The Equivalent Width of the H α emission component (1999)	50
4-8	The derived Equivalent Width of the absorption component (1999)	51
4-9	The <i>sbands</i> -derived Equivalent Width of H α (2001)	53
4-10	The Radial Velocity of Deneb (1999)	54
4-11	Strömgren Photometry of Deneb (Fall 1999)	56
4-12	Strömgren Photometric Colors of Deneb (Fall 1999)	57
4-13	A Color - Color Diagram of Deneb	59
5-1	Scargle periodogram (0 - 100 day periods)	61
5-2	Scargle periodogram (0 - 300 day periods)	62
5-3	Scargle periodogram (0 - 300 day periods)	63
5-4	CLEANed frequencies of Radial Velocities (1931)	66
5-5	CLEANed frequencies of H α net equivalent width	68
5-6	CLEANed frequencies of SiII radial velocities	69

5-7	CLEANed frequencies of Strömgren photometry	70
5-8	CLEANed frequencies of Strömgren photometric colors	71
6-1	Scargle periodogram of the radial velocities	74
6-2	H α Spectra obtained in 2001	75
6-3	Connection between the wind and radial velocities?	82
D-1	Strömgren Photometry of Deneb (Fall 1997)	123
D-2	Strömgren Photometry of Deneb (Spring 1998)	124
D-3	Strömgren Photometry of Deneb (Fall 1998)	125
D-4	Strömgren Photometry of Deneb (Spring 1999)	126
D-5	Strömgren Photometry of Deneb (Spring 2000)	127
D-6	Strömgren Photometry of Deneb (Fall 2000)	128
D-7	Strömgren Photometry of Deneb (Spring 2001)	129

List of Tables

1.1	Stellar Parameters of Deneb	5
2.1	Properties of Ritter Observations	19
2.2	Properties of the Strömgren narrow-band filters	20
2.3	Properties of the Strömgren photometry	22
3.1	Errors in the measurement of the equivalent width of $H\alpha$ from two different spectra.	34
3.2	Estimated errors for the radial velocities measured using the Ritter Observatory spectra.	37
3.3	Published photometry values from the SIMBAD database	40
5.1	Kaufer's Radial Velocity Periods	66
6.1	$H\alpha$ Frequencies and Periods	77

6.2	Photometry and Radial Velocity Frequencies and Periods	80
A.1	1997 Ritter Observations of Deneb	89
A.2	1998 Ritter Observations of Deneb	92
A.3	1999 Ritter Observations of Deneb	94
A.4	2000 Ritter Observations of Deneb	96
A.5	2001 Ritter Observations of Deneb	97
B.1	H α Equivalent Width Measurements	99
C.1	Radial Velocities from Si II $\lambda\lambda$ 6347, 6371	106
D.1	<i>uvby</i> Values and Colors for the Photometric Observations	114

Chapter 1

Introduction

Deneb is the brightest star of the constellation Cygnus, and among the brightest in the sky. Like most bright stars, Deneb has several names, including α Cygni, HR 7924, HD 197345, HIP 102098 and 50 Cygni, and is mentioned in a multitude of catalogs. It is an important astrophysical object. It is an early A-type supergiant (spectral type of A2Iae), and is often considered the prototype of the A-type supergiants. A-type supergiants are signposts for recent star formation, as massive stars evolve into massive supergiants. Massive stars are the origin of many heavy elements as a result of fusion processes and neutron capture processes especially during the terminal supernova explosion. With a great apparent brightness ($m_V = 1.25$), Deneb can be easily studied with small or moderate aperture telescopes. It can be observed

for most of the year at northern latitudes because of its position in the northern sky ($\alpha = 20^{\text{h}} 41^{\text{m}} 25.91^{\text{s}}$, $\delta = 45^{\circ} 16' 49.2''$ for 2000.0). Many papers have been written and much research has been done to understand this star's fundamental parameters and its variability.

A-type supergiants are among the most luminous stars in the optical region of the electromagnetic spectrum. A potential extragalactic distance indicator involving A-type and B-type supergiants was recently developed by Kudritzki et al. (1999a,b). The so-called wind momentum–luminosity relationship (WLR) is based on the theory of radiation driven winds, which predicts a tight relationship between the total mechanical momentum flow ($\dot{M}v_{\infty}$, where \dot{M} is the mass-loss rate, and v_{∞} is the terminal wind speed) and the luminosity (L_*) of the mass-losing star. The relationship is given in Equation 1.1, where α_{eff} represents a dimensionless constant of the order 2/3 and “represents the power law exponent of the distribution function of line strengths of the thousands of lines driving the wind (Kudritzki et al. 1999a) ”.

$$\dot{M}v_{\infty} \propto R_*^{-1/2} L_*^{1/\alpha_{\text{eff}}} \quad (1.1)$$

The WLR shows a different slope depending on the spectral type of the supergiant. Kudritzki et al. observed 14 B-type and 4 A-type supergiants. They used the H α line to determine the parameters \dot{M} and v_{∞} . A few potential problems can

be seen in their observational “proof” that the WLR is valid, especially for A–type supergiants. First, there were only 4 supergiants used with this spectral type. Second, the $H\alpha$ line is variable in Deneb, as with other B and A–type supergiants (i.e. Kaufer et al. 1996). The variability of these objects should be understood before a relationship can be shown. Kudritzki et al. (1999b) did mention that the case of HD 92207 (A0Ia) had almost no variations in the momentum flow (the product of $\dot{M}v_\infty$, with 150 observations), while the terminal wind speed and the mass–loss rate varied significantly.

Much effort has been devoted to determining the fundamental parameters of Deneb. The star was studied by Albayrak (1999, 2000, 2003) in the wavelength range of 3826 – 5212 Å to determine elemental abundances of the star. Albayrak used models to calculate synthetic spectra and found values for many different parameters such as the rotational velocity ($v \sin i$) and the macroturbulent velocity (ζ). The effect of mass–loss on the photospheric lines was investigated and the results showed that either the velocity gradient is too small for there to be an asymmetric line profile or that the mass–loss rate is less than $10^{-6}M_\odot\text{yr}^{-1}$. It was found that there was an under–abundance of helium when compared to solar values. The abundances of carbon, nitrogen, and oxygen were consistent with a dredge-up of these processed materials (C was mildly deficient, N in moderate excess, and O slightly

deficient). Also deficient were aluminum and sulfur. Magnesium and silicon had solar abundances, while most heavier elements (Ca through Ni except Sc, Sr, Y, Zr, Ba, La, and Eu) had above solar abundances.

Aufdenberg et al. (2002) collected observations of the spectral energy distribution of Deneb over most of the electromagnetic spectrum (radio through ultraviolet) and modeled the atmosphere using the PHOENIX stellar atmosphere code to constrain fundamental parameters. A good fit to a typical spectrum in the $H\alpha$ region could not be obtained, which is troubling in the light of the wind momentum–luminosity relationship. Aufdenberg (2006) recently observed Deneb with CHARA (an optical and infrared interferometer operated by Georgia State University) and found Deneb to be approximately 1% oblate. The fundamental parameters derived from various authors are reviewed in Table 1.

The presence of a magnetic field could drastically affect the stellar wind, and thus, the spectral lines that are wind sensitive. Verdugo et al. (2003) began a search for a magnetic field in several A-type supergiants using the MuSiCoS échelle spectropolarimeter at the 2-m Bernard Lyot telescope of the Observatoire de Pic-du-Midi. The longitudinal component of the magnetic field can be measured using a least-squares deconvolution through Zeeman signatures in the Stokes V (circularly polarized) line profiles. Each observation yielded a different longitudinal value of the magnetic field

Table 1.1: Stellar Parameters of Deneb

Parameter	Symbol	Value	Reference [†]
Parallax (mas)	π	1.01 ± 0.57	1
Radius (R_{\odot})	R	$\simeq 180$	2
Luminosity (L_{\odot})	L	$\simeq (1.6 \pm 0.4) \times 10^5$	2
Mass (M_{\odot})	M	$\sim 20 - 25$	2
Surface gravity	$\log g$	$1.1 - 1.6$	2
Effective Temperature (K)	T_{eff}	$8600 \pm 500; 8420 \pm 100$	2
Rotational velocity (km s^{-1})	$v \sin i$	25	3
Mass-loss rate ($M_{\odot} \text{ yr}^{-1}$)	\dot{M}	$(8 \pm 3) \times 10^{-7}$	2
Terminal wind velocity (km s^{-1})	v_{∞}	$\simeq 225$	2
Microturbulent velocity (km s^{-1})	ξ_t	$\simeq 15$	2
Macroturbulent velocity (km s^{-1})	ζ	14	3
Uniform Disk Diameter (mas)	θ_{UD}	2.40 ± 0.06	2

[†]1. Perryman et al. 1997. 2. Aufdenberg et al 2002. 3. Albayrak 1999, 2000.

ranging from $B_l = -19.6 \pm 11.1$ to 2.0 ± 6.0 Gauss. It is questionable, given the error bars, whether this is a positive detection of a magnetic field, especially since no Zeeman signature was seen directly in the spectrum, only after deconvolution. This was not necessarily an upper limit on the field as effects such as rotation could be hiding larger strengths.

Many studies have looked at the variability of the radial velocities of Deneb. Paddock (1935) observed Deneb with the three-prism dispersion of the Mills spectrograph attached to the 36-inch refractor at the Lick observatory. At this point, it had been discovered that Deneb was a radial velocity variable star, although the characteristics of the variability had not been determined. Paddock measured the radial velocity of Deneb by averaging the value from several lines in the blue region of the spectrum. By means of his 399 spectra, Paddock found the velocity variations to have “the characteristics of a Cepheid star, but with only very small, if any, variation of light.” However, the variations appeared to have the same characteristic curve for only a short time. Furthermore, Paddock stated that the “star may have within itself the physical nature of pulsation with a dominant period upon which are imposed other effects.” Thus, Paddock suggested that Deneb was showing these variations mainly due to a pulsation of the atmosphere, rather than due to a planet or a binary.

Abt (1957) observed 9 supergiants, including Deneb, for about a month and found that early- and intermediate-type supergiants all exhibited radial velocity variations. These were said to be pulsations of the stellar atmosphere on the basis that the line profile variations expected for other types of variations, such as turbulence, would produce a much more asymmetric line profile. Also, based on previous work (Paddock 1935, Fath 1935), the variations were thought to be due to pulsations because of the time scales observed. The pulsations could not be modeled by a simple mathematical relation, as in more simple cases, such as Cepheids or β Cephei stars. Further, the value of Q (the pulsational quantity $P \times (\frac{\rho}{\rho_{\odot}})^{1/2}$, where P is the period and ρ is the density) was roughly constant for supergiants ranging from spectral types B through late M.

Using the published radial velocities from Paddock (1935), Lucy (1976) tested the possibility of multiperiodic behavior in the radial velocity variations of supergiants using Deneb as the prototype. The radial velocities were averaged over longer time scales than expected for pulsations, which created variations that were attributed to a binary orbit (the secondary is unseen), with a period of either 846.8 ± 9.3 days or 776.4 ± 10.7 days. This binary period was subtracted out of the radial velocities, and time-series analysis of the residuals was performed to search for pulsational periods. Lucy derived an amplitude spectrum for the year with the most observations (1931),

from which two or three periods were found and subtracted. This was repeated until the amplitude spectrum was essentially all noise. Then, more data were added into the analysis. The derived pulsational periods were the following values: 100.8, 49.1, 40.5, 35.8, 24.2, 18.9, 18.1, 15.6, 14.4, 12.4, 11.4, 10.0, 9.5, 7.8, 7.9, and 6.9 days. Lucy did note that the strengths of the periods decreased as more data were added.

Parthasarathy and Lambert (1987) made 123 spectroscopic observations of Deneb in the near-infrared between 1977 and 1982 at McDonald Observatory. The radial velocity variations were of the same type as that observed by Paddock and found by Lucy, with a similar amplitude. It was claimed that the binary motion was recovered, but the basis of this claim is unclear, as no time-series analysis was performed.

Kaufer et al. (1997) were the first (since Paddock) to obtain a larger data set of radial velocities on which time-series analysis was performed to search for multiple pulsational modes including both radial and non-radial modes. They obtained 49 spectra over 173 nights in 1990 and 74 spectra over 155 nights in 1991. They used cross-correlation to measure the radial velocity for each spectrum obtained. Using the CLEAN algorithm (Roberts et al. 1987), they analyzed each observing season, as well as the radial velocities from 1931 - 1932 taken by Paddock, to find evanescent multiperiodic behavior in Deneb, as well as in 5 other B- and A-type supergiants. Their results support the previous work of Lucy, as the periods change with different

observing seasons, which helps to explain why the strengths of the periods decreased when more data was added.

Studies of the variability of the photometry of Deneb began simultaneously to Paddock's radial velocity measurements. Fath (1935) obtained photometry of Deneb using the 12-inch refractor of the Lick Observatory. This was done to see if there was a relationship between the velocity variations and the brightness, as in the case of Cepheids. Besides Deneb, he also examined the stars α Lyrae and β Canis Majoris. Fath used a photo-electric photometer, and a metal diaphragm pierced with 61 holes to make the observations, with 56 Cygni as a comparison star. No filters were used. Fath found the light curve of Deneb to show variation on the order of hundredths of a magnitude over a few weeks. He compared his observations to the radial velocities obtained by Paddock, and found the maximum light occurred shortly before the minimum velocity. He concluded that these variations were easiest to understand with pulsation of the stellar atmosphere.

The great apparent brightness of Deneb makes photometry difficult, as most photometric telescopes are large and no standard stars of similar brightness are in the neighborhood of Deneb. Thus literature on the photometry of Deneb is scarce. In 1997, Adelman and Albayrak used HIPPARCOS observations of Deneb, as well as other early A-type supergiants, to show that these objects are small or moderate

amplitude variables (a few hundredths or a tenth of a magnitude in amplitude). The light curve was not complete enough to state more than there was a period on the order of about 2 weeks, but there were most likely other effects to take into account. Adelman soon began an observing program on Deneb with the Four College Automated Photoelectric Telescope to examine this variability and to supplement the abundance analysis being performed by Albayrak (1999, 2000).

Another interesting aspect of the variability seen in Deneb, as well as other A-type supergiants, is in the $H\alpha$ profile. In A-type stars, the temperature is such that the hydrogen Balmer lines and the Balmer jump (the limit of the Balmer series, 3646 Å, which represents the energy absorbed when electrons originally in the second energy level of hydrogen are ionized) are maximum in strength. As Deneb has a spectral type of A2Iae, the hydrogen lines are strong. The star has a non-negligible stellar wind, and $H\alpha$ is sensitive to the stellar wind, due to both a high abundance of hydrogen and a large transition probability. $H\alpha$ is the most sensitive spectral line to the stellar wind in the optical region of the spectrum.

The stellar wind creates a P Cygni profile in the $H\alpha$ profile of Deneb and other hot supergiants. P Cygni profiles were first discovered in the spectrum of the luminous blue variable P Cygni. The profile can be explained by assuming the star is losing mass in a spherical distribution. The matter that is lost on a trajectory through the

line of sight will cause scattering out of the line of sight, resulting in an absorption feature. As the scattering material is coming toward the observer, the absorption feature is blue shifted. Matter that is lost with a trajectory perpendicular to the line of sight produces an emission feature that is centered at the rest wavelength. Matter that is lost at trajectories not in the line of sight or perpendicular to the line of sight will emit light that is either blue-shifted or red-shifted. See Figures 1-1 and 1-2.

The $H\alpha$ profile of Deneb (See figure 1-3.) exhibits a weak P Cygni profile. It has been used to estimate the mass-loss rate of the star. For example, Kunasz and Morrison (1982) estimated the mass-loss rate of Deneb to be $(4.0 \pm 1.0) \times 10^{-7} M_{\odot} \text{ yr}^{-1}$ using the $H\alpha$ profile and synthetic spectra based on stellar wind models. Kudritzki et al. (1999) used the strength of the emission component of the P Cygni profile of $H\alpha$ to determine the mass-loss rate \dot{M} , and the absorption of $H\alpha$ to determine the terminal wind speed v_{∞} of several supergiants, without taking into account the potential variability of the profile. For comparison, Hensberge et al. (1982) used low excitation ultraviolet Fe II lines ($\lambda \sim 2279.9$ through 2395.6 \AA) to estimate the mass-loss rate of Deneb to be $(1 - 5) \times 10^{-9} M_{\odot} \text{ yr}^{-1}$. It is interesting to note that the mass-loss rate is still not well known as the different techniques (i.e. $H\alpha$ profile or resonance lines in the ultraviolet) yield results that differ by several orders of magnitude.

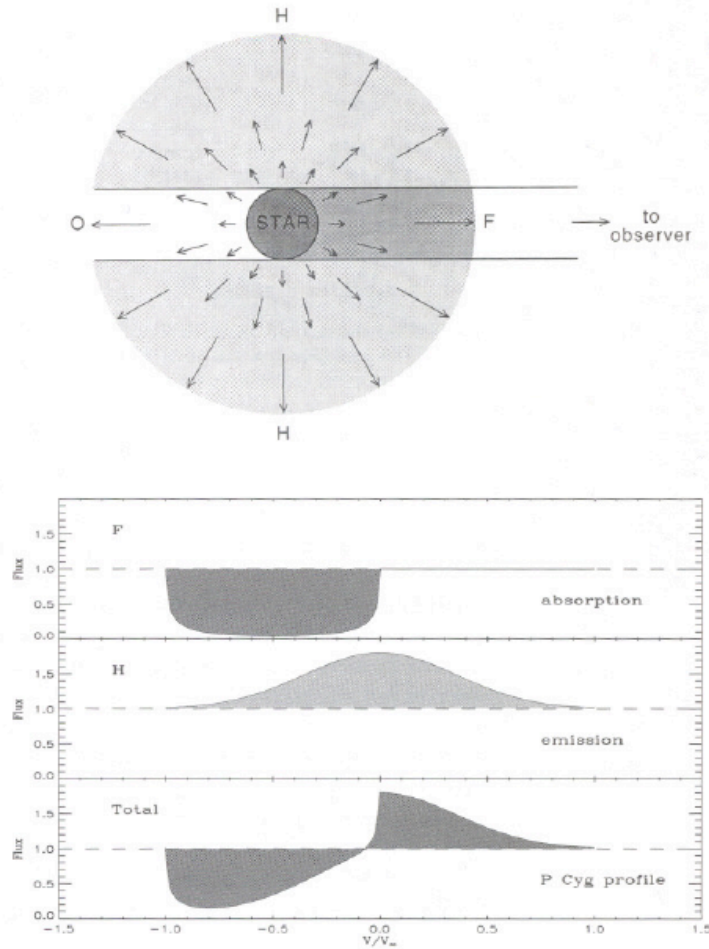


Figure 1-1: The formation of the P Cygni profile. The blue-shifted absorption is formed in the line of sight (region F). The material surrounding the star that is not in the line of sight (region H) will produce emission features that will range from red-shifted to blue-shifted. Region O is occulted, and does not contribute to the spectrum. Figure reproduced from Lamers and Cassinelli, 1999.

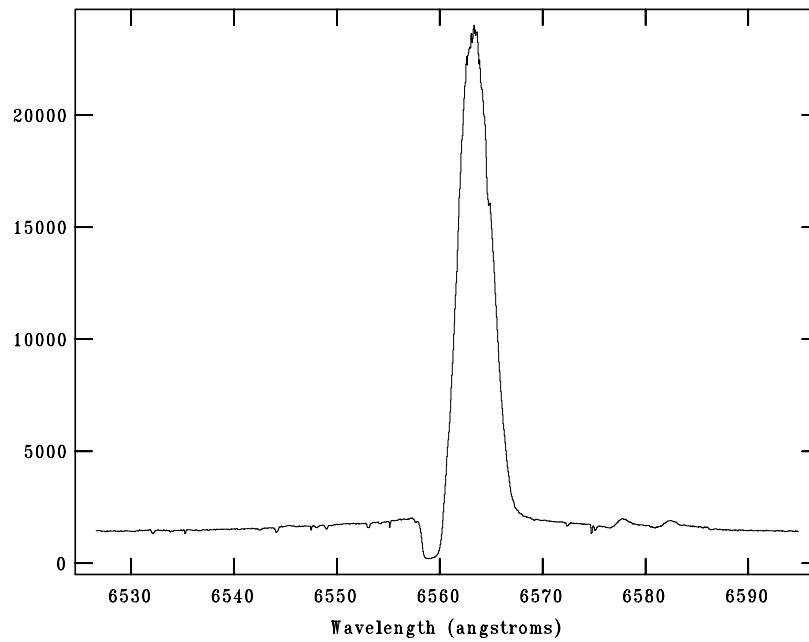


Figure 1-2: The H α region of the spectrum of P Cygni obtained at Ritter Observatory on 04 Oct 2004. Notice the blue-shifted absorption component at 6558 Å, the emission component maximum at approximately the rest wavelength of 6562.817 Å, and the red-shifted emission caused by the receding matter surrounding the star.

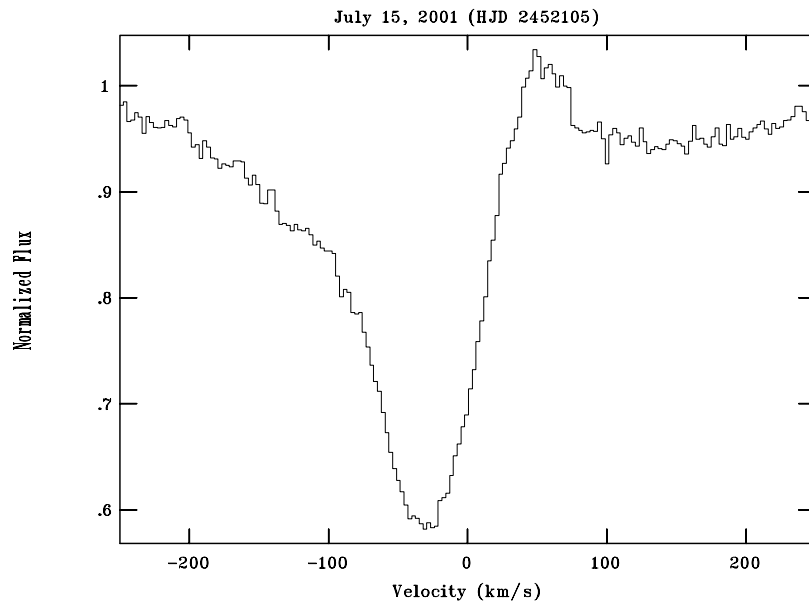


Figure 1-3: The $H\alpha$ spectrum of Deneb from July 15, 2001. The velocity is a measure of the Doppler shift from the rest wavelength of $H\alpha$. This spectrum was obtained by observers Joshua D. Thomas and Dr. Nancy Morrison.

Kaufer et al. (1996) examined the $H\alpha$ profiles of six B- and A-type supergiants, including Deneb, to search for a cause of the variability of the $H\alpha$ profile. Dynamical spectra were constructed for a visual interpretation of the variability of the data sets. Very few variations were observed in the $H\alpha$ profile of Deneb. For each of their stars, the equivalent width of the line was analyzed by observing season with the CLEAN algorithm to search for periodicities. It was found that the periodicities were evanescent in nature, changing each year.

Morrison and Mulliss (1997) reported finding a much more active, and possibly cyclic, variability in the $H\alpha$ profile than that reported by Kaufer et al. Often there are “absorption events” where there is a secondary absorption component on the blue wing of the absorption component of the $H\alpha$ profile. The strength of the emission component is also variable. The absorption events are likely from mass in the line of sight, that was expelled from the atmosphere of Deneb. This could possibly be attributed to a DAC (“Discrete Absorption Component”). A DAC is a feature in a dynamical spectra that allows the terminal wind speed to be determined from secondary absorption component superimposed on the line profile that asymptotically approaches the terminal wind speed with time.

One possible explanation for the variability of the $H\alpha$ profile would be a rotationally modulated wind. This would cause the observed variability to be a cyclic

process. This can be envisioned as a spot on the star having a larger mass loss rate. As the star rotates, the enhanced region of lost mass would cause a spiral-shaped density enhancement in the circumstellar matter. This would explain the DACs that are observed with the winds of some hot stars. Also, this would put a variable density of emitters in the circumstellar environment, causing the emission component strength to vary (Cranmer and Owocki 1996, Dessart 2004).

The purpose of this thesis is to examine the variability of the $H\alpha$ profile, radial velocities, and photometry of Deneb during a five year time period (1997-2001). A study simultaneously encompassing all of these aspects of the variability has not previously been performed. Chapter 2 will detail the observations taken, Chapter 3 will detail the data reductions, Chapter 4 will begin to discuss the results from this study, Chapter 5 will detail the the time-series analysis performed to examine the variability, and Chapter 6 will discuss the results and analysis to draw conclusions about the pulsations of the atmosphere, the $H\alpha$ profile, and the possible binary orbit found by Lucy (1976).

Chapter 2

Observations

This chapter details the observations taken and used in this project. Spectroscopic observations were taken at Ritter Observatory (University of Toledo; Toledo, Ohio), while photometric observations were taken at the Four College Automated Photoelectric Telescope (located in Washington Camp, New Mexico).

2.1 Ritter Observatory

339 red-yellow spectra of Deneb were obtained at Ritter Observatory between 1997 March 20 and 2001 December 21. For the most part, one spectrum was taken per night, although multiple exposures were obtained on some nights.

The starlight was passed through the Cassegrain focus of the 1-meter telescope

onto an optical fiber. The starlight was then transmitted to an entrance slit of an échelle spectrograph. The entrance slit was typically set such that the resolving power was 26,000 in the H α region of the spectrum. However, during the time period between 1997 April 8 and 1997 July 25, the entrance slit of the échelle spectrograph was adjusted for a resolution of approximately 50,000.

The spectra were reduced using standard techniques. This was carried out by the Ritter Research Assistants Chris Mulliss (September 1994 through December 1998), David Knauth (1999 through August 2001), and John Wisniewski (August 2001 through August 2003) by means of an IRAF¹ script. Five to ten “bias” frames were collected every night. These are exposures of essentially zero time where no light is collected on the CCD (Charge Coupled Device). These are averaged in the reduction process. The averaged bias is subtracted from each image to remove background read noise.

The spectra were flat-fielded to remove pixel-to-pixel sensitivity variations. Flat fields are spectra of an approximate continuum lamp source. The spectral energy distribution varies little between pixels with a flat exposure, allowing pixel-to-pixel variations to be determined and divided out of the raw spectrum. The flat exposures are bright and are also used for the order extraction of the échelle orders.

¹IRAF is distributed by the National Optical Astronomy Observatories, which are operated by the Association of Universities for Research in Astronomy, Inc., under contract with the National Science Foundation.

A comparison spectrum was taken before and after each stellar spectrum by means of a Th-Ar discharge lamp mounted on the telescope. The pattern of the emission lines are known, and thus a wavelength calibration can be performed during the reduction process. Many comparison spectra are taken throughout an evening because the CCD chip could be slightly displaced over time. For each stellar spectrum, a time-averaged comparison is created from the surrounding comparison spectra. The root mean square deviation between the known wavelengths and the average comparison spectra is between 0.001 - 0.005 Å (Mulliss 1996).

The typical properties of the spectroscopic observations are summarized in Table 2.1. The individual observations and their properties (date, exposure time, ADU (a measure of the intensity of the light on the spectrograph; a value of 200 ADU typically represents a signal to noise ratio of ~ 200), and the observers) are tabulated in Appendix A.

Table 2.1: Properties of Ritter Observations

Property	H α spectrum
Exposure Times (sec)	60 – 1200
Average Exposure Time (sec)	418
SNR (Range)	50 – 200
Average SNR	100

2.2 The Four College Automated Photoelectric Telescope

370 differential photometric measurements of Deneb were obtained with the Four College Automated Photoelectric Telescope (FCAPT) during the coinciding time period of 1997 October 29 to 2001 July 2. The measurements were made with the Strömngren filter system.

A good review of the Strömngren photometric system is found in Jaschek and Jaschek (1990). It uses four narrow band filters u , v , b , and y , standing for ultraviolet, violet, blue, and yellow. The characteristics of the filters are given in Table 2.2. A plot of the response functions of the filters as a function of wavelength is given in Figure 2-1.

Table 2.2: Properties of the Strömngren narrow-band filters

Filter	Central Wavelength	Width at Base
u	3500 Å	675 Å
v	4100 Å	700 Å
b	4700 Å	700 Å
y	5500 Å	700 Å

The Four College Automated Photoelectric Telescope began operations in the

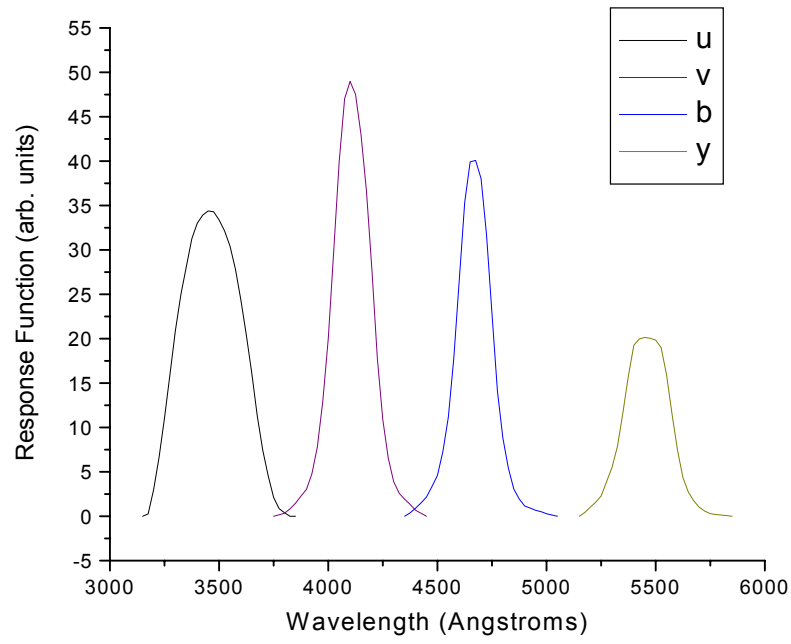


Figure 2-1: The response functions of the Strömrgren filters; this was created from the values tabulated in Jaschek and Jaschek (1990).

autumn of 1990. It is a 0.75-meter telescope located in Washington Camp, Arizona. It chooses its targets from a preset list by means of both priority and proximity to the western horizon. This telescope is owned and operated by four colleges: The College of Charleston (Charleston, SC), The Citadel (Charleston, SC), The University of Nevada, Las Vegas (Las Vegas, NV), and Villanova University (Villanova, PA) (Dukes et al. 1992).

The telescope began taking observations of Deneb in the fall of 1997. As the telescope does not operate in the summer (monsoon season), the measurements were made in the fall and late spring of each year.

Table 2.3: Properties of the Strömgren photometry

Season	Check star	Comparison Star	Estimated Error (magnitudes).
Fall 1997- Spring 1999	HD 197036	HD 198151	0.004
Fall 1999- Fall 2001	HD 198151	HD 199311	0.005

The observations were made differentially relative to two non-variable stars. Each observation consisted of a measurement of the dark count followed by a sequence of sky-ch-c-v-c-v-c-v-c-ch-sky where sky is the reading of the sky in the neighborhood of Deneb, ch is the check star, c is the comparison star, and v is the variable star (in this case Deneb). The check and comparison stars are non-variable stars, where

using two stars allows better photometry as well as a measure of the error. This same process is outlined in Adelman's papers of 1992, 2001, and 2002. The properties of the observations are given in Table 2.2. The estimated error of the measurements comes from the root mean square difference between the check and comparison stars.

In order to avoid saturating the photomultiplier, the light from Deneb (but not that of the comparison and check stars) was passed through a 5 magnitude neutral density filter. The fact that the Strömgen filters have relatively narrow response functions was also helpful.

After HD 197036 had been used as the comparison star for the first two years of data collection, it was discovered that this star is a small amplitude, long period variable star. Thus, it was replaced with HD 198151 for the remainder of these observations, with a new check star, HD 199311.

Chapter 3

Reductions

3.1 H α Spectroscopic Reductions

In order to fully analyze the variability of the H α profile, telluric line removal, doppler correction, and continuum normalization had to be performed. These steps are outlined in this section.

Telluric lines are spectral lines originating in the Earth's atmosphere. In the H α region of the spectrum, a plethora of water vapor lines from Earth's atmosphere litter the spectrum and can create confusion in the interpretation. See figure 3-1 for a typical example of the spectrum of Deneb highlighting the water lines.

Templates of telluric lines were created (both by myself and Kevin Croxall) by

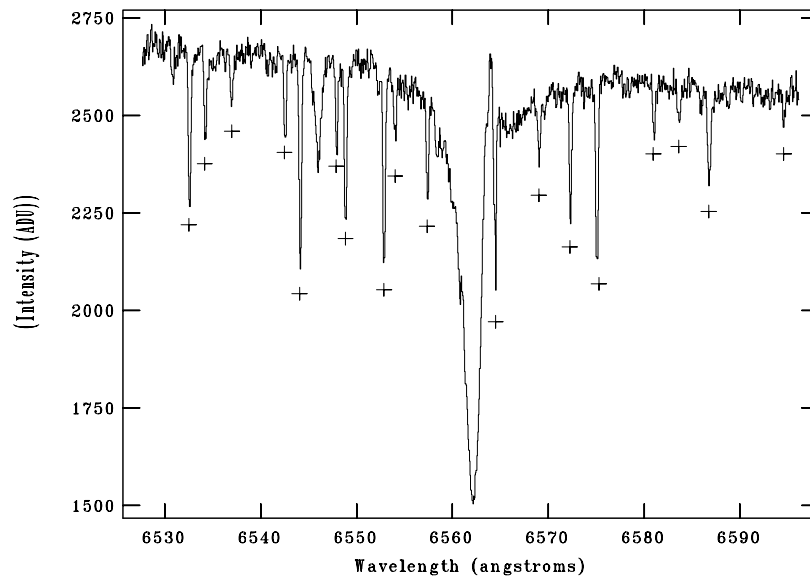


Figure 3-1: In the $H\alpha$ region of the spectrum, there is a plethora of telluric (water) lines, including a few in the absorption and emission components of the P Cygni profile. The strongest telluric features are labeled with '+' signs. This spectrum is from the evening of July 15, 2001. The vertical scale is arbitrary units of intensity.

utilizing spectra taken with the same spectrograph setup of rapidly rotating hot stars that do not exhibit the Be phenomenon. Examples include α Leonis (B7V), σ Sagittarii (B2V), and ζ Aquilae (A0Vn). Telluric lines were fit with Gaussian profiles using the IRAF task *splot* (See Figure 3-2). Then, using the IRAF task *mk1dspec*, template spectra of telluric lines were created (See Figure 3-3).

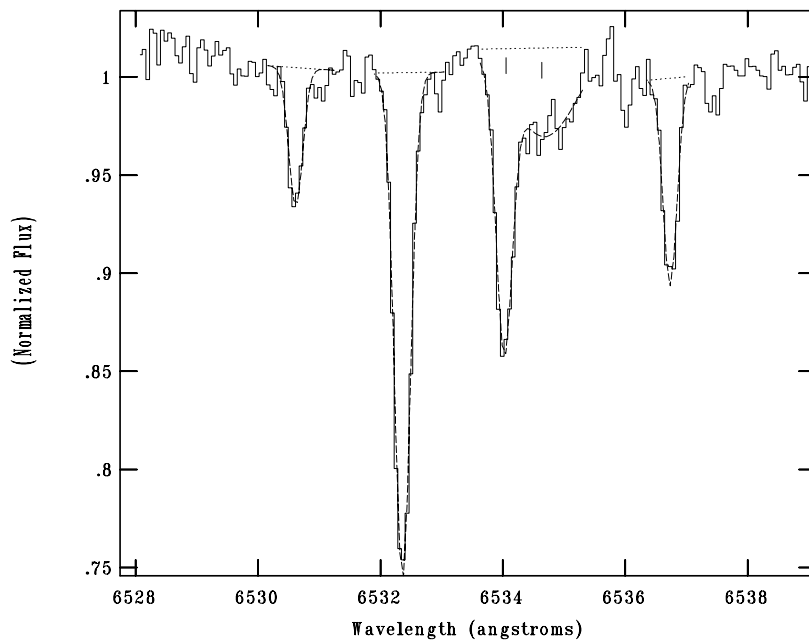


Figure 3-2: Water lines are narrow features from the Earth's atmosphere. They can be fit with Gaussian line profiles to create template spectra.

The IRAF task *telluric* was then employed to divide out the effect of telluric lines. This provides a secondary method of wavelength calibration, with the same wavelength scale as the template. The resultant spectrum should then be entirely

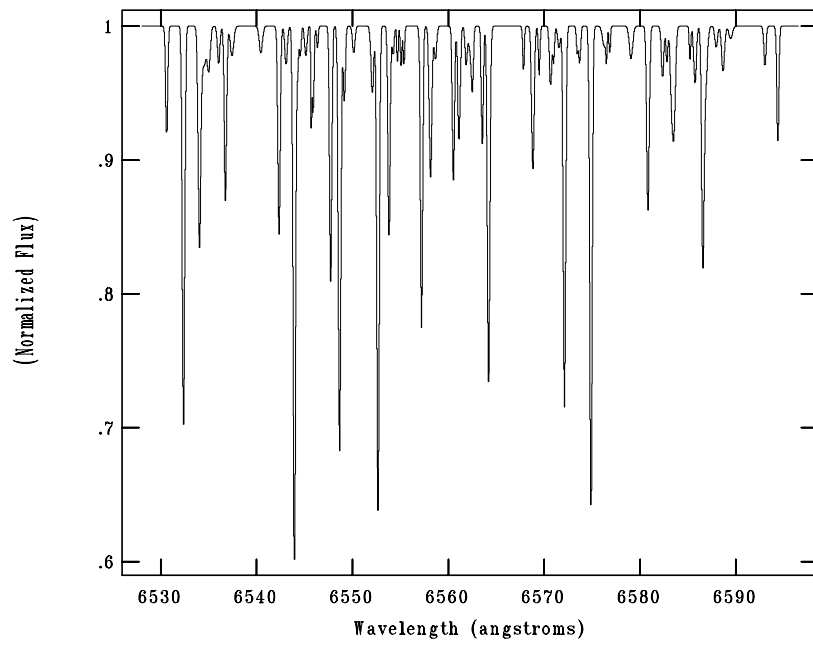


Figure 3-3: A typical water template used in this project.

stellar in origin (See Figure 3-4).

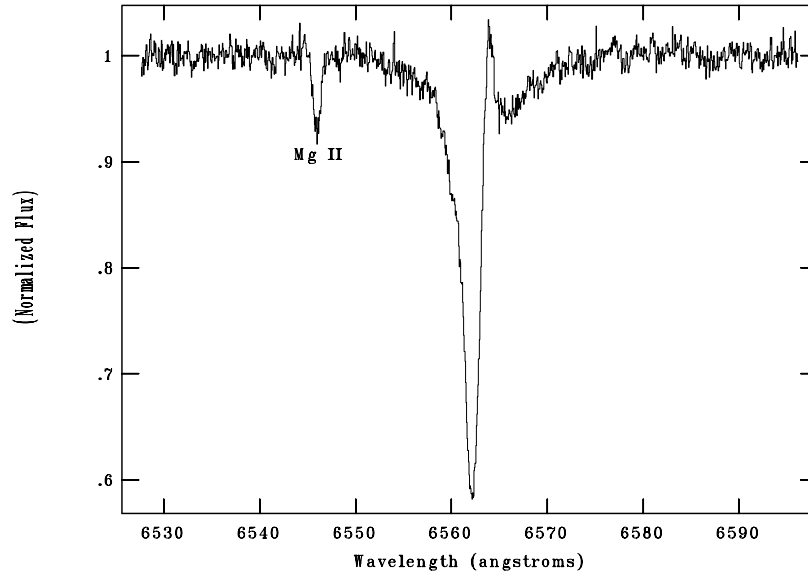


Figure 3-4: This shows a typical resultant spectrum with telluric lines removed (from the same night of July 15, 2001). The resultant spectrum looks much “cleaner” and is easier to analyze.

As the Earth orbits the Sun, it creates a measurable Doppler shift with respect to the line of sight. This is fixed by means of the image keyword *VHELIO*. This keyword is calculated from the known date and time of the observation during the image reduction pipeline process, and it represents the line of sight component of the Earth’s velocity at the time of the observation. This is subtracted by means of the IRAF task *dopcor*, allowing the spectra to be analyzed from the rest frame of the solar system.

The spectra were then normalized so that the continuum value was unity by means of the IRAF task *continuum*. This allows the spectra to be quickly compared for variability, as all of the spectra would have the same continuum value.

There were some nights where more than one spectrum was obtained in an evening. To increase the signal-to-noise ratio (SNR), these spectra were added before being normalized, but after the Doppler correction. The H α profile does not noticeably vary on the time scale of hours (e.g. Kaufer et al. 1996).

3.2 H α Dynamical Spectra

Dynamical spectra provide a method to visually search for variability in large spectroscopic data sets. The spectra are represented three-dimensionally. The spectra (intensity plotted against wavelength) are plotted as a function of time in a dynamical spectrum. The intensity is represented in a color scheme that represents the value of the intensity. This gives a clear representation of the behavior of the spectrum, and has been used in many different settings. For example, Gies and Kullavijaya (1988) used the dynamical spectra to find evidence of multimode non-radial pulsations for the star ϵ Persei. Also, Massa et al. (1995) used this method to find the terminal wind speed for OB stars such as HD 50896, HD 64760, and HD 66811 using resonance lines in the ultraviolet.

Dynamical spectra were constructed for each of the five years of data analyzed in this project. When there were not observations on consecutive days, the spectra were linearly interpolated for the missing observations, provided the gap was less than 10 days. The dynamical spectra created for the Ritter observations will be presented and discussed in Section 4.1.

3.3 The Equivalent Width of H α

The equivalent width of a line, W_λ , is given by Equation 3.1. While the limits of integration are formally 0 and $+\infty$, this can never be observationally reached, as the spectrum has multiple lines, and not all wavelengths are observed. Thus, the integral is evaluated from a minimum to a maximum wavelength (a to b) such that the integral is zero (for the desired line) over the non-integrated spectral regions.

$$W_\lambda = \int_0^\infty \frac{F_c - F_\lambda}{F_c} d\lambda \simeq \int_a^b \frac{F_c - F_\lambda}{F_c} d\lambda \quad (3.1)$$

For each observation, the equivalent width of H α was measured using the same spectral window. By means of the IRAF task *sbands* in the package *onedspec*, a 22 Å filter was constructed to measure the flux centered around H α (See Figure 3-5). Since the continuum flux (F_c) was normalized to unity, and the measured flux ($F_{\text{avg}} \simeq F_\lambda$)

is the average over the 22 \AA window, Equation 3.1 reduces to:

$$W_\lambda = 22 \text{ \AA} \times \frac{1 - F_\lambda}{1} \quad (3.2)$$

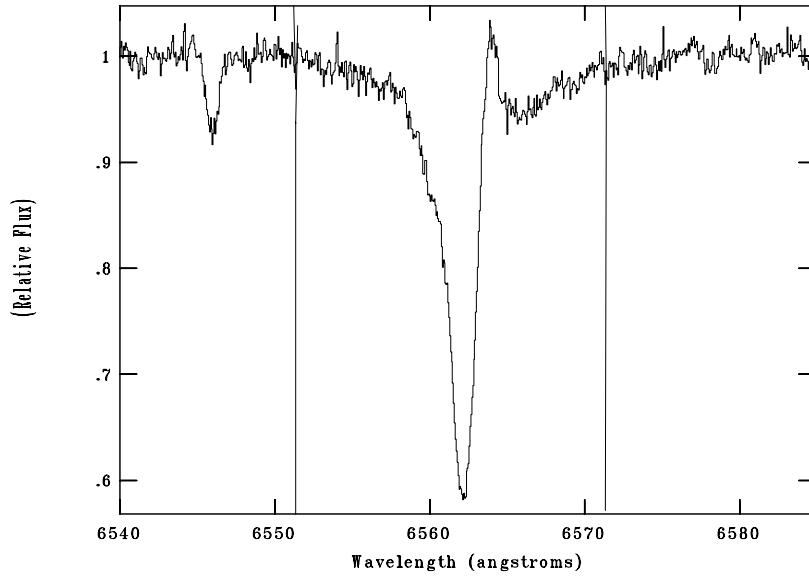


Figure 3-5: The spectral range from which the flux was measured by means of *sbands* is highlighted by two vertical lines, each spaced 11 \AA from the rest wavelength of $\text{H}\alpha$.

This flux was then measured for all of the continuum-normalized $\text{H}\alpha$ spectra. However, this value is the net equivalent width (the sum of absorption and emission component). The emission component's equivalent width (which is negative by convention) was measured using the IRAF task *splot*. Then this value was subtracted to yield an equivalent width of the absorption component of $\text{H}\alpha$ (See Figure 3-6).

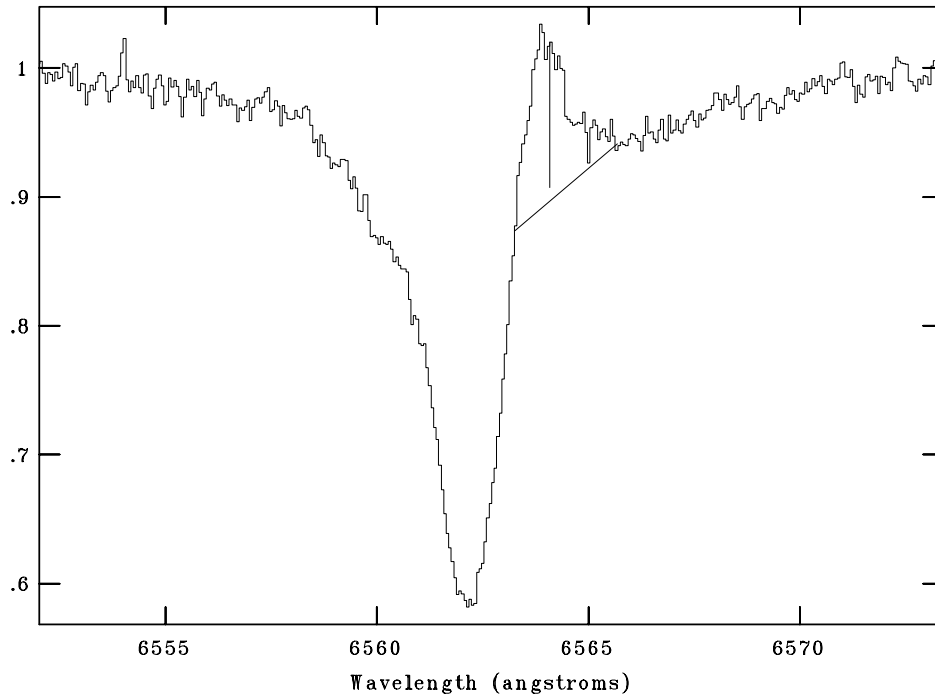


Figure 3-6: The emission component's strength (equivalent width) was measured using the IRAF task *splot*, using the keystroke 'e' in the display window. This was measured in such a way that the emission component was consistently subtracted in each spectrum. This spectrum was obtained on July 15, 2001.

To estimate the error in the measurement of the equivalent width, a few spectra were chosen to analyze. Using *splot*, the window was set to be the same as that of the *sbands* window of 22 Å. The net equivalent width was then measured for each of these spectra five times, where the continuum was placed slightly different each time. Then, by averaging the found value and comparing it to the original values, an estimate of the lower limit of the error could be found. The results are tabulated in Table 3.1. It was found that the error in the *sbands* measurement was on the order of hundredths of an Angstrom, with a comparable value for that of the emission component. In comparison, the errors are much larger for the emission component, as the value for the average of the net equivalent width is 1.318 Å, and the average value for the emission component's equivalent width is -0.20 Å.

3.4 Si II Radial Velocities

In order to investigate the pulsational frequencies and the possible binarity of Deneb, its atmospheric motions were studied. As the atmosphere or star moves toward or away from an observer, the spectral lines are shifted toward the blue or red, respectively, allowing the radial velocity to be measured spectroscopically. This is given by the Doppler shift formula (valid for velocities much less than the speed of light c , which relates the observed velocity (v_{obs}) to the rest wavelength (λ_0) and

Table 3.1: Errors in the measurement of the equivalent width of H α from two different spectra.

<i>sbands</i> derived (net)	Comparison values (net)	Emission Component	Comparison Values
1.441	1.418	-0.087	-0.108
	1.447		-0.120
	1.411		-0.082
	1.490		-0.099
	1.483		-0.091
1.406	1.360	-0.111	-0.102
	1.280		-0.124
	1.392		-0.117
	1.377		-0.135
	1.424		-0.120
Average Differences	net	emission component	
	.009	.013	
	.039	.009	

observed wavelength (λ). See Equation 3.3.

$$v_{obs} = \frac{\lambda - \lambda_0}{\lambda_0} c \quad (3.3)$$

The IRAF task *splot*, also in the package *onedspec*, can be used to find the radial velocities of spectral lines. In order 8 of the Ritter Observatory échelle spectrograph, there is a strong doublet of Si II (rest wavelengths of 6347.11 Å and 6371.36 Å). A typical spectrum in the region of the Si II lines is shown in Figure 3-7. Gaussian curves were fit to the lines of the doublet to measure the line center. On the blue wing of the Si II 6371 Å line, is a weak blended line of Fe II. This line was also fit when determining the radial velocity of the 6371 Å line.

A data set was created of the radial velocities for all of the spectra obtained. As the lines are formed at the same depth in the atmosphere, the radial velocities should be equal for the two lines. Thus the differences in the two lines would yield a measure of the error in the radial velocities. This was performed for each of the observing seasons, with the resultant error estimates listed in Table 3.2 with a sample histogram from which the error was derived shown in Figure 3-8. The root mean square of the difference is also a measure of the error for each observation. This provides a good lower limit to the error, as this does not include effects due to CCD shifts, which would affect both lines of the doublet. It was found in July 2006 that

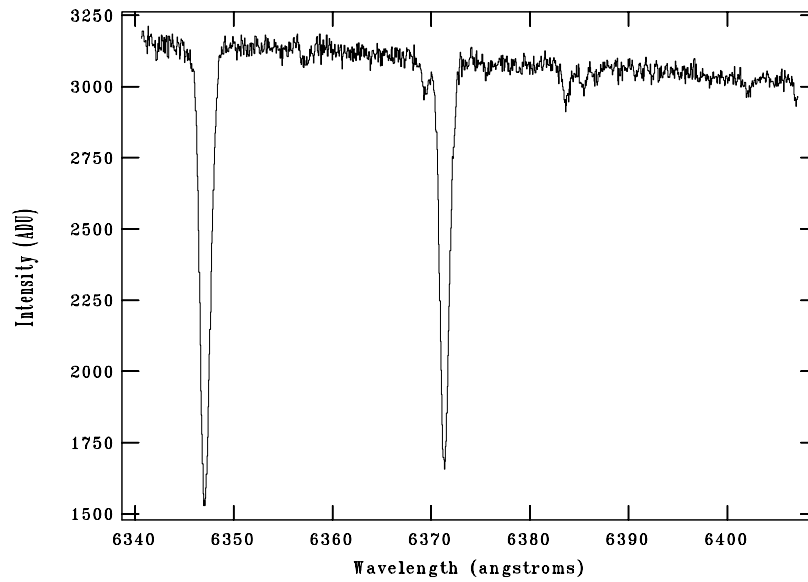


Figure 3-7: The spectrum of Deneb in the region of the Si II doublet ($\lambda\lambda$ 6347, 6371) taken on November 6, 2001. On the blue wing of the 6371 Å line as well as at 6383 Å are two Fe II lines of similar strength. The y-axis is in units of ADU (analog to digital units) which are arbitrary units of intensity that are set in the data acquisition process.

there was an instrumental problem with the comparison lamp used in the fall of 1998 through 1999. This may inflate the actual amount of error in the measurements of that time period.

Table 3.2: Estimated errors for the radial velocities measured using the Ritter Observatory spectra.

Year	Number of Observations	Estimated error (km s ⁻¹)
1997	71	0.50
1998	91	0.45
1999	57	0.69
2000	43	0.47
2001	70	0.48
Average Weighted Error		0.51

On evenings where multiple spectra were obtained, the radial velocity was found for each observation. If the difference was too large ($> 0.5\text{kms}^{-1}$) for one observation from a night with multiple exposures, that measurement was not used in the analysis of the data.

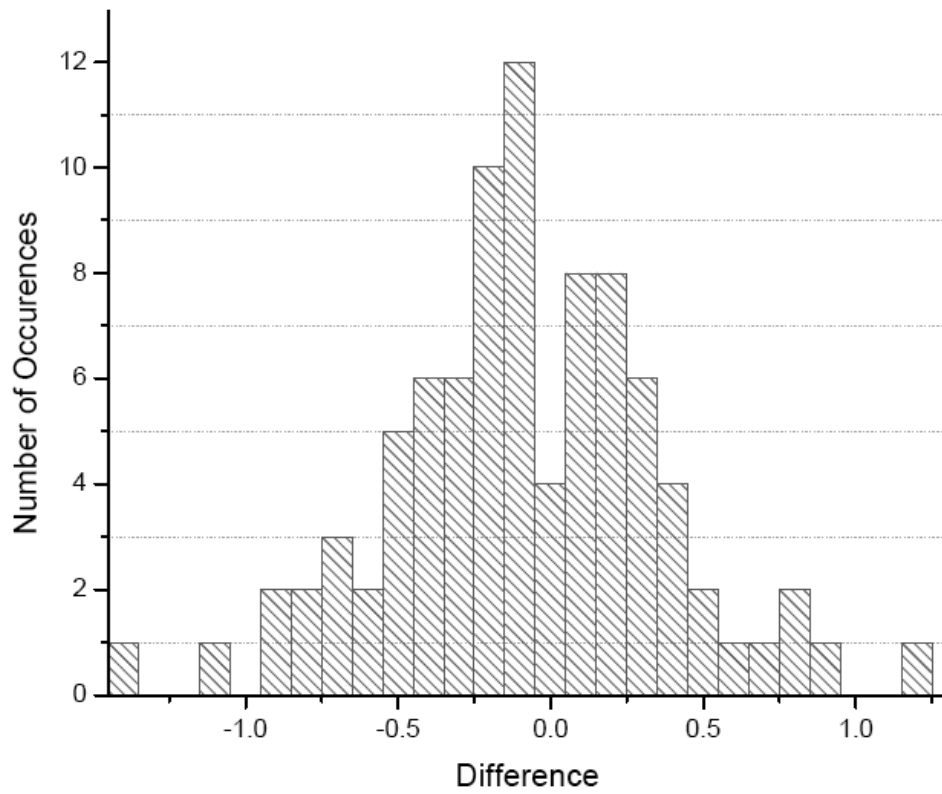


Figure 3-8: A typical histogram of the differences ($v_{r,6371} - v_{r,6347}$) in the units of km s^{-1} of the Si II radial velocities (1998 observing season). The width of a Gaussian curve fit to these data gives an estimate of the average error for a particular time period. For this season, the error is estimated to be 0.45 km s^{-1} .

3.5 Strömgren Photometry

It is desirable to use the actual *uvby* values, rather than the differential measurements. The *y* filter of the Strömgren filter system was designed to give the same value as the Johnson *V* filter. Thus, the *V* magnitude is assumed to be the same as the *y* magnitude. To find the *u*, *v*, and *b* magnitudes, color indices had to be used. *b*−*y* is a standard measurement given for Strömgren standard stars, and can be used to find the *b* magnitude. Similarly, *u* and *v* can be found from the *m*₁ and *c*₁ color indices. *m*₁ is given by Equation 3.4 and is a measure of the metallicity of the star. The *c*₁ color index, given by Equation 3.5, is a measure of the contrast of the stellar flux over the Balmer Jump. The published photometric values (from SIMBAD) are given in Table 3.3.

$$m_1 = (v - b) - (b - y) \quad (3.4)$$

$$c_1 = (u - v) - (v - b) \quad (3.5)$$

The SIMBAD database did not give Strömgren colors for HD 198151. The average differences between the check and comparison stars (HD 198151 and HD 199311) were used to find the Strömgren magnitudes needed for this comparison star.

Table 3.3: Published photometry values from the SIMBAD database

	HD 197036	HD 198151	HD 199311
Spectral Type	B5IV	A3V	A2V
V	6.59	6.31	6.66
$b - y$	0.005	not given	0.370
m_1	0.083	not given	0.187
c_1	0.363	not given	1.068

After the Strömgren magnitudes for the comparison stars were found, the magnitude of Deneb was found for all filters, in the instrumental system. It was discovered that the change of comparison caused a systematic difference in the magnitude observed for Deneb between the first two years and the remaining years. Therefore, the average difference between the two data sets was added to the first data set. The resulting values for the photometry are given in Appendix D.

3.6 Photometric Colors

Photometric colors can give information about a star's fundamental parameters. Two different colors were found (in the instrumental system) using the reduced photometry values. The first color, $u - b$, gave the color across the Balmer jump. While $u - v$ could have been used, the v filter is centered about the $H\delta$ line, which could be

subject to the same type of variability as the $H\alpha$ line, although the variability would likely be much smaller in amplitude. Thus, the $u - b$ is a better choice as the b filter is centered on the continuum for early-type stars.

The second color that was derived was $b - y$. This is essentially a temperature gauge for the star across the continuum. Both filters are centered on continuum regions for early-type stars. No strong lines interfere with the flux that can be measured through the b or y filters. The results are also given in Appendix D.

Chapter 4

Results

4.1 The H α dynamical spectra

The 1997 observing season (Figure 4-1) appears to show semi-regular behavior, with major absorption events occurring approximately every 40 days, around the heliocentric Julian dates 2450640, 2450690, 2450730, and 2450770. If this semi-regular behavior is caused by rotational modulation, this period is either the rotation period or a sub-multiple of the rotational period. The emission is static through most of the year, but strengthens twice (HJD 2450660 and 2450730). It is clear that the H α absorption does not extend to terminal wind speed ($v_\infty \simeq 225\text{km s}^{-1}$; Aufdenberg et al. 2002) and does not exhibit the same behavior seen in DACs. This could be

because there is too little optical depth at great distances from the star or because $H\alpha$ is not a resonance line.

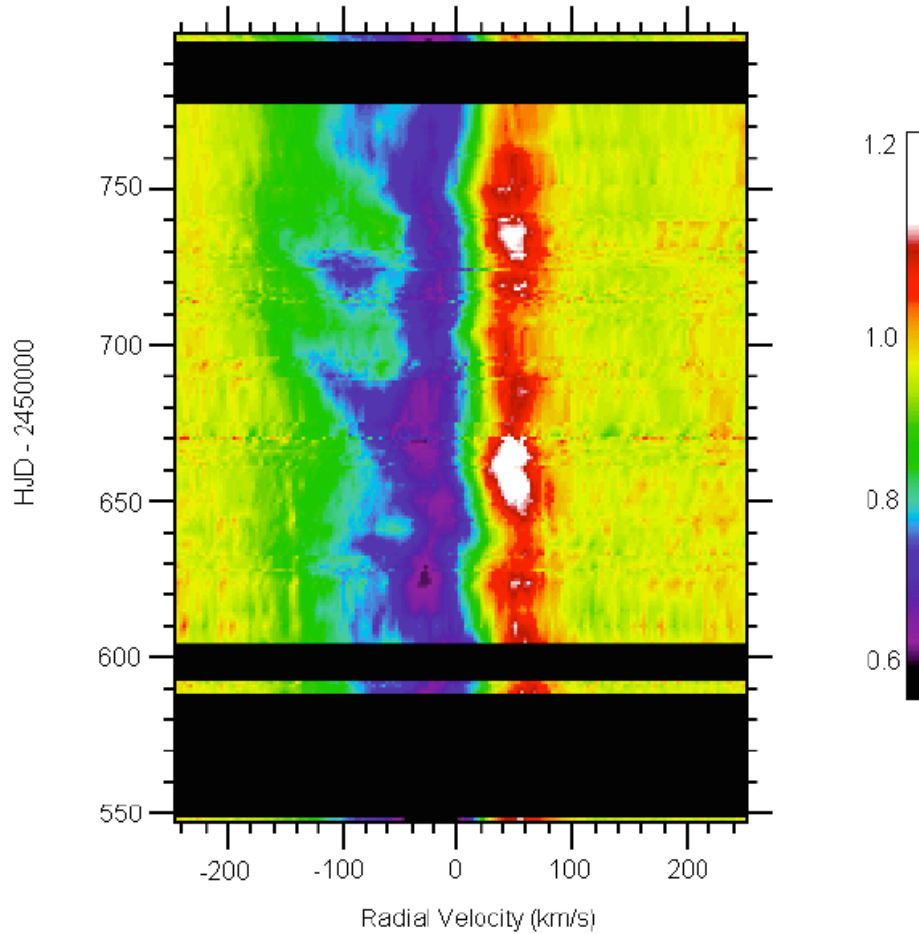


Figure 4-1: A dynamical spectrum of the $H\alpha$ profile for the year 1997.

The 1998 observing season (Figure 4-2) does not show the same cyclic behavior as the 1997 season. There are two absorption events (HJD 2451060 and 2451110) which do not correspond to the 40 day periodicity seen in the 1997 season (if the

40 day period would have continued, the closest events would have been on HJD 2451050, 2451090, and 2451130). The second event is fairly weak compared to the first, and exceptionally weak when compared to the events present in the 1997 season. Unlike the 1997 season, the emission component appears fairly static in this season of observations.

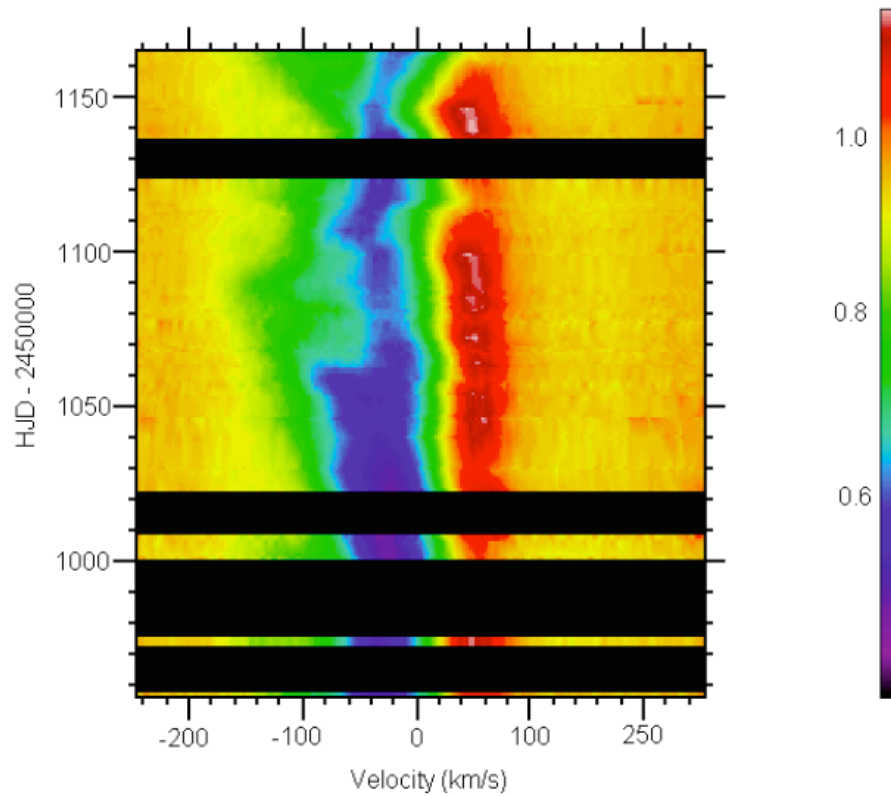


Figure 4-2: A dynamical spectrum of the $H\alpha$ profile for the year 1998 (constructed by Erin Allgaier).

The 1999 observing season (Figure 4-3) showed an nearly static $H\alpha$ profile for

the entire season. There appears to be an excess amount of absorption at the end of the season (HJD 2451520), with no other noteworthy events present. Variations are present, but seem rather small in comparisons to the variability present in other seasons.

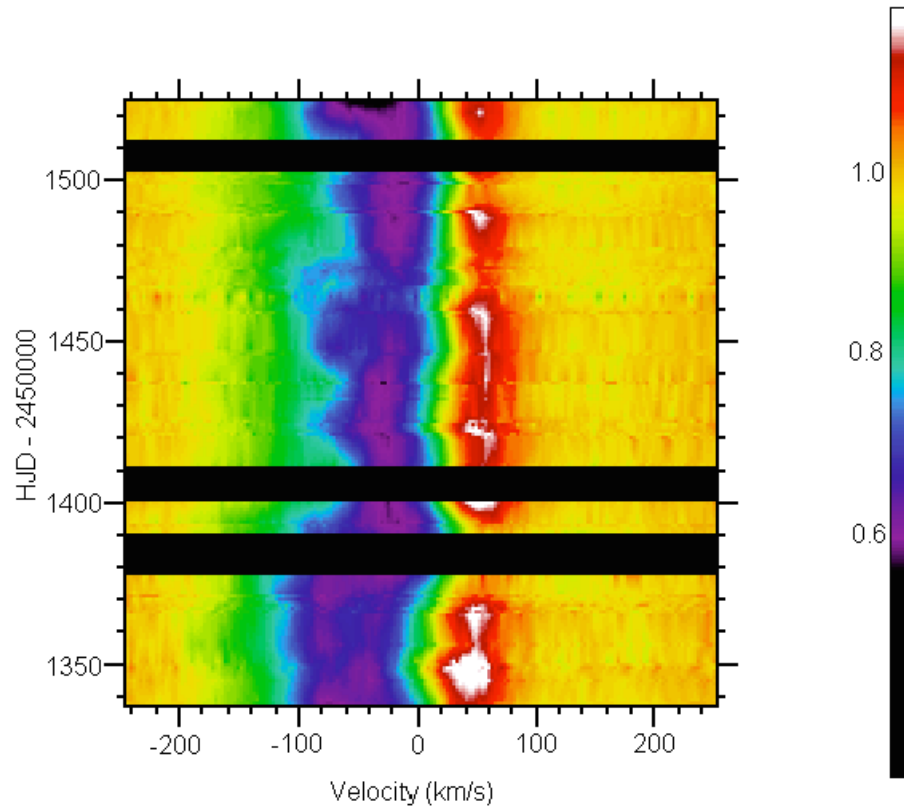


Figure 4-3: A dynamical spectrum of the $H\alpha$ profile for the year 1999 (constructed by Erin Allgaier).

The 2000 observing season (Figure 4-4) was exceptionally short, starting in August of that year, instead of during the spring. (As there was a telescope re-aluminization and camera problems early that year.) One absorption event is ob-

served (HJD 2451815), with the $H\alpha$ profile appearing mostly static for the remainder of the observations.

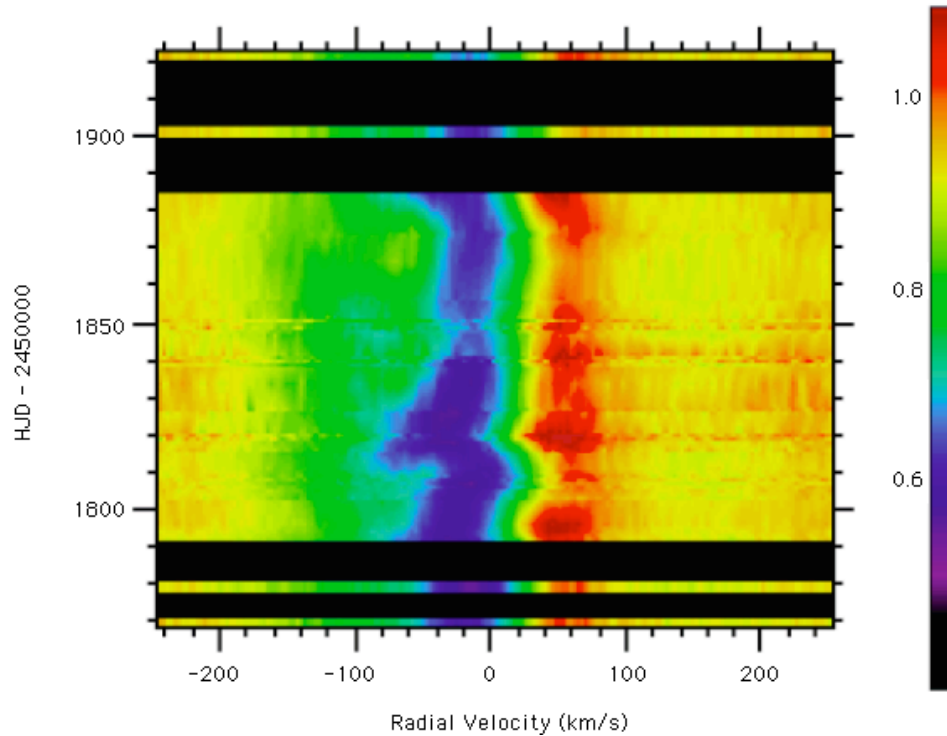


Figure 4-4: A dynamical spectrum of the $H\alpha$ profile for the year 2000 (constructed by Erin Allgaier).

The 2001 observing season (Figure 4-5) started earlier than other years of data collection (March 26), allowing a larger span of data. The absorption component was exceptionally strong at the beginning of the year (HJD 2452000), comparable to the event present at the end of 1999 (HJD 2451520). A small scale absorption event was observed around HJD 2452090. A major absorption event (possibly the superposition of two?) reached a maximum strength on HJD 2452190. During

the same time period, the emission component reached a strength not previously observed in this data set. As this major event subsided (HJD 2452210), the emission component almost vanished from the P Cygni profile.

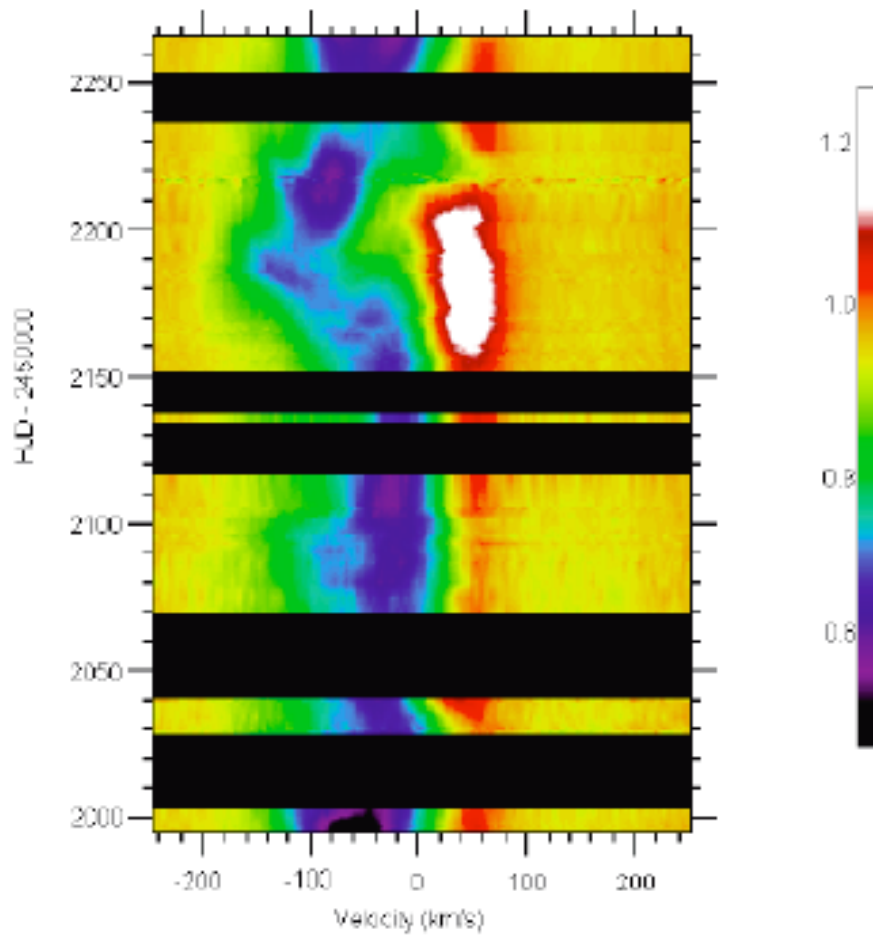


Figure 4-5: A dynamical spectrum of the H α profile for the year 2001.

From these dynamical spectra, it is apparent that the absorption events appeared cyclic in nature only for the 1997 observing season. The multiple events do not show

any hints of being cyclic in nature, but rather appear to be stochastic. Thus, the simple model of spiral shaped density enhancements from DACs should not be used to think of the stellar wind and circumstellar environment of Deneb.

It is also evident that conclusions should not be drawn from only one observing season of supergiant stars. These objects should be monitored for a longer time period. Also, the mass-loss rate probably should not be determined from a single spectrum in the $H\alpha$ region. Further work should be done to examine the wind momentum-luminosity relationship (Kudritzki et al. 1999) with respect to this variability. It should be expected that much scatter in the calculated distance would come from the type of variability exhibited in the $H\alpha$ profile of Deneb. Perhaps another method (such as radio flux) could be employed to use the wind momentum-luminosity relationship, as the $H\alpha$ profile varies in such a way that each spectrum could potentially yield a different mass-loss rate.

4.2 $H\alpha$ Equivalent Width Measurements

The measurements of the $H\alpha$ equivalent width are tabulated in Appendix B. An example is showcased in Figure 4-6, where the 1999 observing season's equivalent width measurements are plotted against the Julian Date of the observation. This season will be discussed due to its "lack" of variability exhibited in the dynamical

spectrum (Figure 4-3). The values can be seen to vary by approximately 0.5 \AA for the equivalent width derived from the *sbands* flux measurements (see Section 3.3, Figure 4-6). The measurements seem to oscillate with time (in a possible periodic way?), although the amplitude of the oscillations is non-stationary.

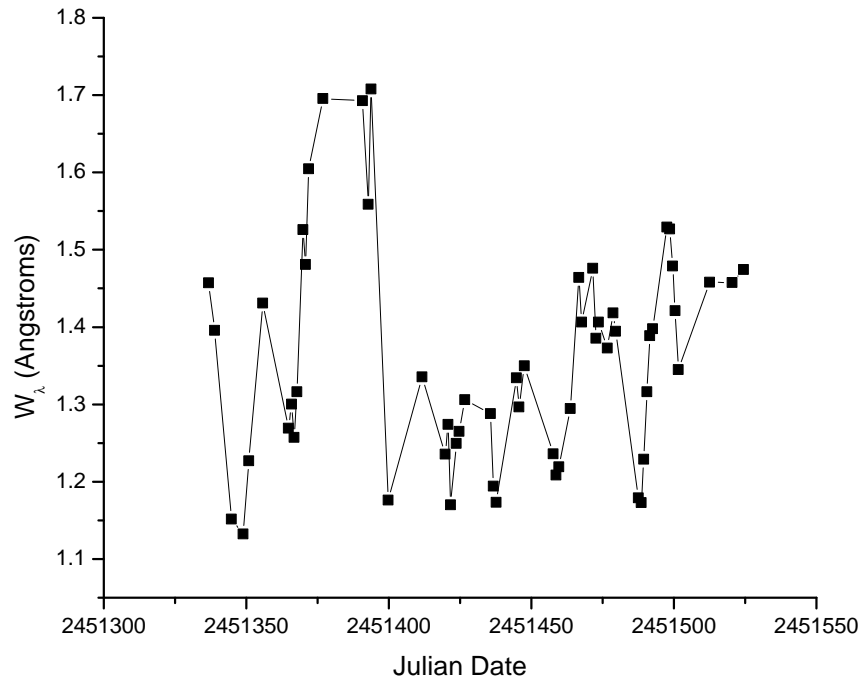


Figure 4-6: The net equivalent width of the $H\alpha$ profile (1999 observing season) as derived from the *sbands* measurements. Note that there is an increase in the equivalent width around Julian Date 2451375. This is also a time of less strength in the emission profile (See the dynamical spectrum, Figure 4-3).

A few features can be seen when the emission component's equivalent width is plotted against Julian date (Figure 4-7) for the same time period as in Figure 4-6.

The strength varies by about 0.3 \AA . It also reflects what is observed in the dynamical spectrum of that year (4-3) in that the emission component shows a minimum around JD 2451375.

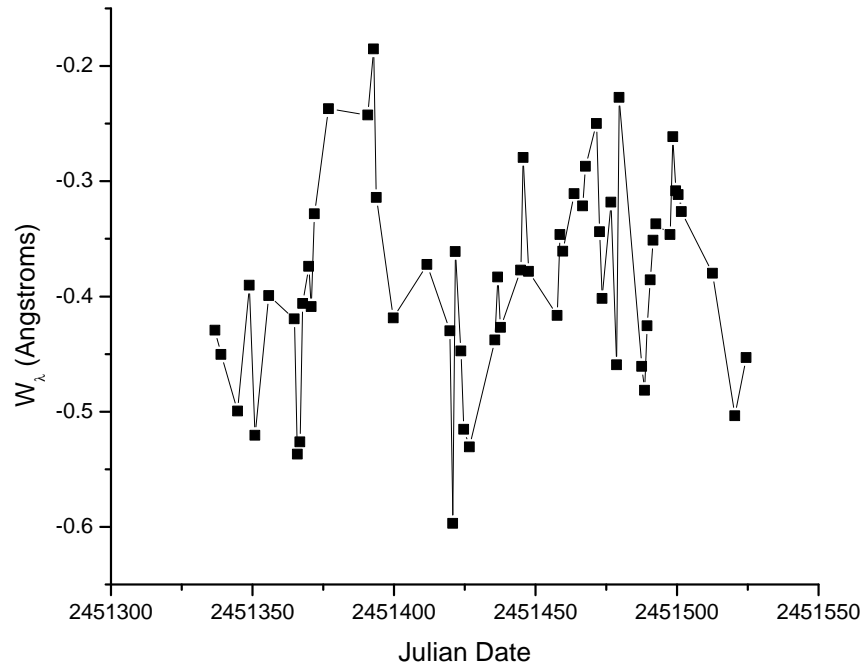


Figure 4-7: The equivalent width of the emission component of $H\alpha$ profile (1999 observing season) as derived from the *splot* measurements. Note that the emission component is weakest during the same period as mentioned in Figure 4-6.

When the equivalent width of the absorption component of $H\alpha$ is plotted as a function of Julian date (Figure 4-8), it becomes clear that the behavior exhibited with the net equivalent width measurements is somewhat representative of the behavior of the absorption component's equivalent width. To fully understand the periodicities

that appear to be present in the data, time-series analysis needs to be employed. Since the two curves tend to have the same trend, and the error is much smaller for the net equivalent width (it is a more consistent approach to the measurement), time-series analysis should be used to analyze the behavior of the net equivalent width.

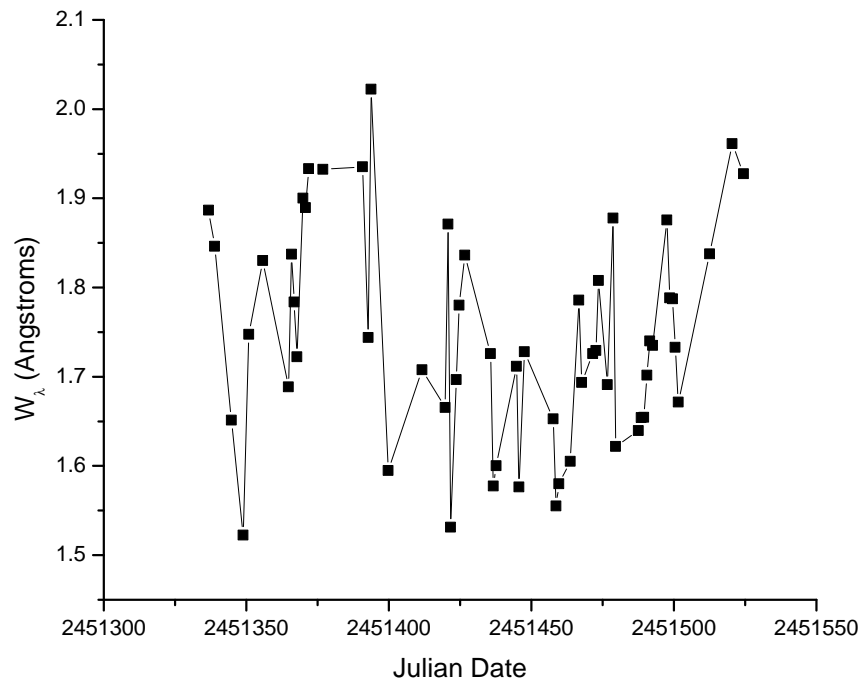


Figure 4-8: The equivalent width of the absorption component (1999 observing season) as derived from subtracting the emission component from the net equivalent width. There do not appear to be any major periods, but the net equivalent width does appear to oscillate between minimum and maximum values in a similar manner as that seen in the net equivalent width.

An interesting trend appeared in the $H\alpha$ equivalent width for the 2001 observing season (Figure 4-9 and the dynamical spectrum in Figure 4-5). From Julian date 2452100 through 2452200, there was a decrease in the overall strength of the $H\alpha$ line, decreasing linearly from a value of 1.4 \AA to about 0.75 \AA . The equivalent width then increased to a relative maximum and decreased again. During this time period, the emission component strengthened to the maximum strength observed, and then quickly declined to a point where it nearly vanished. This is seen at the same time period as the largest absorption event observed (possibly a superposition of two events) for that observing season.

4.3 Radial Velocities

The radial velocity measurements are tabulated in Appendix C. By inspection of the velocity curves, it is apparent that the radial velocity was variable as expected from previous work (e.g. Paddock 1935). The radial velocity curve shows a small (approximately 15 km s^{-1}) amplitude.

Shown in Figure 4-10 is the radial velocity curve for the 1999 observing season. The oscillations are consistent with those published in previous literature (e.g. Paddock 1935, Parthasarathy and Lambert 1987). There are oscillations present that appear to be multi-periodic or random in nature. There are definite (relative) max-

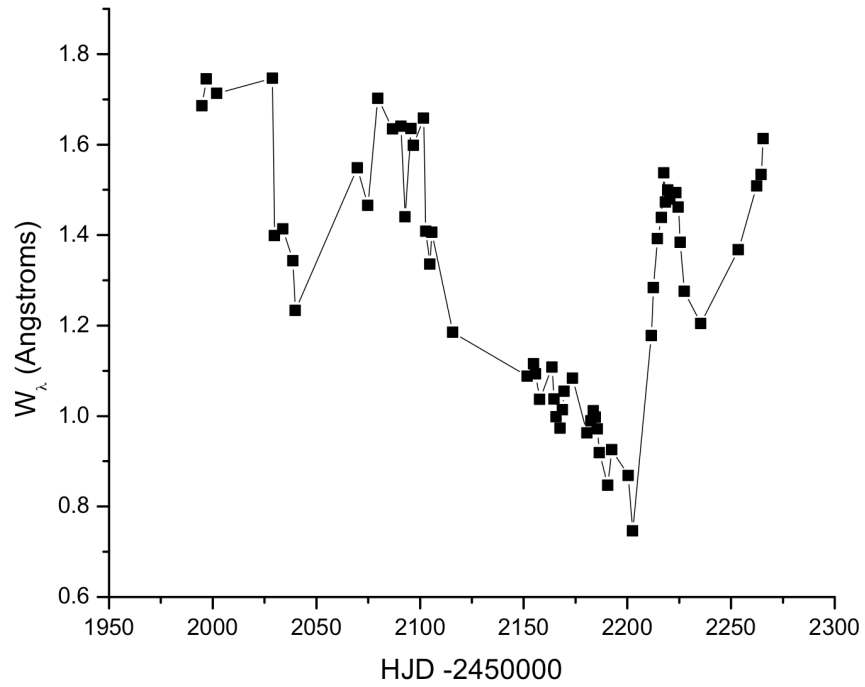


Figure 4-9: The equivalent width of the H α profile as derived from with *sbands* for the 2001 observing season.

ima at Julian dates 2451370, 2451460, and 2451490. Similarly, there are definite (relative) minima at Julian dates 2451390, 2451470, and 2451500.

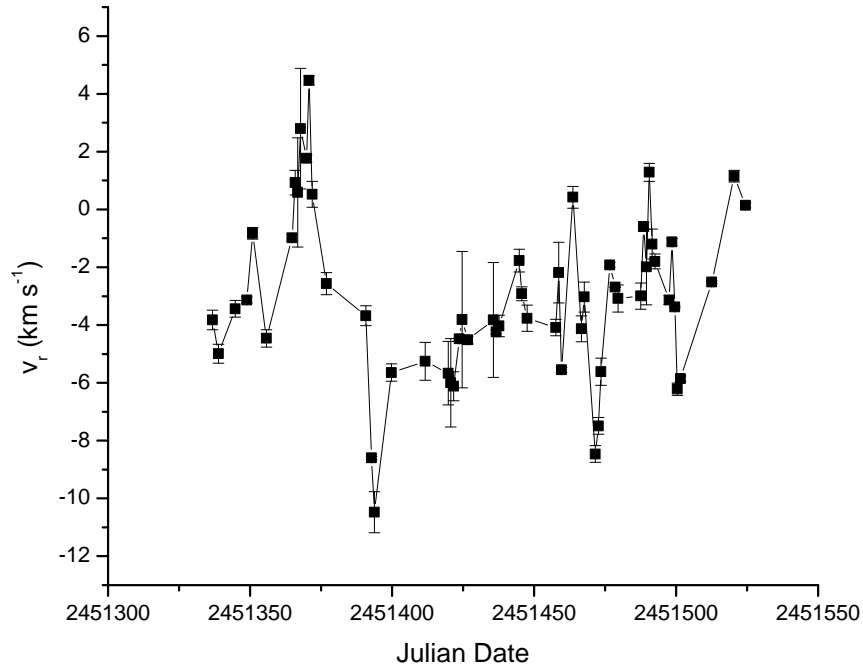


Figure 4-10: The average derived radial velocity of Deneb for the 1999 observing season as derived from with Si II $\lambda\lambda$ 6347, 6371 doublet. The error bars come from the root mean square difference between the two velocities, and is sometimes as small as the data point. The average error for this season is 0.69 km s^{-1} , but may be higher.

To fully understand the oscillations, time-series analysis would need to be performed. This will be discussed in further detail in Chapter 5.

4.4 Light Curves

The *uvby* values were used to construct light curves of Deneb. An example light curve (for the fall of 1999) is given in Figure 4-11. The remaining values and figures are tabulated and shown in Appendix D. The fall of 1999 shows variations in the magnitudes of about 0.06 magnitudes, while appearing almost sinusoidal in nature. There are relative maxima at Julian dates 2451445, 2451460, 2451475, 2451490, and 2451507. This leads to the observation that the dominant light variation is on an approximately 15 day cycle. Also, it should be noted that the radial velocity curve had peaks at Julian dates 2451460 and 2451490, suggesting a correlation between the photometry and the radial velocity.

The light curves immediately show Deneb to be a small amplitude variable, as is expected for early supergiant stars. This is consistent with the work of Fath (1935), who found Deneb to be a variable star with an amplitude of about 0.05 magnitudes. The light curves for the different filters exhibit the same features, consistent with the star having light variations due to pulsations of the atmosphere.

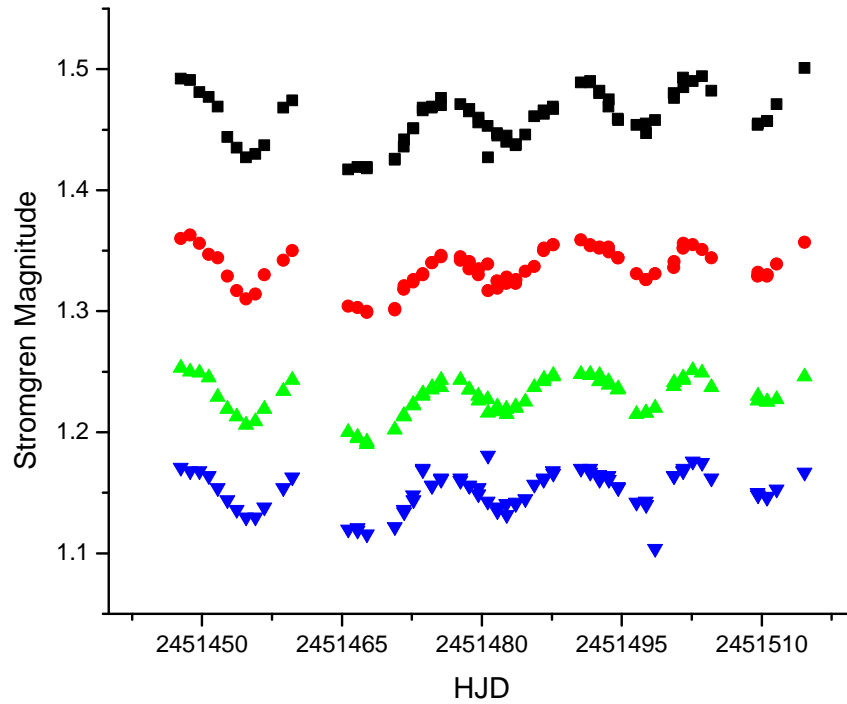


Figure 4-11: Strömgren photometry of Deneb for the fall of 1999. For clarity, the u filter values (black squares) were shifted down 0.75 magnitudes. Also, the b filter values (green triangles) were shifted up by 0.075 magnitudes. The v (red circles) and y values (blue triangles) are left unchanged. The photometry values shown are on the instrumental system. The light curves for the different filters all exhibit the same behavior. On this scale, the error bars for the measurements are comparable to the size of the data points.

4.5 Photometric Colors

As mentioned in Section 3.6, the photometric colors $u - b$ and $b - y$ were derived in order to gain insight into the variations over the Balmer Jump and effective temperature, respectively. A sample set of color curves (for the fall of 1999) is shown in Figure 4-12.

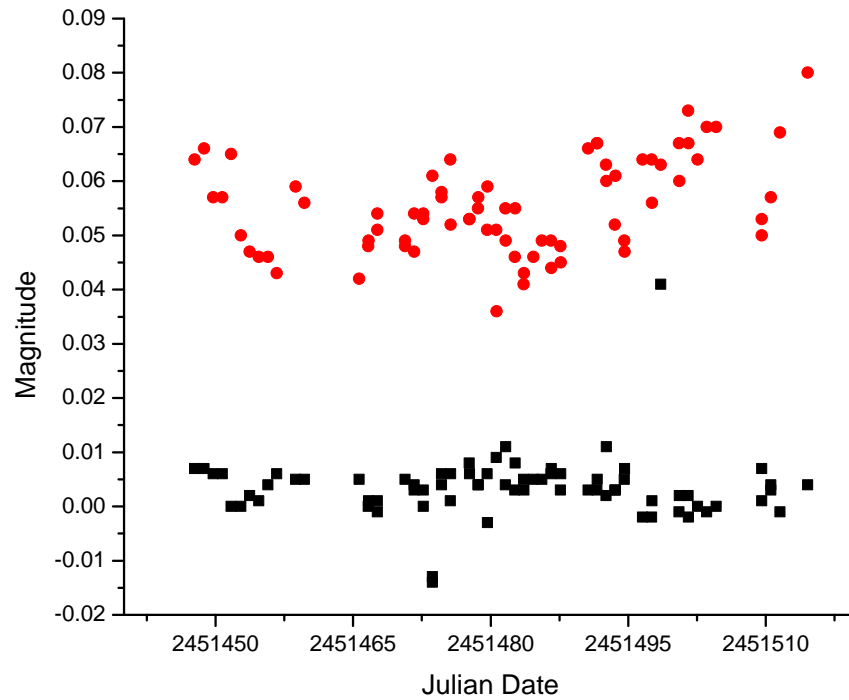


Figure 4-12: Strömrgren photometric colors of Deneb for the fall of 1999. The values have been shifted to show detail in the color curve. $u - b$ measurements are represented by red circles, and shifted down one magnitude to show detail. $b - y$ measurements are represented by black squares.

The $b - y$ colors do not show much variability, implying a minimal color change as Deneb pulsates. The $u - b$ colors exhibit much stronger variability. Thus, the color difference across the Balmer Jump is stronger when compared to that of the change in the effective temperature.

Upon inspection of the color curves, it is easily seen that there is no correlation between the $u - b$ and $b - y$ colors. This is shown in Figure 4-13. Some interesting features are present.

For the 1999 observing season, a trend seems to exist for Julian dates 2451460 through 2451520 for the $u - b$ color. Namely, it seems that $u - b$ has a tendency to increase in the positive direction throughout this time period. While there is some scatter, this same basic trend can be seen with the equivalent width of $H\alpha$ (Figure 4-6).

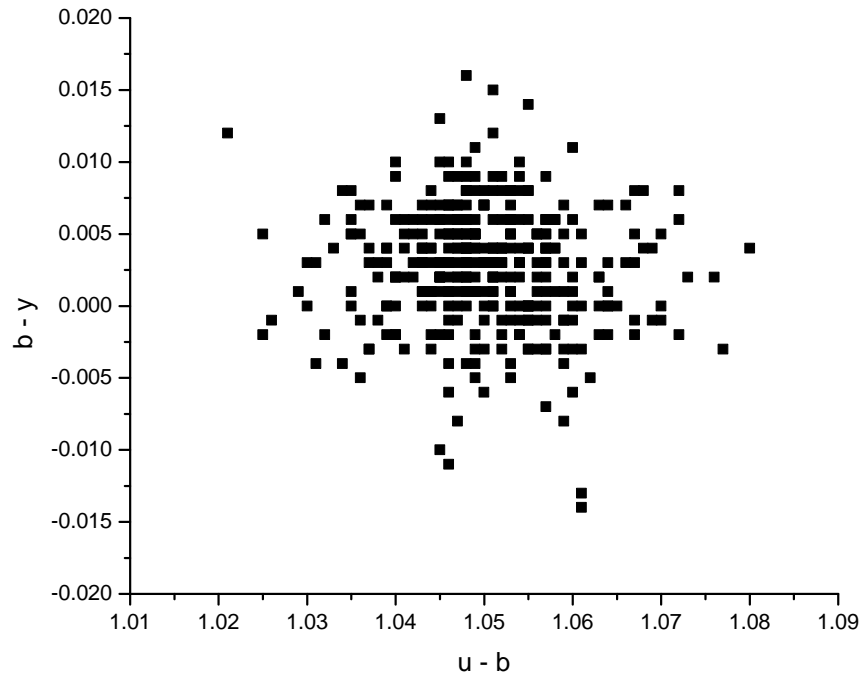


Figure 4-13: The $b - y$ colors plotted as a function of the $u - b$ colors. Clearly, there is no correlation between these two data sets. The effect that is seen where the data appear to break into horizontal lines is due to the fact that the data sampling does not have enough significant figures for a continuous distribution.

Chapter 5

Time-Series Analysis

This chapter outlines the time-series analysis that was performed on the data sets of the $H\alpha$ equivalent widths, radial velocities, and photometry (which are tabulated in Appendices B, C, and D, respectively). Time-series analysis of unequally spaced data points requires more than the basic techniques. A good review of most current time-series analysis tools can be found in Schwarzenberg-Czerny (1993).

5.1 The Scargle Periodogram

Scargle (1982) adapted the periodogram to deal with unevenly spaced data. This method produces a power spectrum which can be used to determine the periodicities present in the data. This method is often used for astronomical time-series analysis,

but it is not ideal for multiperiodic data.

As a test of the Scargle method, the algorithm was run on Paddock's data set, and the results were compared with those obtained on the same data set by Lucy (1976), who used a harmonic analysis, and Kaufer et al. (1997), who used the CLEAN algorithm (Roberts et al. 1987). (See Figures 5-1, 5-2, and 5-3).

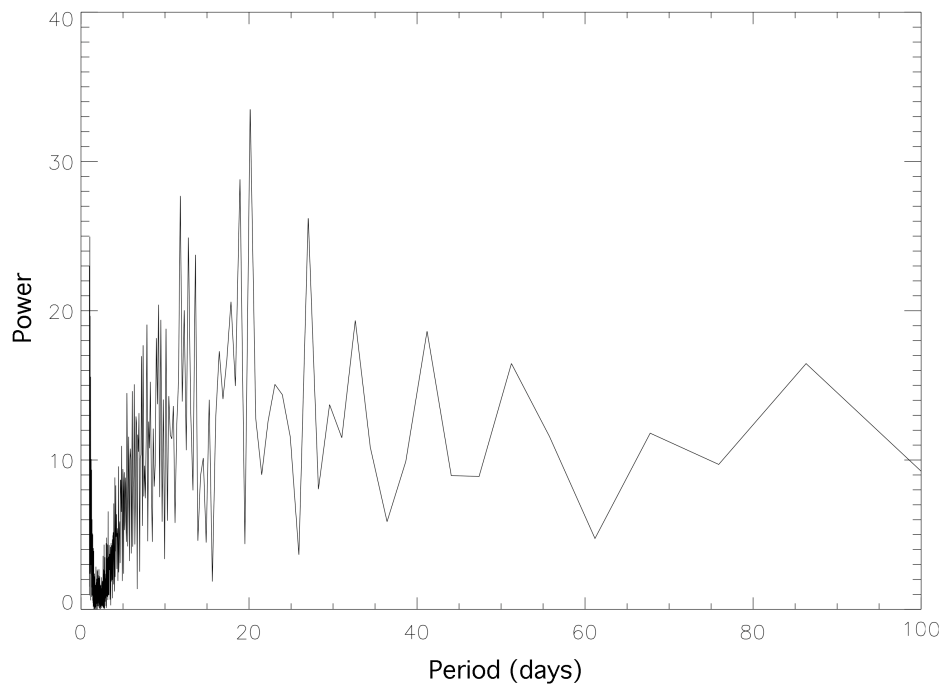


Figure 5-1: The derived Scargle periodogram for Paddock's data set. This window is shown for the period range of 0 to 100 days.

In Figure 5-1, there are several features to note. There is a lot of noise in the power spectrum, meaning that the seven shortest periods found by Lucy can not be reproduced. The 18.9 day period is most likely reproduced. There is a period of

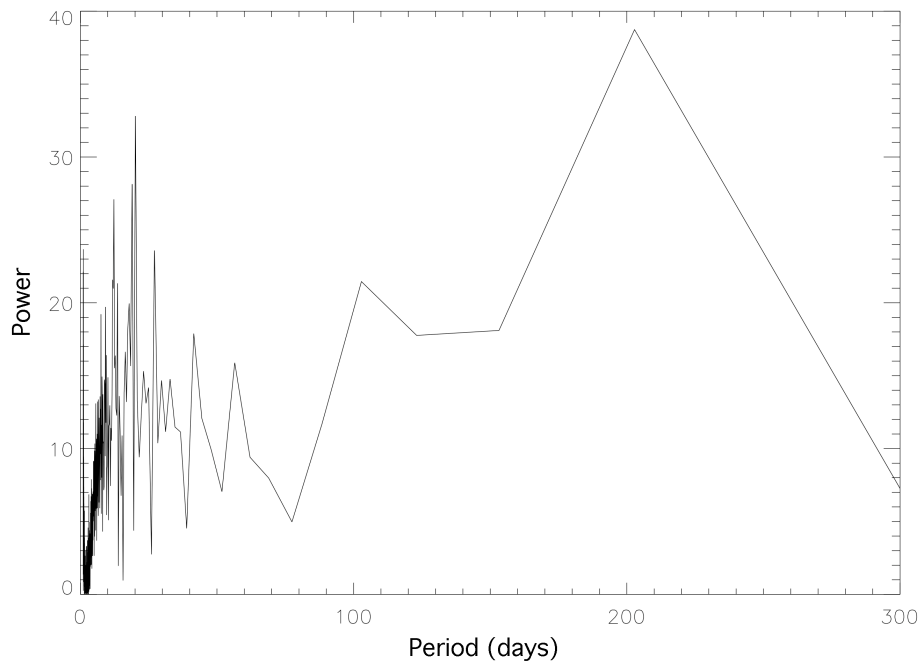


Figure 5-2: The derived Scargle periodogram for Paddock's data set. This window is shown for the period range of 0 to 300 days.

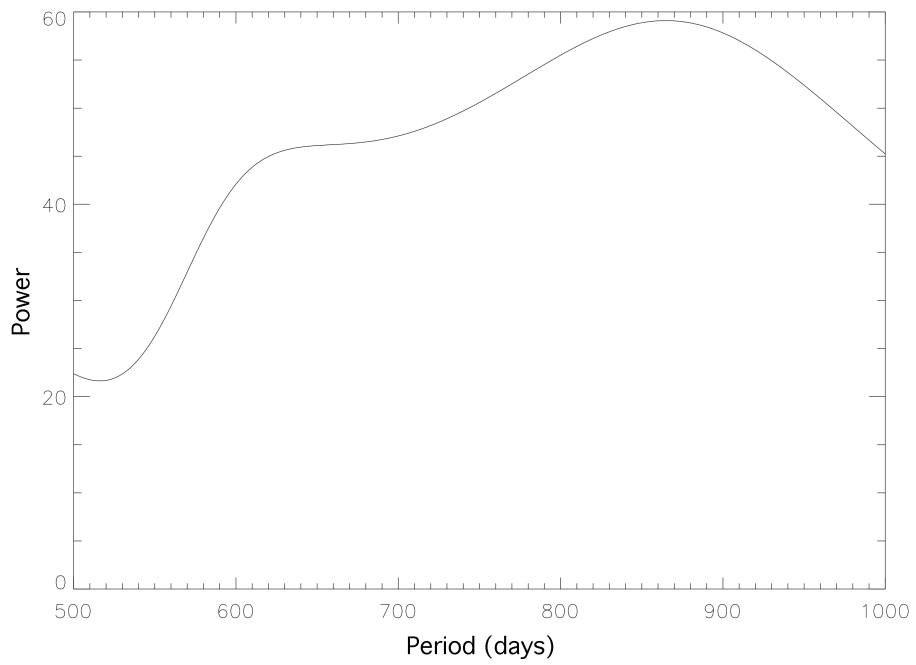


Figure 5-3: The derived Scargle periodogram for Paddock's data set. This window is shown for the period range of 500 to 1000 days.

approximately 20 days that was not found by Lucy. The 40.5 day period also seems to be reproduced, but the 49.1 day period was replaced with a 52 day period.

In Figure 5-2, it becomes apparent that the longest pulsational period of Deneb that Lucy found ($\simeq 100$ days) was reproduced, but another 200 day period is stronger in amplitude. In Figure 5-3, it is clear that the binary period was reproduced (if the binary period is accepted to be the 846.8 ± 9.3 day period, instead of the 776.4 ± 10.7 day period). This period is statistically significant, while many of the others are questionable.

The Scargle periodogram is known to be reliable only for the strongest periodicity in a data set. With so many periods either different or not reproduced, it was decided that a different approach to the time-series analysis should be taken. For reliable identification of multiple periods, the strongest oscillation should be subtracted from the data and the analysis repeated until all significant oscillations have been removed. This is the principle of the CLEAN algorithm.

5.2 The CLEAN algorithm

Roberts et al. (1987) developed another powerful tool for time-series analysis. This algorithm (called CLEAN) was designed for unevenly spaced data with multiple periodicities present. CLEAN produces a power spectrum that is more accurate for

multiperiodic data than any other current algorithm. It works on the same mathematical premise of Fourier inversion as the Scargle periodogram, but it deconvolutes the resultant power spectrum. Kaufer et al. (1996, 1997) used CLEAN to find evanescent periodicities in the $H\alpha$ behavior as well as the radial velocities of B and A type supergiants by analyzing the data by observing season.

Kaufer et al. (1997) re-examined the radial velocities obtained by Paddock (1935). The results were read from their Figure 7 using the program GraphClick¹ and are tabulated in Table 5.1. These data were analyzed in this project to determine the correct gain and number of iterations needed.

With a gain (in practice, only a fraction, g , of the highest peak of the power spectrum is subtracted, where g is the gain) of 0.5, and 1000 iterations, the CLEAN algorithm found all the major periods, but not the exceptionally weak amplitude frequencies claimed by Kaufer et al. (1997). The existence of frequencies exceptionally weak in strength can be questioned. It was determined that a gain of 0.1 and 100,000 iterations produced the same results as with the gain of 0.5 and 1000 iterations (see Figure 5-4). Results from the gain of 0.5 with 1000 iterations were produced much quicker than the results from a gain of 0.1 and 100,000 iterations. Thus, it was decided that the necessary parameters were a gain of 0.5 and 1000 iterations.

¹<http://www.arizona-software.ch/applications/graphclick/en/>

Table 5.1: Published radial velocity periodicities (Kaufer 1997), read from the original graph using GraphClick.

1931 Frequencies (d^{-1})	1931 Period (d)	1932 Frequencies (d^{-1})	1932 Period (d)
0.017	58.82	0.059	16.95
0.018	55.56	0.080	12.50
0.024	41.67	0.110	9.09
0.041	24.39		
0.051	19.61		
0.056	17.86		
0.065	15.38		
0.070	14.29		
0.080	12.50		
0.087	11.49		
0.092	10.87		
0.100	10.00		
0.106	9.43		
0.130	7.69		
0.136	7.35		
0.148	6.76		
0.152	6.58		

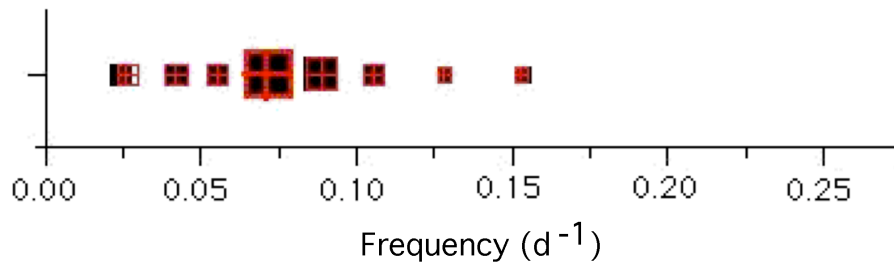


Figure 5-4: CLEANed frequencies of radial velocities published by Paddock for the 1931 observing season, where there were 100 observations. The frequencies represented as black boxes are from a gain of 0.5 with 1000 iterations, while the frequencies represented as red crossed boxes are from a gain of 0.1 and 100,000 iterations. The relative sizes of the data points correspond to the relative powers of the frequencies.

The H α net equivalent width was analyzed for periodic behavior using the CLEAN algorithm, and these results are shown in Figure 5-5. As seen in the results of Kaufer et al. (1996), the dominant period for each observing season changes. Thus, the evanescent periodicities present in this data were recovered. Noteworthy among these results is the approximately 40 day period ($f \simeq 0.025$) present in the first several observing seasons, as well as slowly drifting to smaller frequencies (longer periods). This is the period that appears to be present in the dynamical spectrum for 1997 (Figure 4-1).

In Figure 5-6, the frequencies derived for the radial velocities of the Si II doublet are shown. As the radial velocity curves are in agreement (see Figure 3-8), the periods present in both data sets can be assumed to be real. A few frequencies are only present in one data set. There are significantly more frequencies, as well as different frequencies, present in the radial velocity data than in the H α equivalent width data. This implies that the pulsations are not connected to the variability in the H α profile.

The photometry was also analyzed for periodic behavior. Observing seasons were taken to be the fall of one year and the following spring, as the FCAPT does not operate in the summer. While these observing seasons are different in nature as those from the Ritter data, these data sets provide a better sense of the periodicities

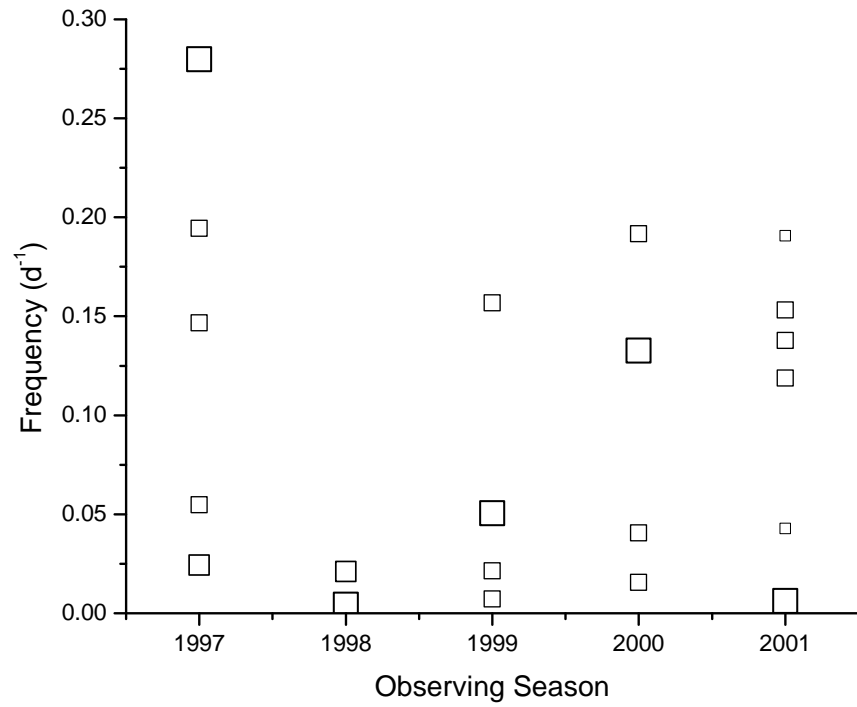


Figure 5-5: CLEANed frequencies of the net equivalent width of $H\alpha$ for each observing season are presented here. The relative sizes of the data points give the relative strengths of the oscillations at the found frequencies.

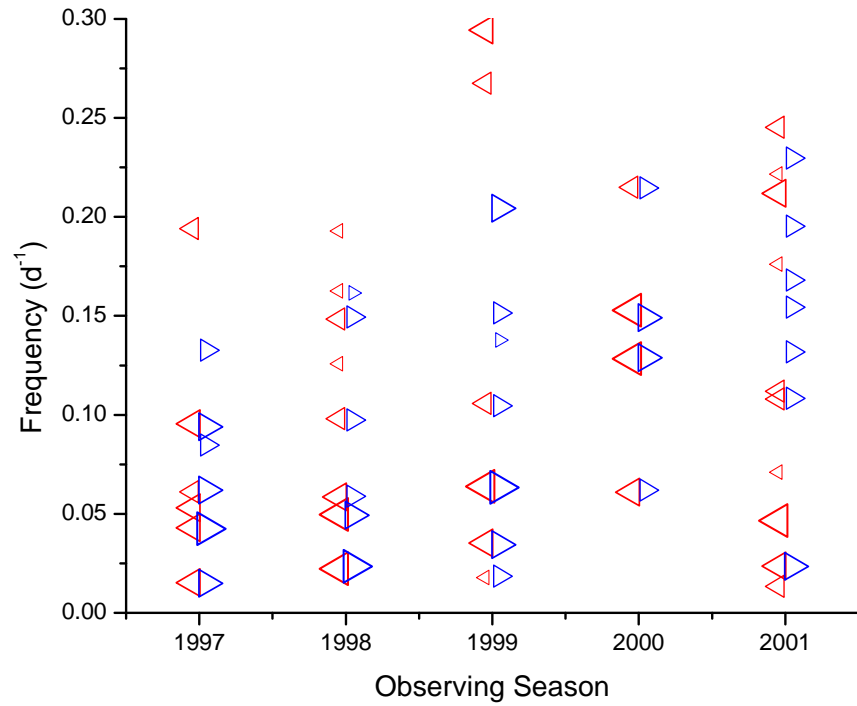


Figure 5-6: CLEANed frequencies of SiII Radial Velocities for each observing season are presented here. The relative sizes of the data points give the relative strengths of the oscillations at the found frequencies. The red triangles are for the velocities derived from Si II λ 6347, while the blue triangles are representative of the velocities from Si II λ 6371.

actually present in the FCAPT data; insight can be gained by then comparing multiple observing seasons of the photometry and radial velocity periodicities present. As seen with the light curves (Figure 4-11 and Appendix D), the variations in the photometry appear extremely periodic in nature. The most prominent feature is that the periods that appear in the light curves are found (periods $\sim 10 - 30$ days, $f \sim 0.025 - 0.10 d^{-1}$) with a second major period found with twice the period.

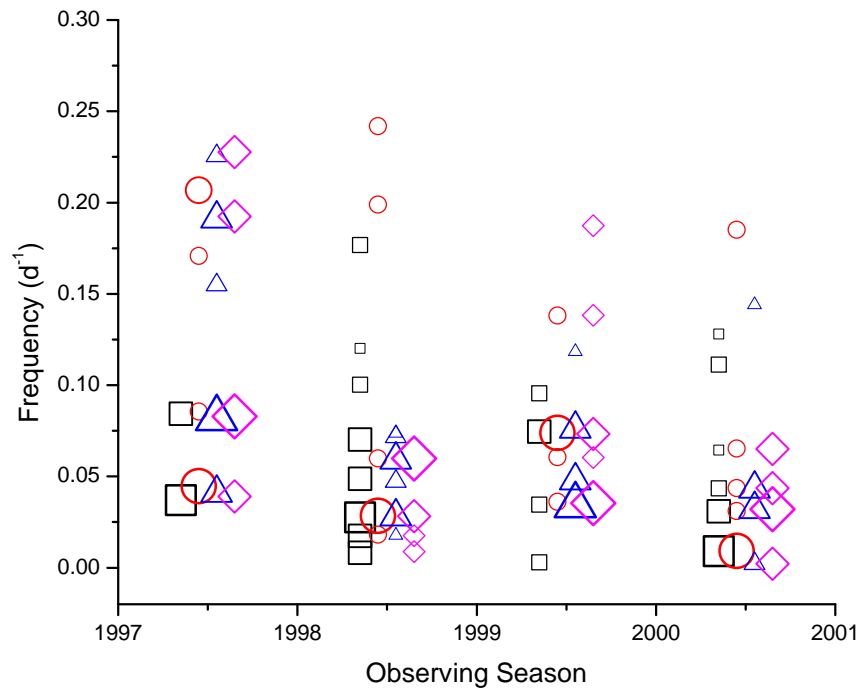


Figure 5-7: CLEANed frequencies of Strömgren photometry obtained each observing season are presented here. The relative sizes of the data points give the relative strengths of the oscillations at the found frequencies. Frequencies are represented as follows: u filter is black squares, v is red circles, b is blue triangles, and y is magenta diamonds.

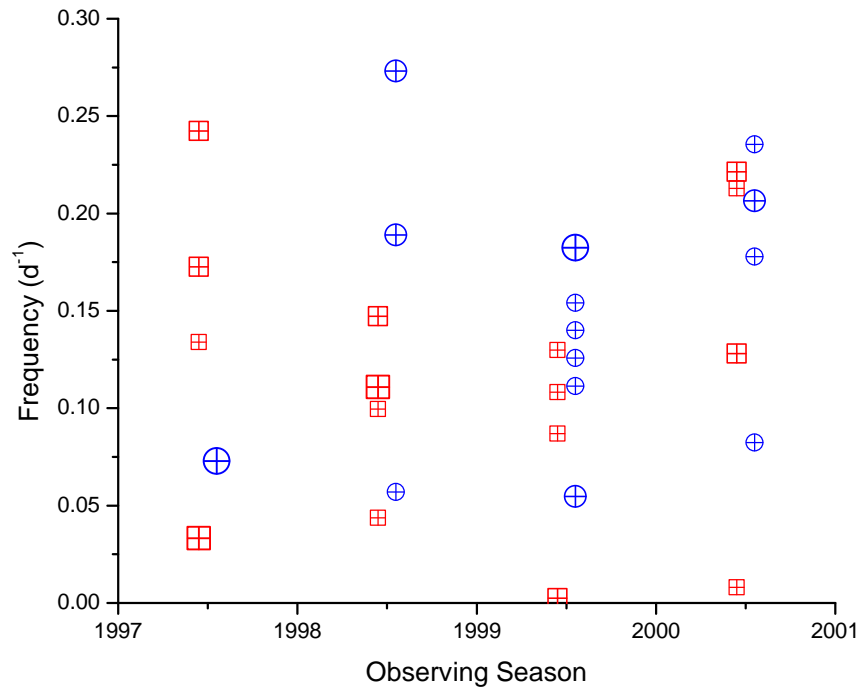


Figure 5-8: CLEANed frequencies of Strömgren photometric colors obtained each observing season are presented here. The relative sizes of the data points give the relative strengths of the oscillations at the found frequencies. $u - b$ is represented by red crossed squares, while $b - y$ is represented as blue crossed circles.

In the same fashion, the photometric colors were analyzed. The periods found for both color sets of these data sets are different, as there was no correlation between the colors $u - b$ and $b - y$ (Figure 4-13). Usually, there are far fewer frequencies for $b - y$ than $u - b$. As the $b - y$ color did not show as much variability as the $u - b$ color, this should be expected. A similar period to the 40 day period in the $H\alpha$ spectroscopic behavior is found in the fall 1997/ spring 1998 observing season.

Chapter 6

Discussion and Conclusions

6.1 Binarity

When the Scargle periodogram was applied to Paddock's data (Figure 5-3), it easily recovered the possible binary period proposed by Lucy (1976). Therefore, it was used to search for this same period in the Ritter radial velocities. Since this is the first data set of comparable size to Paddock's (1935) data set, it is important to see if the variations that were discovered by Lucy (1976) were actually from binary motion.

The resulting periodogram from the Si II radial velocities (Figure 6-1) showed a relative minimum in the region surrounding the possible binary periods (846.8 ± 9.3

days or 776.4 ± 10.7 days) as proposed by Lucy (1976). The periodogram for the radial velocities does not ever escalate to near the power observed for this motion in the values from Paddock. This motion in the radial velocities should not be ascribed to a binary orbit, as that motion would still be present in the radial velocities. Perhaps the variations in the original data set could be attributed to a mass-loss episode which left a large density clump in the wind. This could also be a longer pulsational period in the data. The claim that this binary period found in the measurements made by Parthasarathy and Lambert (1987) should be questioned due to the lack of data points and since time-series analysis was not performed.

6.2 $H\alpha$

The continuum-normalized spectra were overplotted by means of the IRAF task *specplot* in the *onedspec* package. This would allow a quick view of all spectra obtained. This is shown for the spectra obtained between March 26 and December 22, 2001 in Figure 6-2. From this plot, a “minimal activity” phase is hard to define, as is a “maximum activity” phase for the spectra.

As there is the possibility of a correlation between the photometric color $u - b$ and the net equivalent width, it can be seen that the $H\alpha$ profile samples the photosphere as well as the circumstellar environment, as the physics is the same for the Balmer

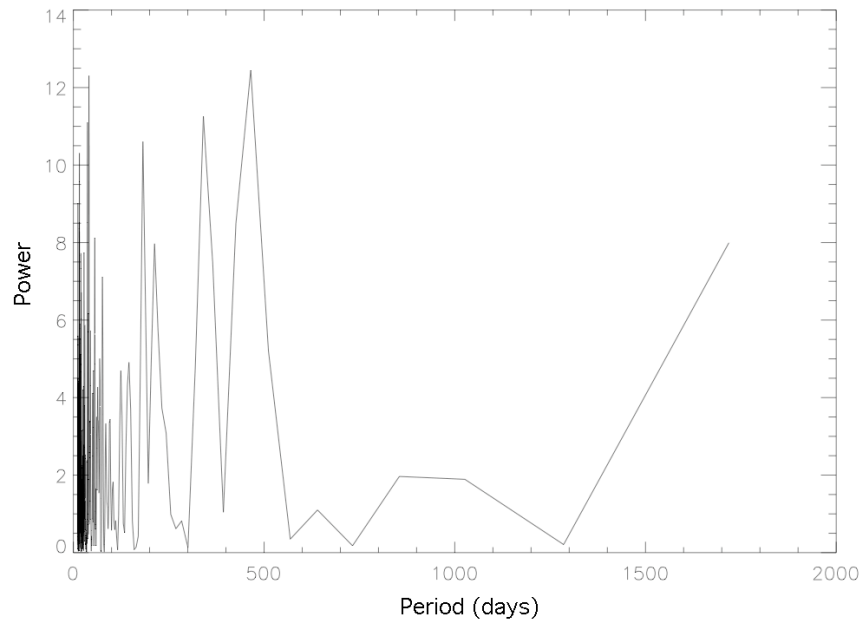


Figure 6-1: The Scargle periodogram as derived from the radial velocities of Si II ($\lambda = 6371 \text{ \AA}$). The periodogram from Paddock's data was at a maximum (with a power $\simeq 59$) for the binary period of $\simeq 850$ days, where the power is at a near minimum for the binary periods proposed by Lucy (1976).

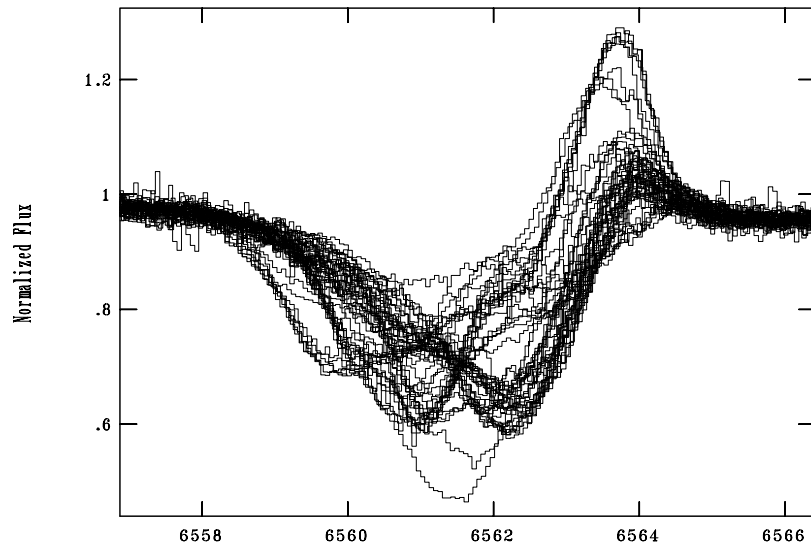


Figure 6-2: The 66 nights of spectroscopic data from 2001 were overplotted by means of the IRAF task *specplot*. There is a wide range of values for the emission component, including a point where it almost vanished. The absorption component usually has a blue-shifted “absorption event” superimposed.

jump as well as for $H\alpha$. The emission component as well as the secondary absorption component are circumstellar in nature. Thus, a star such as η Leonis (an A0Ib supergiant, which does not show the effects of mass-loss in $H\alpha$, but has a slightly higher temperature and gravity) has the potential to be used to find the stellar component of $H\alpha$ in the spectrum of Deneb. It can also be stated that $H\alpha$ does not exhibit the behavior seen in the discrete absorption components, as seen in HD 92207 (Kaufer et al. 1996).

From the dynamical spectra and the time-series analysis of the equivalent width, it can be seen that the periodic behavior is evanescent in nature, as reported by Kaufer et al. (1996). The primary frequency does not remain static between different years of observations. Rather, the dominant period is seen to change with each observing season. The found frequencies and corresponding periods of the net equivalent width of $H\alpha$ are tabulated in Table 6.1. The prominent 40 day period that was seen in the dynamical spectrum of 1997 was found with CLEAN (a 40.6 day period). Some of the found periods are most likely sampling effects, such as a 232.6 day period which would be very similar to the length of the observing season of Deneb, or the 3.6 day period which would be close to the average time between observations throughout an observing season.

The emission component is quite variable. As seen in Figure 6-2, the emission

Table 6.1: Frequencies and Corresponding Periods of the net equivalent width of H α

Observing Season	Frequency	Period	Relative Strength	Comments
1997	0.025	40.6	Strong	
	0.055	18.2	Moderate	
	0.147	6.8	Weak	
	0.195	5.1	Moderate	
	0.280	3.6	Strong	Sampling Effect?
1998	0.004	232.6	Strong	Sampling Effect?
	0.021	47.6	Moderate	
1999	0.007	142.9	Moderate	Sampling Effect?
	0.021	46.7	Moderate	
	0.051	19.7	Strong	
	0.157	6.4	Moderate	
2000	0.015	65.4	Moderate	
	0.045	22.1	Moderate	
	0.131	7.6	Strong	
	0.191	5.2	Moderate	
2001	0.006	163.9	Strong	Sampling Effect?
	0.043	23.5	Strong	
	0.119	8.4	Weak	
	0.137	7.3	Weak	
	0.153	6.5	Moderate	
	0.191	5.2	Moderate	

component varied from almost non-existent to approximately half as strong as the absorption component. With such a strong variability, the wind momentum–luminosity relationship should be re-examined with respect to this sort of variability, especially since the Strömgren filtered photometry does not vary in the same manner as the equivalent width of $H\alpha$.

6.3 Pulsations

The time-series analysis using CLEAN of the radial velocities and Strömgren filtered photometry yielded several different frequencies. As the binarity was not confirmed (no major period was found with the Scargle periodogram, the period found by Lucy (1976) was not recovered, and no periods were found to persist in all observing seasons), these frequencies can be attributed to pulsations of the stellar atmosphere. Pulsations can be either radial or non-radial in nature. It could be said that the frequencies found in both the radial velocities and in the photometry are attributed to radial pulsations. Phase relations would be needed to fully identify this. Other frequencies could be non-radial pulsations as temperature variations do occur locally for non-radial pulsations. The frequencies and corresponding periods found with CLEAN are tabulated in Table 6.2. These values were only the values found for all sets of data (both radial velocity data sets or all filters with the photometry) and

were then averaged to find the “most likely” frequency. This removed most effects of sampling.

Some of the found periods show the signs of being radial pulsations. Specifically, for the photometry the following periods are also found in the radial velocities: 24.8 days (Fall 1997–Spring 1998), 56.6 days (Fall 1998–Spring 1999), 16.1 days (Fall 1998–Spring 1999), and 28.6 days (Fall 1998–Spring 1999). These can be seen in the observing seasons surrounding these seasons. For example, the 24.8 day period is seen in the radial velocities as a 24.4 day period during the 1997 observing season. The 56.6 day period is seen as a 55.2 day period in the 1999 observing season. The 16.1 day period is seen as a 17.0 day period in 1998 and a 15.7 day period in 1999. Finally, the 28.6 day period can be seen as a 28.7 day period in 1999. The other observed periods are most likely due to non-radial pulsations of the atmosphere.

Such close correlations could show direct evidence of radial pulsations in the atmosphere of Deneb with additional phase information. This additional analysis has not yet been performed. The indication that the periods are evanescent in nature, and possibly change slowly (e.g., the 16.1 day period in the photometry, with the corresponding radial velocity periods being 17.0 and 15.7 days) suggest a complicated behavior in the atmosphere of the star. Further work on the variability should be undertaken, possibly using mathematical tools such as wavelets, in order to

Table 6.2: Average Frequencies and Corresponding Periods of the Strömngren photometry and the Radial Velocities.

Observing Season	Frequency (d^{-1})	Period (days)	Relative Strength
Photometry			
Fall 1997 and Spring 1998	0.040	24.8	Strong
	0.084	12.0	Strong
Fall 1998 and Spring 1999	0.018	56.6	Strong
	0.056	17.8	Moderate
	0.062	16.1	Strong
Fall 1999 and Spring 2000	0.035	28.6	Moderate
	0.074	13.4	Strong
Fall 2000 and Spring 2001	0.006	178.6	Moderate
	0.031	31.8	Strong
	0.043	23.0	Strong
Radial Velocities			
1997	0.015	66.2	Strong
	0.043	23.4	Strong
	0.062	16.2	Moderate
	0.095	10.6	Strong
1998	0.023	43.8	Strong
	0.050	20.2	Strong
	0.059	17.0	Moderate
	0.098	10.2	Moderate
1999	0.149	6.7	Moderate
	0.018	55.2	Moderate
	0.035	28.7	Strong
	0.064	15.7	Strong
2000	0.105	9.5	Moderate
	0.062	16.3	Moderate
	0.129	7.8	Strong
	0.151	6.6	Strong
2001	0.215	4.7	Moderate
	0.024	42.5	Strong
	0.110	9.1	Moderate

better understand the mechanisms and the physics that are driving these variations in the atmosphere.

6.4 Connections between pulsations and the wind?

When the periods are compared for the radial velocities or photometry and those of the net equivalent width of $H\alpha$ (assumed to sample the wind), there is no connection seen, as the periods are not the same. The first exception is during the 2000 observing season when the net equivalent width of $H\alpha$ exhibited a 7.6 day period while the radial velocities showed a 7.8 day period. Similarly, in the 2001 observing season, $H\alpha$ showed a 23.5 day period while the photometry exhibited a 20 day period. However, as the periods are evanescent in nature, it can not be assumed that this implies a connection, and is probably coincidence only. Further evidence is shown in Figure 6-3.

6.5 Conclusions

This thesis has examined a five-year campaign on the spectral and photometric variability of Deneb, the prototype A-type supergiant. There was evidence for evanescent periodicities in the equivalent width of $H\alpha$, as well as in pulsations (both

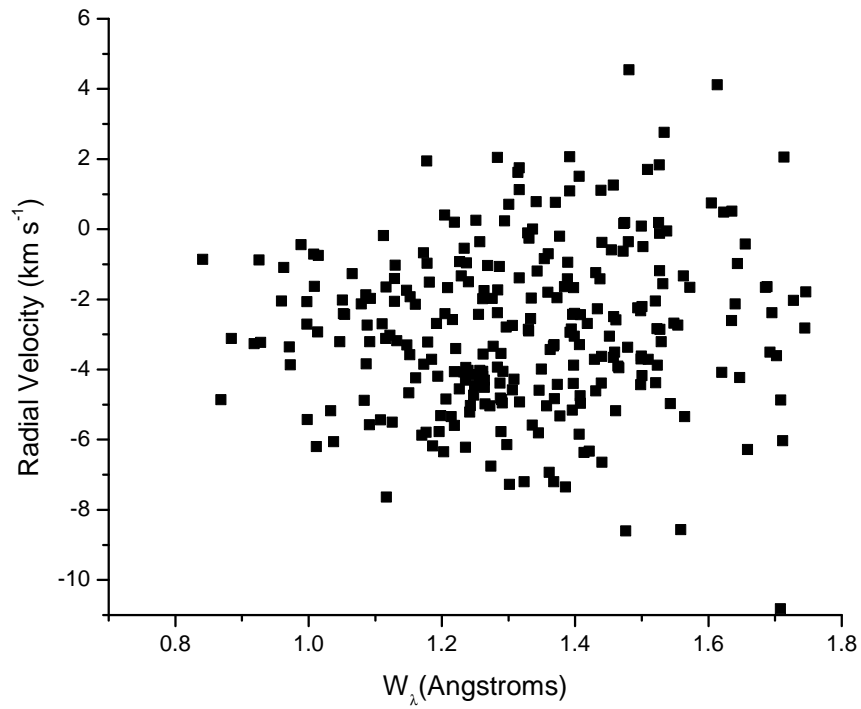


Figure 6-3: The radial velocity is plotted against the net equivalent width of H α . There is no correlation found, further supporting the lack of a connection between the wind and the pulsations. If there was a connection, a time lag is expected. However there should be a trend in this data, which is not present.

in radial velocities and in the photometry), which is consistent with the work of Kaufer et al. (1996, 1997). No evidence of DAC behavior was found in the H α profile, which is sensitive to the wind. This has been the first examination of photometric variability of Deneb using a filtered system, and the first survey since that of Fath (1935).

Further work should be pursued to examine the phase relations of the photometry and radial velocities, to reveal the radial pulsations present in the atmosphere. If several more years of data are examined in detail, a pulsation mechanism may be revealed. Further work to model the H α profile needs to be employed, as no current work has been able to model the profile. Then, models should be made to explain the variability observed (dynamical spectra). Then a detailed analysis of the momentum flow ($\dot{M}v_\infty$) using the H α profile should be performed to search for the variability in this product, which is the foundation of the wind momentum–luminosity relationship.

References

- Abt, H.A. 1957, "The Variability of Supergiants." ApJ **126**: 138.
- Adelman, S.J. 1992, "Photoelectric observations of some bright Be stars." PASP **104**: 392.
- Adelman, S.J. and Meadows, S.A. 2002, "*uvby* photometry of the CP stars HR 149, HD 32966, HD 171782, and HR 7911." A&A **390**: 1023.
- Adelman, S.J. 2001, "Differential *uvby* photometry of 13 Mon (A0Ib)." Baltic Astronomy **10**: 385.
- Adelman, S.J. and B. Alabayrak. 1997, "On the variability of early A-type supergiants." IBVS **4541**: 1.
- Albayrak, B. 1999, "A spectral atlas of Deneb (A2 Iae)." PASP **111**: 917.
- Albayrak, B. 2000, "A spectral atlas of Deneb (A2 Iae)." A&A **364**: 237.

- Albayrak, B. et al. 2003, “A spectroscopic atlas of Deneb (A2 Iae) $\lambda\lambda 3826 - 5212$.”
A&A **400**: 1043.
- Aufdenberg, J.P. et al. 2002, “The spectral energy distribution and mass-loss rate
of the A-type supergiant Deneb.” ApJ **570**: 344.
- Aufdenberg, J.P. 2006, private communication.
- Cranmer, S. R. and S. P. Owocki. 1996, “Hydrodynamical simulations of corotating
interaction regions and discrete absorption components in rotating O-star
winds.” ApJ **462**: 469.
- Dessart, L. 2004, “3D hydrodynamical simulations of corotating interaction regions
in rotating line-driven stellar winds.” A&A **423**: 693.
- Dukes, R.J. et al. 1992 in *ASP Conference Series* **28**: 21. “Report from the Four
College Consortium.”
- Fath, E. 1935, “Pulsation in stellar atmospheres.” Lick Obs. Bull. **17**: 115.
- Gies, D. R. and A. Kullavanijaya. 1988, “The line profile variations of epsilon
Persei. I. Evidence for multimode nonradial pulsations.” ApJ **326**: 813.
- Hensberge, H., Lamers, H.J.G.L.M., de Loore, C. et al. 1982, “Mass loss from α
Cyg (A2Ia) derived from the profiles of low excitation Fe II lines.” A&A **106**:

137.

Jachek, C. and M. Jachek, *The Classification of Stars*, 1990, Cambridge University Press.

Kaufer, A. et al. 1996, “Long term spectroscopic monitoring of BA-type supergiants. I. H alpha line profile variability.” *A&A* **305**: 887.

Kaufer, A. et al. 1997, “Long term spectroscopic monitoring of BA-type supergiants. III. Variability of photospheric lines.” *A&A* **320**: 273.

Kudritzki, R.P. et al. 1999a, “The wind momentum–luminosity relationship in galactic A- and B-supergiants.” *A&A* **350**: 970.

Kudritzki, R.P. et al. 1999b, “The wind momentum–luminosity relationship of blue supergiants.” in *IAU Colloquium* 169: 405.

Kunasz, P. B. and N. D. Morrison. 1982, “Mass loss in alpha Cygni: Synthetic H-alpha profiles.” *ApJ* **263**: 226.

Lamers, H. J. G. L. M. and J. E. Cassinelli. *Introduction to Stellar Winds*. 1999, Cambridge University Press.

Lucy, L. B. 1976, “An analysis of the variable radial velocity of alpha Cygni.” *ApJ* **206**: 499.

- Massa, D. et al. 1995, "The IUE Mega Campaign: Wind variability and rotation in early-type stars." ApJ **452**: L53.
- Morrison, N.D. and C.L. Mulliss. 1997, "Recent results from high-resolution H alpha spectroscopic monitoring of alpha Cygni." BAAS **191**: 125.04.
- Mulliss, C.L., M.S. Thesis. 1996.
- Paddock, G. 1935, "Spectroscopic observations of alpha Cygni." Lick Obs. Bull. **17**: 99.
- Parthasarathy, M. and D. Lambert. 1987, "alpha Cygni as a radial velocity variable." J. Astrophys. Astr. **8**: 51.
- Perryman, M.A.C. et al. 1997, "Double star data in the HIPPARCOS catalogue." A&A **323**: L49.
- Roberts, D.H., J. Lehar, and J.W. Dreher. 1987, "Time series analysis with CLEAN. I. Derivation of a spectrum." AJ **93**: 968.
- Scargle, J.D. 1982, "Studies in astronomical time series analysis. II. Statistical aspects of spectral analysis of unevenly spaced data." ApJ **263**: 835.
- Schwarzenberg-Czerny, A. in *5th ESO / ST-ECF Data Analysis Workshop, April 26-27, 1993*. Eds. Grosbol, P. and R. de Ruijscher. "Analysis of astronomical

time series.”

Verdugo et al. 2003, “Search for magnetic fields in A-type supergiants.” in *212*¹²

IAU Symposium.

Appendix A

Ritter Observations of Deneb

Table A.1: 1997 Ritter Observations of Deneb

Date (YYMMDD)	Exposure Time	ADU	Observer(s)
970408	900	606	NDM,DCK
970520	600	925	DCK
970522	600	795	NDM,DCK
970523	600	626	KSB,AM,CLM
970605	900	655	NDM,HLR,DCK
970610	600	1154	NDM,HLR,DCK
970615	900	1841	NDM
970624	900	1403	NDM
970627	900	1308	KSB
970628	1200	655	CLM
970629	900	1519	NDM

Date (YYMMDD)	Exposure Time	ADU	Observer(s)
970702	900	1689	CLM
970703	900	1997	NDM
970706	900	232	KSB
970711	600	883	KSB,AM
970714	600	879	CLM,AM
970716	600	914	CLM,AM
970720	300	842	NDM,AM
970725	300	263	AM
970728	600	4067	TLS
970731	600	2333	TLS
970801	600	118	DCK
970803	300	1836	AM
970805	300	1466	DCK
970806	300	531	AM
970808	600	529	KSB
970809	600	1418	CLM
970810	600	78	AM
970810	600	3394	AM
970814	300	320	AM
970824	300	1169	AM
970828	420	815	AM
970829	600	2459	KSB
970902	300	1156	NDM
970904	300	373	TLS,CLM
970905	300	1524	NDM,HLR
970913	300	2096	CLM

Date (YYMMDD)	Exposure Time	ADU	Observer(s)
970916	600	147	KSB
970918	300	1059	TLS,AM
970919	300	1864	NDM,HLR
970921	300	2036	AM,CLM
970922	300	1572	AM,CLM
970924	600	573	NDM
970925	600	2804	TLS,AM
970926	600	1856	HLR,NDM,CLM
970927	300	2584	AM,CLM
970928	300	903	CLM
971002	300	1702	TLS
971003	300	1202	NDM,HLR
971004	300	1422	CLM
971006	300	1198	AM,CLM
971007	300	1352	KSB,CLM
971008	300	369	NDM
971009	600	3541	AM
971010	600	525	CLM,AM
971011	600	2813	CLM
971015	300	1897	NDM,HLR
971018	300	228	CLM
971019	300	1526	AM,CLM
971020	1200	327	AM
971021	300	1398	KSB,CLM
971022	300	749	NDM,HLR,DCK
971029	300	976	NDM,HLR
971031	300	397	NDM
971109	600	2487	CLM
971113	600	2577	AM,TLS
971118	300	1412	AM,CLM
971125	600	3007	KSB
971216	600	2144	KSB,CLM
971217	300	1713	NDM,HLR,WJF
971218	300	1462	TLS,AM

Table A.2: 1998 Ritter Observations of Deneb

Date (YYMMDD)	Exposure Time	ADU	Observer(s)
980517	150	177	CLM,PAO
980522	300	122	KSB
980608	300	1845	NDM
980705	300	1018	NDM
980706	600	1348	NDM
980710	600	375	KSB
980712	600	173	CLM
980727	300	199	NDM
980727	300	166	NDM
980727	300	204	NDM
980727	300	512	NDM
980802	300	395	CLM,NDM
980802	60	125	CLM,NDM
980802	60	210	CLM,NDM
980802	60	215	CLM,NDM
980802	60	147	CLM,NDM
980802	60	153	CLM,NDM
980802	60	184	CLM,NDM
980802	60	219	CLM,NDM
980803	600	743	NDM
980813	600	751	TLS
980819	900	1506	DCK
980820	600	1169	TLS
980820	600	963	TLS
980826	900	1714	DCK
980827	600	696	TLS
980830	300	144	CLM
980901	300	305	NDM
980901	300	248	NDM
980901	60	101	NDM
980901	60	114	NDM
980901	60	114	NDM
980905	300	811	NDM,PAO
980906	300	461	NDM
980909	300	261	DCK,CLM
980910	300	184	TS
980911	600	443	CLM
980912	600	1387	HR,CLM
980914	600	1785	NDM,WJF

Date (YYMMDD)	Exposure Time	ADU	Observer(s)
980919	600	2833	CLM,HR
980921	600	345	NDM
980923	600	624	CLM
980924	600	481	TS
980927	600	439	CLM
980929	600	1517	KSB,TS
981002	600	518	CLM
981010	600	507	CLM
981011	600	1024	CLM
981012	300	377	NDM
981012	300	419	NDM
981016	600	72	CLM
981016	600	232	CLM
981019	300	107	NDM,CLM
981019	300	140	NDM,CLM
981019	300	142	NDM,CLM
981020	300	518	NDM,CLM
981023	600	347	CLM
981024	300	672	NDM,PAO
981025	600	1202	CLM
981027	600	842	KSB
981029	300	219	TLS
981029	600	782	TLS
981104	600	98	DCK,CLM
981104	600	78	DCK,CLM
981118	300	138	DCK,CLM
981118	900	360	DCK,CLM
981120	900	160	CLM
981120	900	79	CLM
981124	1200	899	KSB
981127	300	252	NDM
981127	300	347	NDM
981127	300	419	NDM
981127	300	380	NDM
981128	300	461	NDM
981129	600	684	CLM
981202	300	450	DCK,CLM
981210	300	452	NDM
981212	300	430	NDM,PAO
981213	600	795	CLM
981215	300	96	KSB,NDM
981215	300	164	KSB,NDM
981216	300	404	NDM,CLM

Table A.3: 1999 Ritter Observations of Deneb

Date (YYMMDD)	Exposure Time	ADU	Observer(s)
990607	300	681	NDM
990609	300	560	DCK,AM
990615	300	402	WJF,NDM
990619	600	683	NDM,DH
990621	300	531	NDM
990626	300	452	NDM
990705	300	622	NDM
990706	300	560	WJF
990707	300	415	WJF
990708	600	861	AM,NDM
990710	300	468	HR,NDM
990711	300	437	NDM,DH
990712	300	633	WJF
990717	300	252	HR,NDM
990731	600	545	NDM
990802	300	296	WJF
990803	600	694	WJF
990809	300	648	NDM
990821	300	681	NDM
990829	300	202	NDM
990830	600	890	NDM,DCK
990831	300	1051	DCK
990902	600	859	DCK,AM
990903	300	583	KSB
990905	300	485	NDM
990914	600	752	DCK
990915	600	1029	KSB,WJF
990916	600	875	DCK,AM
990923	300	446	DCK,AM
990924	300	298	KSB,WJF
990926	300	533	AM

Date (YYMMDD)	Exposure Time	ADU	Observer(s)
991006	300	380	KSB,WJF
991007	300	448	DCK,AM
991008	300	261	KSB,WJF
991012	600	743	DCK
991015	300	296	KSB,JPW,AM
991016	300	292	AM
991020	300	382	KSB
991021	600	952	DCK,AM
991022	300	333	KSB
991025	300	369	AM,DCK
991027	300	206	KSB,WJF
991028	300	349	DCK,JPW,AM
991105	600	663	KSB,AM
991106	300	294	AM
991107	300	435	AM
991108	300	386	AM,DCK
991109	300	382	AM
991110	300	413	KSB,WJF
991115	300	406	AM
991116	300	432	AM
991117	300	377	KSB,AM,WJF
991118	300	342	KSB,AM
991119	600	290	KSB,WJF
991130	300	496	AM
991208	300	261	KSB
991212	300	380	DCK,AM

Table A.4: 2000 Ritter Observations of Deneb

Date (YYYYMMDD)	Exposure Time	ADU	Observer(s)
20000810	300	170	DCK,JPW
20000810	600	434	DCK,JPW
20000821	300	286	AM,DCK
20000903	600	453	NDM
20000905	300	263	AM,DCK
20000905	300	204	AM,DCK
20000907	300	196	WJF
20000913	300	228	KSB,AM
20000914	300	252	WJF,AM
20000916	300	260	NDM,AM
20000917	300	260	NDM
20000918	300	353	AM
20000919	300	212	AM,WJF
20000920	300	163	KSB,AM
20000922	300	128	KSB
20000922	300	160	KSB
20000926	600	301	AM
20000927	300	237	KSB,AM
20000929	300	301	NDM
20000930	300	291	NDM
20001001	900	213	NDM
20001002	600	550	DCK
20001007	600	506	NDM
20001008	300	353	NDM
20001015	600	574	NDM
20001019	600	977	WJF,DCK
20001020	300	312	KSB
20001021	300	239	NDM,AM
20001023	600	704	DCK
20001028	300	370	NDM
20001029	600	715	AM,DCK
20001030	600	372	DCK
20001101	600	585	KSB
20001105	300	426	NDM,DCK
20001106	300	526	DCK
20001116	300	244	WJF
20001123	300	229	NDM
20001125	300	199	NDM
20001204	300	164	AM
20001222	600	138	AM

Table A.5: 2001 Ritter Observations of Deneb

Date (YYYYMMDD)	Exposure Time	ADU	Observer(s)
20010110	300	124	NDM,AM,DCK
20010111	600	71	AM,DCK
20010326	900	458	NDM,DCK
20010328	900	456	KSB,JPW,JT,AM
20010402	300	216	NDM
20010429	300	372	NDM,JT,DCK
20010430	300	142	NDM,JT,DCK
20010430	600	149	NDM,JT,DCK
20010504	600	452	AM
20010509	900	617	KSB,AM
20010510	600	390	WJF,DCK
20010609	300	362	NDM,JT
20010614	600	152	DCK
20010619	300	353	NDM
20010626	300	251	NDM,JT,AG
20010630	600	427	NDM
20010702	600	455	NDM,JT,AG
20010705	300	268	NDM
20010706	300	232	NDM
20010706	300	273	NDM
20010710	300	183	JPW
20010710	500	248	JPW
20010712	300	197	JPW
20010714	300	229	NDM,JT
20010715	300	305	JT,NDM
20010725	600	86	WJF
20010725	600	174	WJF
20010814	300	153	JPW
20010830	300	315	JPW
20010902	300	253	JT,JPW
20010903	300	192	JT,DCK
20010905	300	283	NDM,PAS,AG,LAS,DS,AM
20010905	300	323	NDM,PAS,AG,LAS,DS,AM
20010905	300	258	NDM,PAS,AG,LAS,DS,AM
20010906	300	297	JPW
20010907	300	315	NDM
20010911	300	325	JPW
20010912	300	337	NDM
20010913	300	447	JPW
20010915	600	682	AM

Date (YYYYMMDD)	Exposure Time	ADU	Observer(s)
20010916	300	387	JPW,AM
20010917	300	498	JT,DCK
20010921	300	371	NDM
20010928	441	457	NDM,LAS,PAS,AG,DS
20010930	300	425	JPW
20011001	300	535	JT
20011002	300	476	JPW
20011003	300	342	NDM,LAS,PAS,AG
20011004	300	409	JPW
20011008	300	155	JT
20011008	300	520	JT
20011010	600	752	LAS,PAS,AG,NDM
20011018	300	543	JPW
20011020	300	827	JPW
20011020	300	373	JPW
20011029	300	443	JT,JPW
20011030	300	374	JPW
20011101	300	508	JPW
20011103	300	308	AM
20011104	300	305	AM
20011105	300	295	JT
20011106	300	312	JPW
20011107	300	254	NDM,AG,LAS,PAS
20011110	300	181	AM
20011111	300	398	JPW,AM
20011112	300	373	NDM
20011112	300	287	NDM
20011113	300	468	JPW
20011122	300	508	NDM,AM
20011210	300	383	JT
20011219	300	397	NDM
20011221	300	265	NDM,JPW
20011222	300	307	NDM,JPW

Appendix B

H α Measurements

Table B.1: H α Equivalent Width Measurements

Julian Date	W_λ (net)	W_λ (emission)	W_λ (absorption)
2450546.91051251	1.461	-0.285	1.746
2450588.86303180	1.240	-0.206	1.446
2450590.84395394	1.264	-0.214	1.478
2450591.85544913	1.284	-0.178	1.462
2450604.79591576	1.214	-0.202	1.416
2450609.87109713	1.261	-0.197	1.458
2450614.84276841	1.374	-0.217	1.591
2450623.77241360	1.129	-0.271	1.400
2450626.77451461	1.289	-0.224	1.513
2450627.73838157	1.207	-0.237	1.444
2450628.78655021	1.239	-0.241	1.480
2450631.77347052	1.333	-0.154	1.487
2450632.84827024	1.306	-0.158	1.464
2450635.85337284	1.451	-0.149	1.600
2450640.80576980	1.287	-0.175	1.462
2450643.76409389	1.203	-0.173	1.376
2450645.78557716	1.264	-0.172	1.436

Julian Date	W_λ (net)	W_λ (emission)	W_λ (absorption)
2450649.89552412	1.199	-0.200	1.399
2450654.69862821	1.117	-0.276	1.393
2450660.74224343	1.233	-0.312	1.545
2450661.78846059	1.091	-0.286	1.377
2450663.72390025	1.126	-0.307	1.433
2450665.74104598	1.148	-0.291	1.439
2450666.73503305	1.160	-0.247	1.407
2450668.73985444	1.130	-0.262	1.392
2450669.69969583	0.841	-0.226	1.067
2450670.69620772	1.332	-0.227	1.559
2450674.64682815	1.324	-0.224	1.548
2450684.61903913	1.236	-0.285	1.521
2450688.67315596	1.205	-0.208	1.413
2450689.70227578	1.216	-0.261	1.477
2450693.67658389	1.243	-0.229	1.472
2450695.72257290	1.196	-0.234	1.430
2450696.70105945	1.186	-0.148	1.334
2450704.69342104	1.153	-0.223	1.376
2450707.60930136	1.262	-0.195	1.457
2450709.72386113	1.221	-0.183	1.404
2450710.58845668	1.283	-0.176	1.459
2450712.61052209	1.264	-0.174	1.438
2450713.62311954	1.242	-0.226	1.468
2450715.60945511	1.258	-0.233	1.491
2450716.60215994	1.248	-0.222	1.470
2450717.57613373	1.256	-0.208	1.464
2450718.55766077	1.246	-0.202	1.448
2450719.57555580	1.219	-0.249	1.468
2450723.53224540	1.308	-0.276	1.584
2450724.50313663	1.346	-0.203	1.549
2450725.53217602	1.291	-0.219	1.510
2450727.59407425	1.272	-0.211	1.483
2450728.63555574	1.226	-0.195	1.421
2450729.52496529	1.151	-0.213	1.364
2450730.58291626	1.161	-0.209	1.370
2450731.64684010	1.087	-0.202	1.289
2450732.55339146	1.047	-0.209	1.256
2450736.53490734	1.079	-0.230	1.309
2450739.56125069	1.066	-0.206	1.272
2450740.58932877	1.111	-0.201	1.312
2450741.53111076	1.117	-0.224	1.341
2450742.50016212	1.129	-0.235	1.364
2450743.50555947	1.178	-0.188	1.366
2450750.55849728	1.051	-0.228	1.279

Julian Date	W_λ (net)	W_λ (emission)	W_λ (absorption)
2450752.56531801	1.113	-0.230	1.343
2450762.49980709	1.182	-0.167	1.349
2450765.51684137	1.316	-0.131	1.447
2450770.47501183	1.262	-0.123	1.385
2450777.49181747	1.284	-0.139	1.423
2450798.47763920	1.499	-0.121	1.620
2450799.48850632	1.527	-0.101	1.628
2450800.52262673	1.500	-0.125	1.625
2450950.88095748	1.229	-0.461	1.899
2450955.85326243	1.438	-0.500	1.859
2450972.84059198	1.359	-0.326	1.946
2450999.77149517	1.620	-0.463	2.172
2451000.73309465	1.709	-0.520	2.063
2451004.79542603	1.543	-0.461	1.901
2451006.80721263	1.440	-0.362	1.731
2451021.75284438	1.369	-0.434	1.957
2451027.69932164	1.523	-0.380	1.880
2451028.69395310	1.500	-0.507	1.861
2451038.67103865	1.354	-0.357	1.725
2451044.79884184	1.368	-0.518	1.879
2451045.76414008	1.361	-0.473	1.881
2451051.67669180	1.408	-0.500	1.933
2451052.74531801	1.433	-0.435	1.958
2451055.70155940	1.523	-0.483	2.004
2451057.67934585	1.521	-0.404	1.773
2451061.74683731	1.369	-0.371	1.763
2451062.70667893	1.392	-0.367	1.798
2451065.65878460	1.431	-0.409	1.838
2451066.63236443	1.429	-0.350	1.747
2451067.60498553	1.397	-0.419	1.776
2451068.71211093	1.357	-0.415	1.692
2451070.72930597	1.277	-0.332	1.662
2451075.53823459	1.330	-0.384	1.747
2451077.54643286	1.363	-0.359	1.676
2451079.57380094	1.317	-0.382	1.680
2451080.59926455	1.298	-0.460	1.749
2451083.61306955	1.289	-0.403	1.801
2451085.60670703	1.398	-0.449	1.826
2451088.57064794	1.377	-0.478	1.715
2451096.56685999	1.237	-0.479	1.698
2451097.55166005	1.219	-0.454	1.705
2451098.53583451	1.251	-0.378	1.679
2451102.52214259	1.301	-0.333	1.623
2451105.61378888	1.290	-0.375	1.667

Julian Date	W_λ (net)	W_λ (emission)	W_λ (absorption)
2451106.58253566	1.292	-0.352	1.683
2451109.63728077	1.331	-0.352	1.681
2451110.50936285	1.329	-0.296	1.638
2451111.50936280	1.342	-0.291	1.763
2451113.57118501	1.472	-0.285	1.795
2451115.51881552	1.510	-0.347	1.736
2451121.53755176	1.389	-0.464	1.497
2451135.58661100	1.033	-0.416	1.300
2451137.51457740	0.884	-0.427	1.355
2451141.54538907	0.928	-0.475	1.434
2451144.47399910	0.959	-0.484	1.481
2451145.46913573	0.997	-0.380	1.389
2451146.48616081	1.009	-0.393	1.585
2451149.50689755	1.192	-0.304	1.590
2451157.49058970	1.286	-0.236	1.628
2451159.50352561	1.392	-0.172	1.627
2451160.50281023	1.455	-0.220	1.719
2451162.53478797	1.499	-0.192	1.691
2451163.47022251	1.499	-0.429	1.886
2451336.80563403	1.457	-0.450	1.846
2451338.84190551	1.396	-0.500	1.652
2451344.80036071	1.152	-0.390	1.522
2451348.85423465	1.132	-0.521	1.748
2451350.84189368	1.227	-0.399	1.830
2451355.82954285	1.431	-0.420	1.689
2451364.80753528	1.269	-0.537	1.837
2451365.84349881	1.300	-0.526	1.783
2451366.81577188	1.257	-0.406	1.722
2451367.81323986	1.316	-0.374	1.900
2451369.87641275	1.526	-0.409	1.890
2451370.83326650	1.481	-0.328	1.933
2451371.86956697	1.605	-0.237	1.932
2451376.84562954	1.695	-0.243	1.936
2451390.79296231	1.693	-0.185	1.744
2451392.81798543	1.559	-0.314	2.022
2451393.77638712	1.708	-0.419	1.595
2451399.79525191	1.176	-0.372	1.708
2451411.69902630	1.336	-0.430	1.666
2451419.73773457	1.236	-0.597	1.871
2451420.72246949	1.274	-0.361	1.531
2451421.64964821	1.170	-0.447	1.696
2451423.63147511	1.249	-0.515	1.780
2451424.65571363	1.265	-0.531	1.837
2451426.69744491	1.306	-0.438	1.726

Julian Date	W_λ (net)	W_λ (emission)	W_λ (absorption)
2451435.62443607	1.288	-0.383	1.577
2451436.65566424	1.194	-0.427	1.600
2451437.67301701	1.173	-0.377	1.711
2451444.75422616	1.334	-0.280	1.577
2451445.67147021	1.297	-0.378	1.728
2451447.60288468	1.350	-0.417	1.653
2451457.69956882	1.236	-0.346	1.555
2451458.67892679	1.209	-0.361	1.580
2451459.67170132	1.219	-0.311	1.605
2451463.68991441	1.294	-0.322	1.786
2451466.66316974	1.464	-0.287	1.693
2451467.67782688	1.406	-0.250	1.726
2451471.61100990	1.476	-0.344	1.730
2451472.62301844	1.386	-0.402	1.808
2451473.53323194	1.406	-0.318	1.691
2451476.66490172	1.373	-0.459	1.877
2451478.61499964	1.418	-0.227	1.621
2451479.55320231	1.394	-0.461	1.640
2451487.60409752	1.179	-0.482	1.655
2451488.59862064	1.173	-0.426	1.655
2451489.49557849	1.229	-0.386	1.702
2451490.57043052	1.316	-0.351	1.740
2451491.58998624	1.389	-0.337	1.735
2451492.51301154	1.398	-0.346	1.875
2451497.55375277	1.529	-0.261	1.788
2451498.55827275	1.527	-0.308	1.787
2451499.56391749	1.479	-0.312	1.733
2451500.48317052	1.421	-0.326	1.671
2451501.58749059	1.345	-0.380	1.838
2451512.50205306	1.458	-0.504	1.962
2451520.44426611	1.458	-0.453	1.927
2451524.45578348	1.474	-0.290	1.792
2451766.65352529	1.502	-0.303	1.991
2451777.69434071	1.688	-0.416	2.063
2451790.67409622	1.647	-0.438	1.846
2451792.64695412	1.408	-0.472	1.734
2451794.65323420	1.262	-0.365	1.735
2451800.64645313	1.370	-0.298	1.942
2451801.66190175	1.644	-0.332	1.833
2451803.70268037	1.501	-0.274	1.897
2451804.69867070	1.623	-0.345	2.073
2451805.66527417	1.728	-0.281	1.813
2451806.60222468	1.532	-0.250	1.822
2451807.66589659	1.572	-0.238	1.893

Julian Date	W_λ (net)	W_λ (emission)	W_λ (absorption)
2451809.61068368	1.655	-0.346	2.057
2451812.58110413	1.711	-0.370	1.810
2451814.64967713	1.440	-0.401	1.840
2451816.66153546	1.439	-0.502	1.649
2451817.70606781	1.147	-0.535	1.482
2451818.64572957	0.947	-0.375	1.689
2451819.56642114	1.314	-0.423	1.882
2451824.51645752	1.459	-0.426	1.683
2451825.49550015	1.257	-0.423	1.800
2451832.63255561	1.377	-0.293	1.548
2451836.56151493	1.255	-0.313	1.875
2451837.56111674	1.562	-0.338	1.346
2451838.58314765	1.008	-0.280	1.366
2451839.49245117	1.086	-0.385	1.437
2451840.51696936	1.052	-0.204	1.768
2451845.50436195	1.564	-0.259	1.813
2451846.50508201	1.554	-0.337	1.459
2451847.64089982	1.122	-0.272	1.668
2451849.47802808	1.396	-0.279	1.806
2451853.47955711	1.527	-0.211	1.732
2451854.48402400	1.521	-0.315	1.840
2451864.47505721	1.525	-0.404	1.764
2451871.54475050	1.360	-0.309	1.639
2451873.50126078	1.330	-0.355	1.754
2451882.45217583	1.399	-0.222	1.606
2451901.47514821	1.384	-0.268	1.478
2451919.48566920	1.210	-0.181	1.867
2451994.89469939	1.686	-0.164	1.909
2451996.89223833	1.745	-0.144	1.857
2452001.97258815	1.713	-0.136	1.882
2452028.82093231	1.746	-0.140	1.539
2452029.80038531	1.399	-0.120	1.519
2452033.78390954	1.413	-0.200	1.613
2452038.74861894	1.343	-0.217	1.560
2452039.81000001	1.234	-0.110	1.344
2452069.86191237	1.548	-0.113	1.661
2452074.87611819	1.466	-0.059	1.525
2452079.73171166	1.702	-0.078	1.780
2452086.86035902	1.635	-0.055	1.690
2452090.78253705	1.640	-0.088	1.728
2452092.78033792	1.441	-0.055	1.496
2452095.77715713	1.635	-0.068	1.703
2452096.80859715	1.598	-0.060	1.658
2452101.71120681	1.659	-0.107	1.766

Julian Date	W_λ (net)	W_λ (emission)	W_λ (absorption)
2452102.75962414	1.408	-0.124	1.532
2452104.84014659	1.336	-0.111	1.447
2452105.75722569	1.406	-0.119	1.525
2452115.71436255	1.185	-0.138	1.323
2452151.66575579	1.088	-0.164	1.252
2452154.77190308	1.116	-0.208	1.324
2452155.75065970	1.093	-0.186	1.279
2452157.66480292	1.037	-0.235	1.272
2452158.63577953	1.015	-0.244	1.259
2452159.60004226	1.092	-0.262	1.354
2452163.66854221	1.108	-0.362	1.470
2452164.64596066	1.038	-0.361	1.399
2452165.59930458	0.998	-0.377	1.375
2452167.65179817	0.973	-0.434	1.407
2452168.64343776	1.014	-0.406	1.420
2452169.54733498	1.054	-0.411	1.465
2452173.51536406	1.084	-0.382	1.466
2452180.52505513	0.963	-0.470	1.433
2452182.53683153	0.989	-0.503	1.492
2452183.55028786	1.012	-0.433	1.445
2452184.52438114	0.998	-0.464	1.462
2452185.57601779	0.971	-0.436	1.407
2452186.52787653	0.919	-0.499	1.418
2452190.51306572	0.847	-0.413	1.260
2452192.50230576	0.926	-0.359	1.285
2452200.49032799	0.868	-0.357	1.225
2452202.51007565	0.746	-0.431	1.177
2452211.54627200	1.177	-0.208	1.385
2452212.53254794	1.284	-0.135	1.419
2452214.46641976	1.392	-0.110	1.502
2452216.49511221	1.439	-0.167	1.606
2452217.53935808	1.538	-0.050	1.588
2452218.46923395	1.473	-0.048	1.521
2452219.47158286	1.500	-0.026	1.526
2452220.54794420	1.480	-0.049	1.529
2452223.46755044	1.494	-0.046	1.540
2452224.50767394	1.461	-0.070	1.531
2452225.48495306	1.384	-0.074	1.458
2452227.49988936	1.276	-0.099	1.375
2452235.45532754	1.204	-0.142	1.346
2452253.46989869	1.367	-0.132	1.499
2452262.46741699	1.509	-0.102	1.611
2452264.49168601	1.534	-0.089	1.623
2452265.50806281	1.613	-0.072	1.685

Appendix C

Radial Velocities

Table C.1: Radial Velocities from Si II $\lambda\lambda$ 6347, 6371

Julian Date	$v_{r,6347}$	$v_{r,6371}$	Difference
2450546.91051251	-5.18	-4.88	-0.30
2450588.86303180	-1.50	-1.91	0.41
2450590.84395394	-1.75	-1.57	-0.18
2450591.85544913	-1.73	-1.59	-0.14
2450604.79591576	-5.35	-4.69	-0.66
2450609.87109713	-4.20	-4.19	-0.01
2450614.84276841	-4.43	-4.53	0.10
2450623.77241360	-2.05	-1.91	-0.14
2450626.77451461	-3.54	-4.14	0.60
2450627.73838157	-4.84	-4.68	-0.16
2450628.78655021	-4.03	-3.83	-0.20
2450631.77347052	-2.55	-2.67	0.12
2450632.84827024	-2.75	-3.12	0.37
2450635.85337284	-3.05	-3.52	0.47
2450640.80576980	-4.39	-4.66	0.27
2450643.76409389	-6.35	-5.55	-0.80

Julian Date	$v_{r,6347}$	$v_{r,6371}$	Difference
2450645.78557716	-4.51	-4.55	0.04
2450649.89552412	-5.32	-5.76	0.44
2450654.69862821	-7.64	-6.88	-0.76
2450660.74224343	-4.07	-4.08	0.01
2450661.78846059	-5.58	-5.43	-0.15
2450663.72390025	-5.50	-5.53	0.03
2450665.74104598	-3.30	-3.11	-0.19
2450666.73503305	-2.14	-2.49	0.35
2450668.73985444	-1.02	-1.58	0.56
2450669.69969583	-0.86	-1.27	0.41
2450670.68505478	-2.36	-3.58	1.22
2450670.70736065	-2.31	-2.93	0.62
2450674.64682815	-7.20	-6.88	-0.32
2450684.61903913	-4.31	-3.94	-0.37
2450688.67315596	-2.41	-2.60	0.19
2450689.70227578	-2.58	-2.27	-0.31
2450693.67658389	-5.03	-4.10	-0.93
2450695.72257290	-5.77	-5.46	-0.31
2450696.70105945	-6.19	-5.45	-0.74
2450704.69342104	-1.93	-1.64	-0.29
2450707.60930136	-1.98	-1.96	-0.02
2450709.72386113	-3.41	-4.29	0.88
2450710.58845668	-3.94	-3.76	-0.18
2450712.61052209	-4.31	-4.35	0.04
2450713.62311954	-5.21	-4.18	-1.03
2450715.60945511	-4.15	-3.39	-0.76
2450716.60215994	-4.74	-3.66	-1.08
2450717.57613373	-4.43	-3.75	-0.68
2450718.55766077	-4.15	-3.72	-0.43
2450719.57555580	-4.06	-4.11	0.05
2450723.53224540	-4.28	-4.50	0.22
2450724.50313663	-4.60	-5.35	0.75
2450725.53217602	-4.95	-5.29	0.34
2450727.59407425	-5.04	-5.39	0.35
2450728.63555574	-4.55	-4.93	0.38
2450729.52496529	-4.67	-4.91	0.24
2450730.58291626	-4.24	-4.15	-0.09
2450731.64684010	-3.84	-4.26	0.42
2450732.55339146	-3.21	-3.22	0.01
2450736.53490734	-2.14	-1.55	-0.59
2450739.56125069	-1.27	-1.70	0.43
2450740.58932877	-2.70	-2.27	-0.43
2450741.53111076	-1.65	-1.19	-0.46
2450742.50016212	-1.41	-1.19	-0.22
2450743.50555947	-0.97	-1.14	0.17

Julian Date	$v_{r,6347}$	$v_{r,6371}$	Difference
2450750.55849728	-2.02	-0.97	-1.05
2450752.56531801	-0.18	0.79	-0.97
2450762.49980709	-1.51	-2.54	1.03
2450765.51684137	-1.39	-1.35	-0.04
2450770.47501183	-4.05	-4.24	0.19
2450777.49181747	-2.38	-2.73	0.35
2450798.47763920	-2.33	-2.26	-0.07
2450799.48850632	-2.86	-2.39	-0.47
2450800.52262673	-3.62	-3.31	-0.31
2450950.88095748	-1.45	-1.20	-0.25
2450955.85326243	-1.42	-1.49	0.07
2450972.84059198	-1.80	-2.02	0.22
2450999.77149517	-4.09	-4.24	0.15
2451000.73309465	-4.88	-4.72	-0.16
2451004.79542603	-4.98	-4.69	-0.29
2451006.80721263	-3.62	-3.51	-0.11
2451021.75284438	-4.83	-4.75	-0.08
2451021.76163625	-4.69	-5.08	0.39
2451021.76670584	-5.01	-4.84	-0.17
2451021.78053951	-4.84	-4.92	0.08
2451027.69932164	-3.88	-4.06	0.18
2451027.70550926	-4.00	-3.87	-0.13
2451027.70720374	-3.68	-3.85	0.17
2451027.71100937	-3.74	-3.69	-0.05
2451027.71446083	-3.85	-3.84	-0.01
2451027.71669699	-4.04	-4.28	0.24
2451027.71894705	-3.81	-3.75	-0.06
2451027.72786389	-3.88	-3.63	-0.25
2451028.69395310	-4.17	-4.08	-0.09
2451038.67103865	-0.84	-0.47	-0.37
2451044.79884184	-7.21	-7.41	0.20
2451045.76414008	-6.93	-6.24	-0.69
2451051.67669180	-2.44	-2.37	-0.07
2451052.74531801	-2.27	-2.05	-0.22
2451055.70155940	-2.84	-2.84	0.00
2451057.67934585	-4.38	-4.74	0.36
2451057.68515138	-4.05	-4.52	0.47
2451057.69147774	-4.43	-4.17	-0.26
2451057.69390134	-3.78	-4.02	0.24
2451057.69750549	-4.61	-4.36	-0.25
2451057.69908189	-4.13	-4.46	0.33
2451061.74683731	-3.30	-2.73	-0.57
2451062.70667893	-2.94	-2.39	-0.55
2451065.65878460	-1.24	-0.97	-0.27
2451066.63236443	-3.71	-2.60	-1.11

Julian Date	$v_{r,6347}$	$v_{r,6371}$	Difference
2451067.60498553	-4.40	-3.89	-0.51
2451068.71211093	-5.04	-4.62	-0.42
2451070.72930597	-3.34	-2.85	-0.49
2451075.53823459	-2.91	-2.74	-0.17
2451077.54643286	-3.43	-2.99	-0.44
2451079.57380094	-4.92	-4.74	-0.18
2451080.59926455	-6.14	-5.66	-0.48
2451083.61306955	-5.77	-5.03	-0.74
2451085.60670703	-3.88	-3.48	-0.40
2451088.57064794	-5.33	-5.38	0.05
2451096.56685999	-0.96	-0.59	-0.37
2451097.55166005	0.20	0.18	0.02
2451098.53583451	0.26	0.86	-0.60
2451098.55019512	0.56	0.62	-0.06
2451102.52214259	-7.28	-5.87	-1.41
2451102.53394770	-6.81	-6.69	-0.12
2451105.61378888	-4.86	-3.97	-0.89
2451105.61961504	-4.65	-4.35	-0.30
2451105.65845382	-4.79	-5.58	0.79
2451106.58253566	-4.06	-3.31	-0.75
2451109.63728077	-0.26	-0.25	-0.01
2451110.50936285	-0.11	0.56	-0.67
2451111.50936280	0.79	0.96	-0.17
2451113.57118501	-0.63	-0.57	-0.06
2451115.51881552	-3.71	-3.94	0.23
2451115.53198855	-3.70	-4.05	0.35
2451121.53755176	-1.42	-1.28	-0.14
2451121.55744668	-2.48	-1.72	-0.76
2451135.58661100	-5.17	-6.07	0.90
2451135.59424952	-5.14	-5.46	0.32
2451137.51457740	-3.11	-2.82	-0.29
2451137.52761842	-3.25	-3.87	0.62
2451141.54538907	-3.23	-2.81	-0.42
2451144.47399910	-2.05	-2.16	0.11
2451144.48307500	-1.98	-2.11	0.13
2451144.49132458	-2.28	-2.62	0.34
2451144.50578224	-2.53	-2.64	0.11
2451145.46913573	-2.07	-1.61	-0.46
2451146.48616081	-1.63	-1.49	-0.14
2451149.50689755	-2.69	-2.54	-0.15
2451157.49058970	-1.07	-1.13	0.06
2451159.50352561	1.09	0.69	0.40
2451160.50281023	-0.59	-1.38	0.79
2451162.53478797	-3.70	-3.90	0.20
2451162.54174597	-2.97	-3.31	0.34

Julian Date	$v_{r,6347}$	$v_{r,6371}$	Difference
2451163.47022251	-4.44	-4.72	0.28
2451336.80563403	-3.66	-4.00	0.34
2451338.84190551	-5.16	-4.83	-0.33
2451344.80036071	-3.58	-3.29	-0.29
2451348.85423465	-3.19	-3.08	-0.11
2451350.84189368	-0.93	-0.73	-0.20
2451355.82954285	-4.61	-4.32	-0.29
2451364.80753528	-1.04	-0.93	-0.11
2451365.84349881	0.71	1.14	-0.43
2451366.81577188	-0.36	1.53	-1.89
2451367.81323986	1.75	3.84	-2.09
2451369.87641275	1.83	1.70	0.13
2451370.83326650	4.54	4.39	0.15
2451371.86956697	0.75	0.30	0.45
2451376.84562954	-2.38	-2.76	0.38
2451390.79296231	-3.51	-3.85	0.34
2451392.81798543	-8.57	-8.63	0.06
2451393.77638712	-10.83	-10.12	-0.71
2451399.79525191	-5.80	-5.50	-0.30
2451411.69902630	-5.58	-4.93	-0.65
2451419.73773457	-6.22	-5.12	-1.10
2451420.72246949	-6.76	-5.23	-1.53
2451421.64964821	-5.87	-6.37	0.50
2451423.63147511	-4.46	-4.50	0.04
2451424.65571363	-4.99	-2.63	-2.36
2451426.69744491	-4.58	-4.45	-0.13
2451435.62443607	-4.82	-2.83	-1.99
2451436.65566424	-4.20	-4.28	0.08
2451437.67301701	-3.85	-4.22	0.37
2451444.75422616	-1.97	-1.58	-0.39
2451445.67147021	-2.80	-3.04	0.24
2451447.60288468	-3.99	-3.54	-0.45
2451457.69956882	-3.94	-4.23	0.29
2451458.67892679	-1.66	-2.71	1.05
2451459.67170132	-5.60	-5.51	-0.09
2451463.68991441	0.23	0.61	-0.38
2451466.66316974	-3.91	-4.36	0.45
2451467.67782688	-3.29	-2.77	-0.52
2451471.61100990	-8.61	-8.32	-0.29
2451472.62301844	-7.35	-7.63	0.28
2451473.53323194	-5.85	-5.38	-0.47
2451476.66490172	-1.96	-1.88	-0.08
2451478.61499964	-2.69	-2.70	0.01
2451479.55320231	-2.85	-3.32	0.47
2451487.60409752	-3.22	-2.77	-0.45

Julian Date	$v_{r,6347}$	$v_{r,6371}$	Difference
2451488.59862064	-0.67	-0.51	-0.16
2451489.49557849	-1.34	-2.64	1.30
2451490.57043052	1.13	1.44	-0.31
2451491.58998624	-0.94	-1.46	0.52
2451492.51301154	-1.67	-1.93	0.26
2451497.55375277	-3.21	-3.06	-0.15
2451498.55827275	-1.19	-1.07	-0.12
2451499.56391749	-3.36	-3.39	0.03
2451500.48317052	-6.33	-6.11	-0.22
2451501.58749059	-5.81	-5.91	0.10
2451512.50205306	-2.49	-2.54	0.05
2451520.44426611	1.25	1.05	0.20
2451524.45578348	0.18	0.10	0.08
2451766.65352529	-0.50	-0.59	0.09
2451766.66085250	0.42	0.07	0.35
2451777.69434071	-1.64	-1.62	-0.02
2451790.67409622	-4.23	-3.86	-0.37
2451792.64695412	-4.75	-4.71	-0.04
2451792.70771749	-4.89	-4.55	-0.34
2451794.65323420	-3.57	-3.03	-0.54
2451800.64645313	0.77	0.32	0.45
2451801.66190175	-0.99	-1.18	0.19
2451803.70268037	-2.21	-2.58	0.37
2451804.69867070	0.49	0.12	0.37
2451805.66527417	-2.03	-2.08	0.05
2451806.60222468	-1.56	-1.85	0.29
2451807.66589659	-1.66	-1.41	-0.25
2451809.61068368	-0.42	-0.46	0.04
2451809.61707244	-0.61	-0.31	-0.30
2451812.58110413	-6.04	-6.30	0.26
2451814.64967713	-6.64	-6.02	-0.62
2451816.66153546	-4.39	-3.72	-0.67
2451817.70606781	-1.74	-1.81	0.07
2451818.64572957	9.14	8.26	0.88
2451819.56642114	1.62	1.67	-0.05
2451824.51645752	-3.51	-3.64	0.13
2451825.49550015	-4.03	-4.36	0.33
2451832.63255561	-0.20	0.24	-0.44
2451836.56151493	-2.43	-1.63	-0.80
2451837.56111674	-1.34	-1.69	0.35
2451838.58314765	-0.71	-1.07	0.36
2451839.49245117	-1.88	-1.98	0.10
2451840.51696936	-2.42	-3.43	1.01
2451845.50436195	-5.35	-4.89	-0.46
2451846.50508201	-2.74	-2.37	-0.37

Julian Date	$v_{r,6347}$	$v_{r,6371}$	Difference
2451847.64089982	-3.02	-1.85	-1.17
2451849.47802808	-2.43	-1.64	-0.79
2451853.47955711	-0.11	-0.16	0.05
2451854.48402400	-2.05	-2.00	-0.05
2451864.47505721	0.19	0.14	0.05
2451871.54475050	-0.70	-0.56	-0.14
2451873.50126078	-2.86	-3.34	0.48
2451882.45217583	-2.40	-1.89	-0.51
2451901.47514821	-1.65	-2.02	0.37
2451994.89469939	-1.66	-1.55	-0.11
2451996.89223833	-2.82	-3.62	0.80
2452001.97258815	2.06	1.85	0.21
2452028.82093231	-1.79	-1.50	-0.29
2452029.80038531	-3.06	-2.88	-0.18
2452033.78390954	-6.37	-6.04	-0.33
2452038.74861894	-1.19	-0.82	-0.37
2452039.81000001	-0.55	-1.33	0.78
2452069.86191237	-2.68	-2.92	0.24
2452074.87611819	-3.95	-3.26	-0.69
2452079.73171166	-3.61	-3.87	0.26
2452086.86035902	-2.61	-2.40	-0.21
2452090.78253705	-2.14	-2.33	0.19
2452092.78033792	-0.38	-0.35	-0.03
2452095.77715713	0.51	0.47	0.04
2452096.81705811	-1.46	-1.72	0.26
2452101.71120681	-6.28	-6.60	0.32
2452102.75962414	-4.96	-4.84	-0.12
2452104.84014659	0.00	0.71	-0.71
2452105.75722569	1.51	2.93	-1.42
2452115.71436255	-3.72	-3.94	0.22
2452135.68774092	-0.58	-0.48	-0.10
2452151.66575579	-2.73	-2.69	-0.04
2452154.77190308	-3.12	-2.40	-0.72
2452155.75065970	-1.98	-1.75	-0.23
2452157.66480292	-3.81	-3.50	-0.31
2452158.63577953	-0.75	-0.32	-0.43
2452159.60004226	-3.21	-2.82	-0.39
2452163.66854221	-5.43	-4.88	-0.55
2452164.64596066	-6.06	-5.55	-0.51
2452165.59930458	-5.42	-5.01	-0.41
2452167.65179817	-3.87	-2.95	-0.92
2452168.64343776	-2.93	-2.33	-0.60
2452169.54733498	-2.43	-2.24	-0.19
2452173.51536406	-4.88	-4.71	-0.17
2452180.52505513	-1.10	-0.33	-0.77

Julian Date	$v_{r,6347}$	$v_{r,6371}$	Difference
2452182.53683153	-0.44	-0.12	-0.32
2452183.55028786	-6.20	-6.58	0.38
2452184.52438114	-2.71	-2.17	-0.54
2452185.57601779	-3.36	-2.98	-0.38
2452186.52787653	-3.26	-2.94	-0.32
2452190.51306572	0.12	-0.13	0.25
2452192.50230576	-0.88	-1.09	0.21
2452200.49032799	-4.86	-4.65	-0.21
2452202.51007565	-3.96	-3.18	-0.78
2452211.54627200	1.94	1.19	0.75
2452212.53254794	2.05	1.65	0.40
2452214.46641976	2.06	1.35	0.71
2452216.49511221	1.10	0.04	1.06
2452217.53935808	-0.05	-1.15	1.10
2452218.46923395	0.16	0.41	-0.25
2452219.47158286	0.09	0.05	0.04
2452220.54794420	-0.36	-0.13	-0.23
2452223.46755044	-2.24	-1.95	-0.29
2452224.50767394	-2.59	-2.19	-0.40
2452225.48495306	-2.30	-2.47	0.17
2452227.49988936	-1.97	-1.86	-0.11
2452235.45532754	0.40	0.75	-0.35
2452253.46989869	-3.33	-2.82	-0.51
2452262.46741699	1.70	2.14	-0.44
2452264.49168601	2.76	3.34	-0.58
2452265.50806281	4.11	4.31	-0.20

Appendix D

Photometry

Table D.1: *uvby* Values and Colors for the Photometric Observations in the instrumental system

Julian Date	<i>u</i>	<i>v</i>	<i>b</i>	<i>y</i>	<i>u - b</i>	<i>b - y</i>
2450750.6404	2.229	1.347	1.172	1.171	1.057	0.001
2450751.6399	2.222	1.336	1.164	1.158	1.058	0.006
2450752.6566	2.215	1.332	1.158	1.153	1.057	0.005
2450753.6364	2.210	1.322	1.155	1.141	1.055	0.014
2450754.6564	2.197	1.314	1.142	1.142	1.055	0.000
2450756.6545	2.174	1.299	1.124	1.121	1.050	0.003
2450757.6456	2.178	1.295	1.122	1.119	1.056	0.003
2450760.6463	2.181	1.312	1.134	1.128	1.047	0.006
2450767.6317	2.186	1.305	1.133	1.128	1.053	0.005
2450768.6054	2.182	1.297	1.123	1.124	1.059	-0.001
2450769.6084	2.175	1.292	1.121	1.121	1.054	0.000
2450771.6043	2.187	1.306	1.129	1.128	1.058	0.001
2450772.5904	2.176	1.288	1.118	1.112	1.058	0.006
2450781.5898	2.164	1.285	1.109	1.109	1.055	0.000
2450782.5898	2.166	1.284	1.108	1.104	1.058	0.004
2450792.5734	2.197	1.301	1.134	1.132	1.063	0.002

Julian Date	u	v	b	y	$u - b$	$b - y$
2450793.5734	2.184	1.306	1.133	1.121	1.051	0.012
2450919.9904	2.203	1.329	1.147	1.145	1.056	0.002
2450920.9905	2.209	1.333	1.148	1.148	1.061	0.000
2450921.9873	2.209	1.340	1.156	1.154	1.053	0.002
2450922.9855	2.203	1.423	1.155	1.154	1.048	0.001
2450926.9763	2.191	1.322	1.140	1.137	1.051	0.003
2450928.9701	2.181	1.301	1.132	1.124	1.049	0.008
2450931.9586	2.186	1.311	1.128	1.130	1.058	-0.002
2450932.9547	2.182	1.315	1.137	1.134	1.045	0.003
2450933.9526	2.192	1.318	1.139	1.134	1.053	0.005
2450934.9499	2.195	1.328	1.147	1.139	1.048	0.008
2450936.9446	2.196	1.322	1.141	1.141	1.055	0.000
2450938.9448	2.195	1.317	1.139	1.139	1.056	0.000
2450940.9372	2.226	1.338	1.163	1.156	1.063	0.007
2450942.9296	2.223	1.351	1.166	1.162	1.057	0.004
2450943.9234	2.217	1.347	1.167	1.163	1.050	0.004
2450944.9278	2.207	1.344	1.175	1.151	1.032	0.024
2450946.9188	2.201	1.322	1.145	1.140	1.056	0.005
2450948.9128	2.200	1.335	1.152	1.142	1.048	0.010
2450949.9104	2.203	1.336	1.153	1.146	1.050	0.007
2450951.9033	2.208	1.345	1.164	1.163	1.044	0.001
2450957.8895	2.206	1.342	1.159	1.155	1.047	0.004
2450959.8865	2.195	1.329	1.145	1.142	1.050	0.003
2450960.8905	2.185	1.329	1.126	1.127	1.059	-0.001
2450961.8762	2.180	1.320	1.138	1.132	1.042	0.006
2450962.8976	2.179	1.309	1.133	1.126	1.046	0.007
2450965.8725	2.199	1.317	1.135	1.135	1.064	0.000
2450966.8626	2.201	1.315	1.141	1.140	1.060	0.001
2450966.8776	2.210	1.314	1.138	1.140	1.072	-0.002
2450968.8595	2.230	1.340	1.160	1.155	1.070	0.005
2450968.8668	2.230	1.337	1.158	1.150	1.072	0.008
2450969.8564	2.237	1.346	1.169	1.161	1.068	0.008
2450969.9585	2.239	1.336	1.163	1.161	1.076	0.002
2450970.8536	2.242	1.359	1.175	1.167	1.067	0.008
2450970.8604	2.241	1.353	1.172	1.168	1.069	0.004
2450972.8473	2.233	1.340	1.161	1.155	1.072	0.006
2450972.8626	2.229	1.343	1.161	1.157	1.068	0.004
2450973.8455	2.202	1.319	1.181	1.169	1.021	0.012
2450974.8404	2.193	1.314	1.134	1.133	1.059	0.001
2450977.8316	2.187	1.317	1.146	1.142	1.041	0.004
2450977.8396	2.197	1.334	1.149	1.140	1.048	0.009
2450977.8466	2.190	1.315	1.135	1.138	1.055	-0.003
2450977.8545	2.201	1.327	1.146	1.142	1.055	0.004
2450977.8612	2.192	1.326	1.143	1.142	1.049	0.001
2450977.8694	2.192	1.331	1.145	1.140	1.047	0.005

Julian Date	u	v	b	y	$u - b$	$b - y$
2450977.8764	2.179	1.320	1.144	1.144	1.035	0.000
2450977.8843	2.187	1.325	1.141	1.141	1.046	0.000
2450977.8909	2.189	1.321	1.150	1.143	1.039	0.007
2450977.8993	2.190	1.328	1.143	1.143	1.047	0.000
2450977.9063	2.182	1.321	1.138	1.141	1.044	-0.003
2450977.9140	2.183	1.327	1.147	1.140	1.036	0.007
2450977.9204	2.192	1.322	1.140	1.142	1.052	-0.002
2450977.9289	2.191	1.326	1.143	1.138	1.048	0.005
2450977.9366	2.188	1.320	1.143	1.141	1.045	0.002
2450977.9436	2.191	1.325	1.145	1.138	1.046	0.007
2450977.9505	2.188	1.319	1.143	1.140	1.045	0.003
2450978.8370	2.187	1.323	1.143	1.142	1.044	0.001
2450978.8445	2.188	1.318	1.149	1.145	1.039	0.004
2450978.8516	2.194	1.329	1.149	1.144	1.045	0.005
2450978.8596	2.189	1.327	1.149	1.143	1.040	0.006
2450978.8666	2.193	1.316	1.147	1.142	1.046	0.005
2450978.8745	2.190	1.320	1.150	1.141	1.040	0.009
2450978.8812	2.195	1.324	1.148	1.143	1.047	0.005
2450978.8894	2.194	1.318	1.148	1.142	1.046	0.006
2450978.8964	2.189	1.320	1.146	1.142	1.043	0.004
2450978.9043	2.195	1.323	1.147	1.145	1.048	0.002
2450978.9103	2.189	1.321	1.144	1.143	1.045	0.001
2450978.9193	2.193	1.325	1.145	1.142	1.048	0.003
2450978.9263	2.193	1.324	1.145	1.141	1.048	0.004
2450978.9342	2.194	1.322	1.147	1.143	1.047	0.004
2450978.9405	2.196	1.327	1.146	1.145	1.050	0.001
2450978.9489	2.197	1.333	1.146	1.144	1.051	0.002
2450978.9566	2.196	1.330	1.148	1.144	1.048	0.004
2450979.8275	2.191	1.319	1.142	1.144	1.049	-0.002
2450979.8348	2.194	1.321	1.148	1.143	1.046	0.005
2450979.8425	2.195	1.324	1.144	1.144	1.051	0.000
2450979.8497	2.200	1.326	1.147	1.142	1.053	0.005
2450979.8574	2.198	1.322	1.144	1.142	1.054	0.002
2450979.8646	2.201	1.321	1.147	1.144	1.054	0.003
2450979.8701	2.186	1.322	1.142	1.136	1.044	0.006
2450979.8786	2.196	1.321	1.148	1.142	1.048	0.006
2450979.8866	2.198	1.319	1.147	1.143	1.051	0.004
2450979.8938	2.195	1.315	1.151	1.143	1.044	0.008
2450979.9004	2.196	1.330	1.145	1.145	1.051	0.000
2450979.9086	2.196	1.323	1.145	1.141	1.051	0.004
2450979.9143	2.189	1.316	1.141	1.138	1.048	0.003
2450979.9209	2.197	1.323	1.146	1.143	1.051	0.003
2450979.9292	2.197	1.328	1.145	1.141	1.052	0.004
2450979.9365	2.197	1.323	1.146	1.144	1.051	0.002
2450979.9439	2.198	1.324	1.147	1.145	1.051	0.002

Julian Date	u	v	b	y	$u - b$	$b - y$
2450980.8304	2.197	1.326	1.148	1.144	1.049	0.004
2450980.8389	2.201	1.326	1.148	1.149	1.053	-0.001
2450982.8244	2.212	1.330	1.155	1.146	1.057	0.009
2450983.8176	2.205	1.339	1.154	1.139	1.051	0.015
2450983.9336	2.214	1.339	1.157	1.152	1.057	0.005
2450984.8142	2.204	1.346	1.157	1.156	1.047	0.001
2450984.8205	2.210	1.347	1.159	1.157	1.051	0.002
2450985.8176	2.206	1.345	1.161	1.154	1.045	0.007
2450985.8255	2.210	1.349	1.167	1.160	1.043	0.007
2450985.8328	2.208	1.353	1.163	1.157	1.045	0.006
2450985.8405	2.212	1.355	1.164	1.156	1.048	0.008
2450985.8476	2.217	1.348	1.160	1.163	1.057	-0.003
2450985.8555	2.208	1.353	1.161	1.156	1.047	0.005
2450985.8625	2.214	1.345	1.165	1.156	1.049	0.009
2450985.8703	2.213	1.349	1.165	1.157	1.048	0.008
2450985.8776	2.209	1.350	1.161	1.156	1.048	0.005
2450985.8852	2.210	1.346	1.158	1.154	1.052	0.004
2450985.8925	2.214	1.347	1.163	1.155	1.051	0.008
2450985.9003	2.204	1.340	1.164	1.154	1.040	0.010
2450985.9075	2.209	1.352	1.157	1.155	1.052	0.002
2450985.9149	2.212	1.349	1.162	1.154	1.050	0.008
2450985.9224	2.215	1.343	1.160	1.154	1.055	0.006
2450985.9296	2.211	1.343	1.163	1.157	1.048	0.006
2450985.9375	2.215	1.354	1.160	1.160	1.055	0.000
2450985.9448	2.209	1.343	1.161	1.159	1.048	0.002
2450985.9524	2.212	1.343	1.160	1.157	1.052	0.003
2450985.9596	2.212	1.343	1.165	1.156	1.047	0.009
2450985.9673	2.211	1.348	1.161	1.154	1.050	0.007
2450986.8146	2.205	1.341	1.159	1.165	1.046	-0.006
2450986.8903	2.210	1.338	1.158	1.154	1.052	0.004
2450987.8073	2.214	1.346	1.159	1.151	1.055	0.008
2450988.8035	2.206	1.333	1.152	1.144	1.054	0.008
2450988.8825	2.212	1.340	1.153	1.146	1.059	0.007
2450989.8029	2.203	1.333	1.148	1.149	1.055	-0.001
2450990.8066	2.199	1.349	1.153	1.146	1.046	0.007
2450990.8864	2.206	1.339	1.153	1.145	1.053	0.008
2450991.7985	2.201	1.343	1.156	1.143	1.045	0.013
2450991.8876	2.207	1.343	1.154	1.147	1.053	0.007
2450992.7955	2.193	1.344	1.161	1.155	1.032	0.006
2450993.7905	2.207	1.346	1.157	1.154	1.050	0.003
2450994.7875	2.194	1.340	1.150	1.149	1.044	0.001
2450994.9665	2.202	1.333	1.155	1.148	1.047	0.007
2450995.8553	2.199	1.325	1.146	1.145	1.053	0.001
2450996.9302	2.195	1.316	1.149	1.140	1.046	0.009
2451081.6695	2.202	1.324	1.159	1.156	1.043	0.003

Julian Date	u	v	b	y	$u - b$	$b - y$
2451082.6023	2.212	1.337	1.166	1.167	1.046	-0.001
2451083.6003	2.211	1.340	1.165	1.164	1.046	0.001
2451084.6002	2.211	1.334	1.162	1.158	1.049	0.004
2451085.6203	2.211	1.337	1.163	1.156	1.048	0.007
2451086.6404	2.214	1.325	1.159	1.160	1.055	-0.001
2451087.6235	2.214	1.331	1.157	1.160	1.057	-0.003
2451090.6225	2.213	1.334	1.167	1.165	1.046	0.002
2451091.6253	2.212	1.338	1.164	1.163	1.048	0.001
2451092.6186	2.208	1.346	1.170	1.168	1.038	0.002
2451093.6176	2.217	1.347	1.169	1.165	1.048	0.004
2451096.6155	2.194	1.332	1.161	1.157	1.033	0.004
2451097.6146	2.185	1.321	1.154	1.151	1.031	0.003
2451098.6035	2.183	1.319	1.146	1.143	1.037	0.003
2451101.6001	2.206	1.323	1.154	1.146	1.052	0.008
2451102.5998	2.217	1.336	1.163	1.165	1.054	-0.002
2451103.5885	2.215	1.333	1.168	1.162	1.047	0.006
2451104.5883	2.224	1.343	1.179	1.169	1.045	0.010
2451105.5875	2.237	1.346	1.183	1.174	1.054	0.009
2451105.6244	2.230	1.358	1.176	1.170	1.054	0.006
2451113.5905	2.188	1.334	1.130	1.152	1.058	-0.022
2451115.5894	2.194	1.320	1.149	1.147	1.045	0.002
2451116.5905	2.199	1.338	1.158	1.152	1.041	0.006
2451118.5911	2.201	1.331	1.159	1.157	1.042	0.002
2451119.5885	2.210	1.348	1.166	1.162	1.044	0.004
2451120.5902	2.213	1.340	1.168	1.166	1.045	0.002
2451121.5694	2.224	1.351	1.176	1.172	1.048	0.004
2451122.5690	2.225	1.354	1.176	1.174	1.049	0.002
2451123.6403	2.218	1.346	1.175	1.174	1.043	0.001
2451131.5902	2.195	1.314	1.150	1.148	1.045	0.002
2451132.5875	2.196	1.313	1.147	1.142	1.049	0.005
2451133.5875	2.193	1.316	1.144	1.139	1.049	0.005
2451136.5709	2.197	1.329	1.163	1.155	1.034	0.008
2451290.9885	2.244	1.374	1.198	1.188	1.046	0.010
2451295.9834	2.221	1.364	1.186	1.180	1.035	0.006
2451298.9703	2.214	1.354	1.179	1.174	1.035	0.005
2451299.9647	2.214	1.349	1.177	1.173	1.037	0.004
2451300.9609	2.213	1.347	1.175	1.172	1.038	0.003
2451302.9603	2.234	1.349	1.175	1.183	1.059	-0.008
2451303.9644	2.242	1.354	1.182	1.182	1.060	0.000
2451304.9593	2.231	1.346	1.174	1.172	1.057	0.002
2451306.9786	2.225	1.335	1.168	1.169	1.057	-0.001
2451308.9736	2.208	1.339	1.163	1.165	1.045	-0.002
2451310.9669	2.196	1.324	1.149	1.150	1.047	-0.001
2451312.9293	2.193	1.324	1.150	1.146	1.043	0.004
2451313.9683	2.192	1.329	1.153	1.150	1.039	0.003

Julian Date	u	v	b	y	$u - b$	$b - y$
2451314.9254	2.203	1.334	1.160	1.155	1.043	0.005
2451315.9213	2.197	1.322	1.154	1.154	1.043	0.000
2451317.9453	2.203	1.329	1.156	1.154	1.047	0.002
2451318.9275	2.204	1.331	1.155	1.154	1.049	0.001
2451319.9283	2.200	1.336	1.157	1.156	1.043	0.001
2451320.9249	2.193	1.334	1.158	1.153	1.035	0.005
2451321.9326	2.190	1.334	1.160	1.157	1.030	0.003
2451322.9175	2.191	1.338	1.156	1.155	1.035	0.001
2451323.9184	2.193	1.335	1.158	1.150	1.035	0.008
2451324.9273	2.192	1.330	1.156	1.157	1.036	-0.001
2451325.9233	2.196	1.337	1.159	1.162	1.037	-0.003
2451326.9074	2.197	1.338	1.158	1.154	1.039	0.004
2451447.7241	2.242	1.360	1.178	1.171	1.064	0.007
2451448.7296	2.241	1.363	1.175	1.168	1.066	0.007
2451449.7205	2.231	1.356	1.174	1.168	1.057	0.006
2451450.7197	2.227	1.347	1.170	1.164	1.057	0.006
2451451.7045	2.219	1.344	1.154	1.154	1.065	0.000
2451452.7455	2.194	1.329	1.144	1.144	1.050	0.000
2451453.7328	2.185	1.317	1.138	1.136	1.047	0.002
2451454.7100	2.177	1.310	1.131	1.130	1.046	0.001
2451455.7241	2.180	1.314	1.134	1.130	1.046	0.004
2451456.6853	2.187	1.330	1.144	1.138	1.043	0.006
2451458.7142	2.218	1.342	1.159	1.154	1.059	0.005
2451459.6947	2.224	1.350	1.168	1.163	1.056	0.005
2451465.6754	2.167	1.304	1.125	1.120	1.042	0.005
2451466.6700	2.169	1.303	1.121	1.121	1.048	0.000
2451466.6785	2.169	1.303	1.120	1.119	1.049	0.001
2451467.6596	2.169	1.299	1.115	1.116	1.054	-0.001
2451467.6671	2.168	1.300	1.117	1.116	1.051	0.001
2451470.6645	2.175	1.301	1.127	1.122	1.048	0.005
2451470.6801	2.176	1.302	1.127	1.122	1.049	0.005
2451471.6534	2.186	1.318	1.139	1.136	1.047	0.003
2451471.6601	2.192	1.321	1.138	1.134	1.054	0.004
2451472.6501	2.201	1.324	1.148	1.148	1.053	0.000
2451472.6584	2.201	1.326	1.147	1.144	1.054	0.003
2451473.6546	2.216	1.330	1.155	1.169	1.061	-0.014
2451473.6601	2.218	1.331	1.157	1.170	1.061	-0.013
2451474.6496	2.218	1.340	1.160	1.156	1.058	0.004
2451474.6571	2.219	1.340	1.162	1.156	1.057	0.006
2451475.6285	2.226	1.345	1.162	1.161	1.064	0.001
2451475.6361	2.220	1.346	1.168	1.162	1.052	0.006
2451477.6890	2.221	1.345	1.168	1.160	1.053	0.008
2451477.6974	2.221	1.342	1.168	1.162	1.053	0.006
2451478.6262	2.215	1.335	1.160	1.156	1.055	0.004
2451478.6670	2.217	1.341	1.160	1.156	1.057	0.004

Julian Date	u	v	b	y	$u - b$	$b - y$
2451479.6305	2.206	1.330	1.155	1.149	1.051	0.006
2451479.6656	2.210	1.335	1.151	1.154	1.059	-0.003
2451480.6300	2.203	1.339	1.152	1.143	1.051	0.009
2451480.6700	2.177	1.317	1.141	1.181	1.036	-0.040
2451481.6254	2.197	1.325	1.142	1.138	1.055	0.004
2451481.6664	2.195	1.319	1.146	1.135	1.049	0.011
2451482.6301	2.190	1.323	1.144	1.141	1.046	0.003
2451482.6700	2.195	1.328	1.140	1.132	1.055	0.008
2451483.6185	2.187	1.323	1.146	1.141	1.041	0.005
2451483.6595	2.188	1.326	1.145	1.142	1.043	0.003
2451484.6565	2.196	1.333	1.150	1.145	1.046	0.005
2451485.6060	2.211	1.337	1.162	1.157	1.049	0.005
2451486.6090	2.216	1.350	1.167	1.161	1.049	0.006
2451486.6435	2.213	1.352	1.169	1.162	1.044	0.007
2451487.6077	2.219	1.355	1.171	1.168	1.048	0.003
2451487.6486	2.217	1.355	1.172	1.166	1.045	0.006
2451491.6033	2.240	1.354	1.173	1.170	1.067	0.003
2451491.6371	2.239	1.355	1.172	1.167	1.067	0.005
2451490.6306	2.239	1.359	1.173	1.170	1.066	0.003
2451492.5950	2.230	1.352	1.167	1.165	1.063	0.002
2451492.6351	2.232	1.353	1.172	1.161	1.060	0.011
2451493.5753	2.219	1.353	1.167	1.164	1.052	0.003
2451493.6274	2.225	1.349	1.164	1.161	1.061	0.003
2451494.5721	2.209	1.344	1.160	1.155	1.049	0.005
2451494.6242	2.208	1.344	1.161	1.154	1.047	0.007
2451496.5732	2.204	1.331	1.140	1.142	1.064	-0.002
2451497.5650	2.205	1.326	1.141	1.143	1.064	-0.002
2451497.6161	2.197	1.326	1.141	1.140	1.056	0.001
2451498.5655	2.208	1.331	1.145	1.104	1.063	0.041
2451500.5725	2.230	1.336	1.163	1.164	1.067	-0.001
2451500.6043	2.226	1.341	1.166	1.164	1.060	0.002
2451501.5722	2.243	1.352	1.170	1.168	1.073	0.002
2451501.6023	2.235	1.356	1.168	1.170	1.067	-0.002
2451502.6026	2.240	1.355	1.176	1.176	1.064	0.000
2451503.5947	2.244	1.351	1.174	1.175	1.070	-0.001
2451504.5942	2.232	1.344	1.162	1.162	1.070	0.000
2451509.5782	2.204	1.329	1.151	1.150	1.053	0.001
2451509.5857	2.205	1.332	1.155	1.148	1.050	0.007
2451510.5704	2.207	1.329	1.150	1.146	1.057	0.004
2451510.5857	2.207	1.330	1.150	1.147	1.057	0.003
2451511.5856	2.221	1.339	1.152	1.153	1.069	-0.001
2451514.5860	2.251	1.357	1.171	1.167	1.080	0.004
2451656.9855	2.212	1.345	1.155	1.155	1.057	0.000
2451657.9781	2.215	1.342	1.161	1.151	1.054	0.010
2451658.9770	2.205	1.342	1.157	1.153	1.048	0.004

Julian Date	u	v	b	y	$u - b$	$b - y$
2451659.9720	2.206	1.334	1.147	1.144	1.059	0.003
2451660.9784	2.199	1.325	1.139	1.133	1.060	0.006
2451661.9866	2.185	1.318	1.133	1.124	1.052	0.009
2451663.9785	2.223	1.318	1.127	1.124	1.096	0.003
2451664.9700	2.185	1.316	1.134	1.130	1.051	0.004
2451665.9786	2.183	1.320	1.141	1.138	1.042	0.003
2451666.9701	2.184	1.327	1.144	1.144	1.040	0.000
2451667.9671	2.191	1.324	1.140	1.137	1.051	0.003
2451668.9628	2.186	1.318	1.137	1.134	1.049	0.003
2451669.9658	2.173	1.314	1.129	1.125	1.044	0.004
2451670.9425	2.167	1.308	1.127	1.125	1.040	0.002
2451671.9491	2.166	1.312	1.126	1.124	1.040	0.002
2451672.9501	2.177	1.319	1.128	1.123	1.049	0.005
2451673.9472	2.181	1.325	1.133	1.132	1.048	0.001
2451674.9462	2.192	1.345	1.149	1.145	1.043	0.004
2451684.9161	2.181	1.318	1.140	1.138	1.041	0.002
2451686.9565	2.179	1.314	1.515	1.127	0.664	0.388
2451689.9027	2.202	1.329	1.149	1.143	1.053	0.006
2451698.9054	2.169	1.328	1.137	1.139	1.032	-0.002
2451699.8961	2.164	1.324	1.139	1.134	1.025	0.005
2451700.9000	2.166	1.329	1.137	1.136	1.029	0.001
2451704.8900	2.214	1.354	1.158	1.153	1.056	0.005
2451705.8823	2.208	1.342	1.157	1.156	1.051	0.001
2451706.8807	2.225	1.348	1.164	1.167	1.061	-0.003
2451707.8820	2.231	1.360	1.168	1.168	1.063	0.000
2451708.8798	2.232	1.354	1.171	1.166	1.061	0.005
2451709.8760	2.231	1.360	1.174	1.171	1.057	0.003
2451710.8847	2.235	1.359	1.187	1.171	1.048	0.016
2451711.8690	2.231	1.353	1.167	1.164	1.064	0.003
2451712.8621	2.218	1.348	1.161	1.155	1.057	0.006
2451729.8198	2.169	1.304	1.122	1.130	1.047	-0.008
2451809.6045	2.198	1.327	1.148	1.149	1.050	-0.001
2451810.6860	2.197	1.330	1.145	1.148	1.052	-0.003
2451815.6754	2.215	1.357	1.175	1.177	1.040	-0.002
2451816.6651	2.220	1.360	1.183	1.176	1.037	0.007
2451817.6596	2.224	1.373	1.185	1.185	1.039	0.000
2451823.6563	2.191	1.318	1.141	1.147	1.050	-0.006
2451823.6432	2.184	1.313	1.146	1.147	1.038	-0.001
2451825.6436	2.192	1.321	1.146	1.148	1.046	-0.002
2451830.6280	2.220	1.325	1.160	1.163	1.060	-0.003
2451831.6222	2.212	1.332	1.159	1.164	1.053	-0.005
2451833.6201	2.193	1.317	1.144	1.149	1.049	-0.005
2451834.6195	2.190	1.317	1.141	1.144	1.049	-0.003
2451842.6092	2.181	1.319	1.144	1.147	1.037	-0.003
2451844.5860	2.185	1.316	1.149	1.144	1.036	0.005

Julian Date	u	v	b	y	$u - b$	$b - y$
2451847.6401	2.200	1.330	1.152	1.151	1.048	0.001
2451849.5932	2.197	1.328	1.151	1.155	1.046	-0.004
2451850.5907	2.193	1.323	1.153	1.151	1.040	0.002
2451857.5724	2.187	1.311	1.146	1.149	1.041	-0.003
2451861.5700	2.201	1.329	1.162	1.164	1.039	-0.002
2451864.5691	2.192	1.328	1.153	1.153	1.039	0.000
2451867.5690	2.169	1.309	1.144	1.146	1.025	-0.002
2451869.5677	2.175	1.310	1.141	1.145	1.034	-0.004
2451874.5741	2.174	1.310	1.138	1.143	1.036	-0.005
2451875.5665	2.179	1.314	1.149	1.149	1.030	0.000
2451877.5662	2.194	1.330	1.154	1.156	1.040	-0.002
2452030.9561	2.163	1.314	1.137	1.138	1.026	-0.001
2452031.9505	2.171	1.318	1.140	1.144	1.031	-0.004
2452034.9587	2.196	1.332	1.152	1.154	1.044	-0.002
2452035.9681	2.209	1.336	1.154	1.157	1.055	-0.003
2452036.9480	2.237	1.344	1.160	1.163	1.077	-0.003
2452037.9403	2.221	1.340	1.161	1.162	1.060	-0.001
2452038.9407	2.213	1.344	1.157	1.158	1.056	-0.001
2452039.9422	2.216	1.344	1.162	1.164	1.054	-0.002
2452044.9106	2.221	1.343	1.159	1.164	1.062	-0.005
2452045.9322	2.216	1.337	1.163	1.159	1.053	0.004
2452046.9203	2.219	1.340	1.159	1.165	1.060	-0.006
2452050.8982	2.208	1.330	1.145	1.147	1.063	-0.002
2452051.9021	2.196	1.325	1.142	1.139	1.054	0.003
2452052.9008	2.193	1.321	1.134	1.138	1.059	-0.004
2452053.8872	2.184	1.320	1.136	1.134	1.048	0.002
2452055.8843	2.180	1.315	1.123	1.130	1.057	-0.007
2452058.8930	2.189	1.322	1.145	1.142	1.044	0.003
2452061.8678	2.184	1.323	1.138	1.149	1.046	-0.011
2452062.9052	2.191	1.310	1.138	1.142	1.053	-0.004
2452064.8663	2.192	1.311	1.136	1.139	1.056	-0.003
2452073.8330	2.202	1.323	1.156	1.153	1.046	0.003
2452074.8332	2.200	1.313	1.151	1.155	1.049	-0.004
2452074.8305	2.193	1.318	1.149	1.149	1.044	0.000
2452076.8383	2.167	1.307	1.119	1.123	1.048	-0.004
2452084.8073	2.167	1.294	1.122	1.132	1.045	-0.010
2452087.8001	2.185	1.303	1.135	1.138	1.050	-0.003
2452088.7921	2.188	1.310	1.136	1.137	1.052	-0.001
2452092.9283	2.204	1.338	1.164	1.162	1.040	0.002

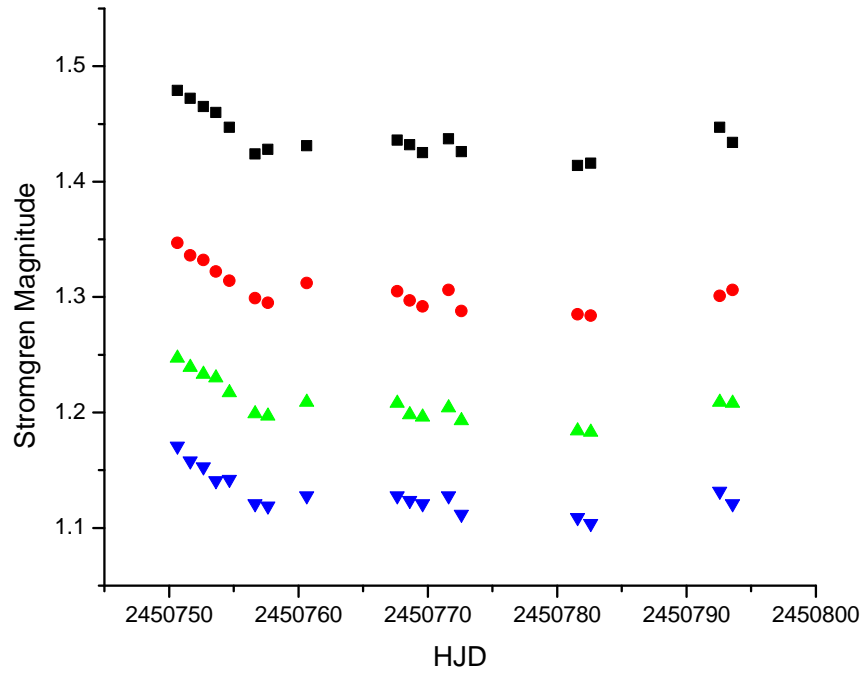


Figure D-1: Strömrgren photometry of Deneb for the fall of 1997. The values have been shifted to show detail in the light curve in the same manner as Figure 4-11.

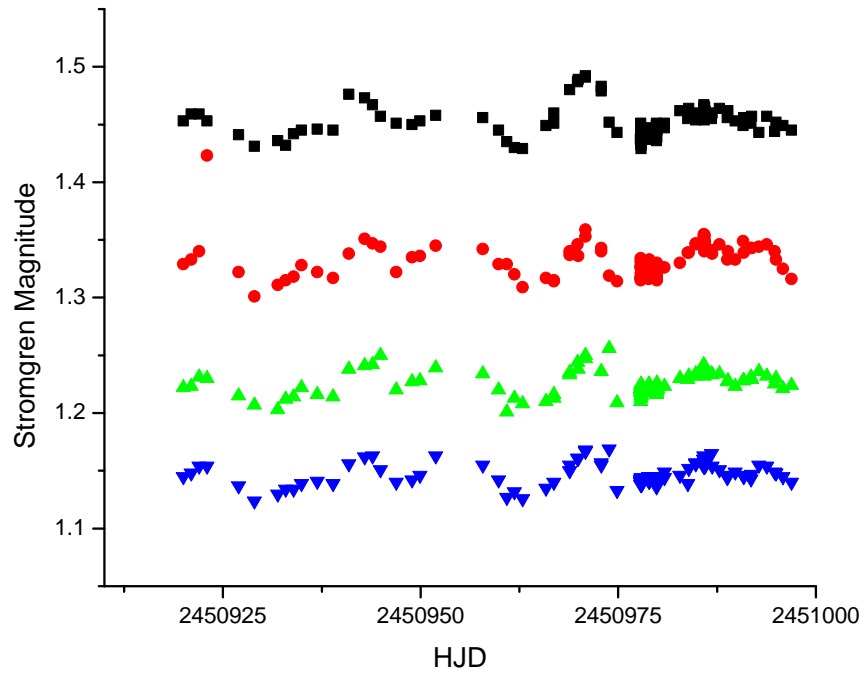


Figure D-2: Strömrgren photometry of Deneb for the spring of 1998. The values have been shifted to show detail in the light curve in the same manner as Figure 4-11.

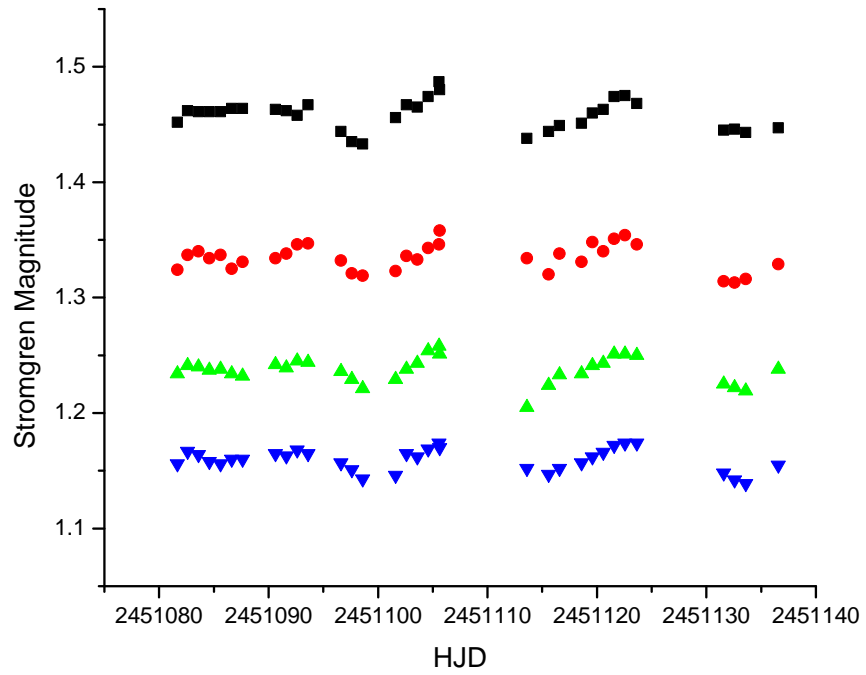


Figure D-3: Strömgen photometry of Deneb for the fall of 1998. The values have been shifted to show detail in the light curve in the same manner as Figure 4-11.

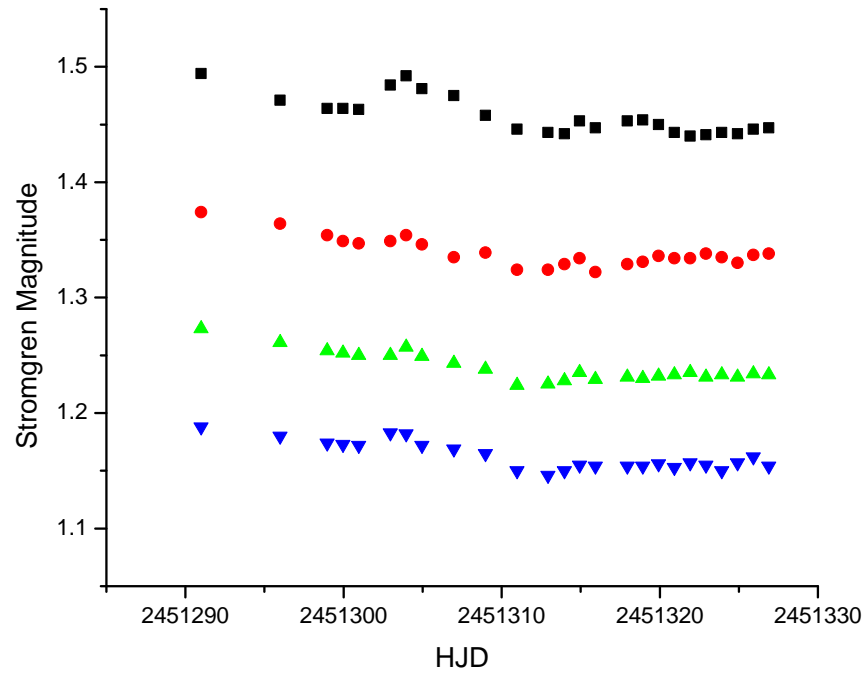


Figure D-4: Strömrgren photometry of Deneb for the spring of 1999. The values have been shifted to show detail in the light curve in the same manner as Figure 4-11.

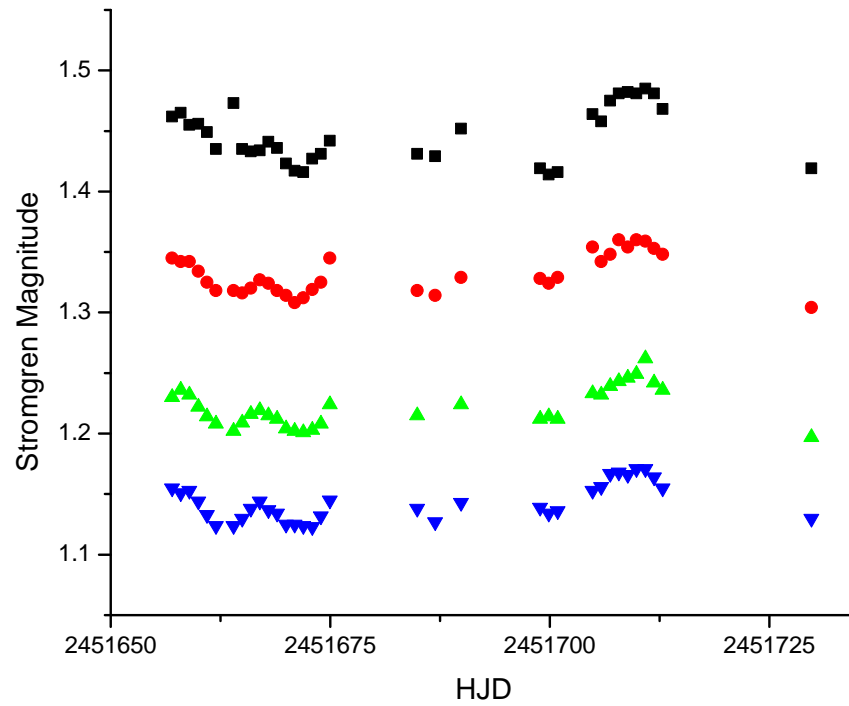


Figure D-5: Strömrgren photometry of Deneb for the spring of 2000. The values have been shifted to show detail in the light curve in the same manner as Figure 4-11.

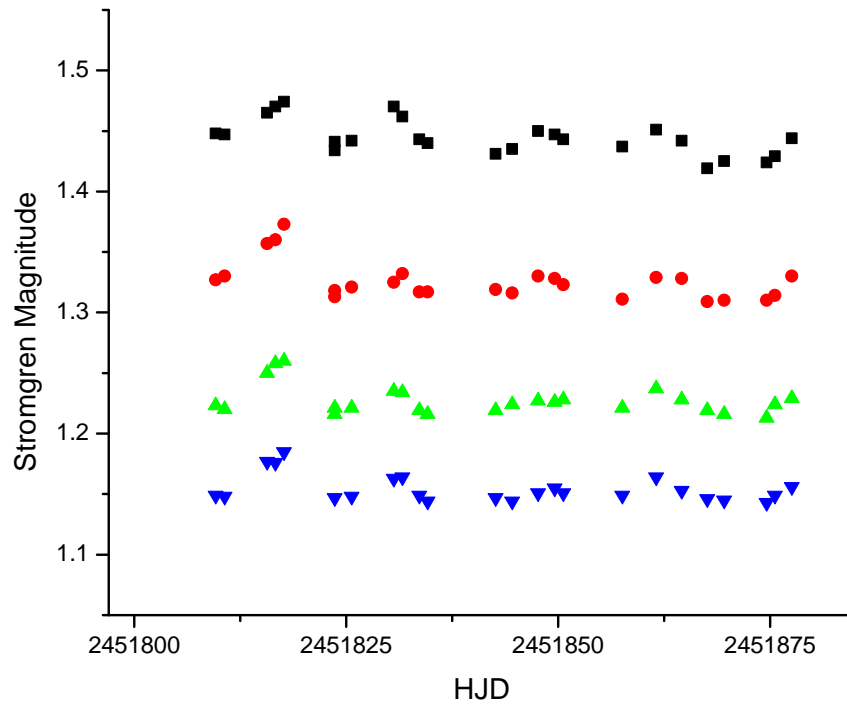


Figure D-6: Strömrgren photometry of Deneb for the fall of 2000. The values have been shifted to show detail in the light curve in the same manner as Figure 4-11.

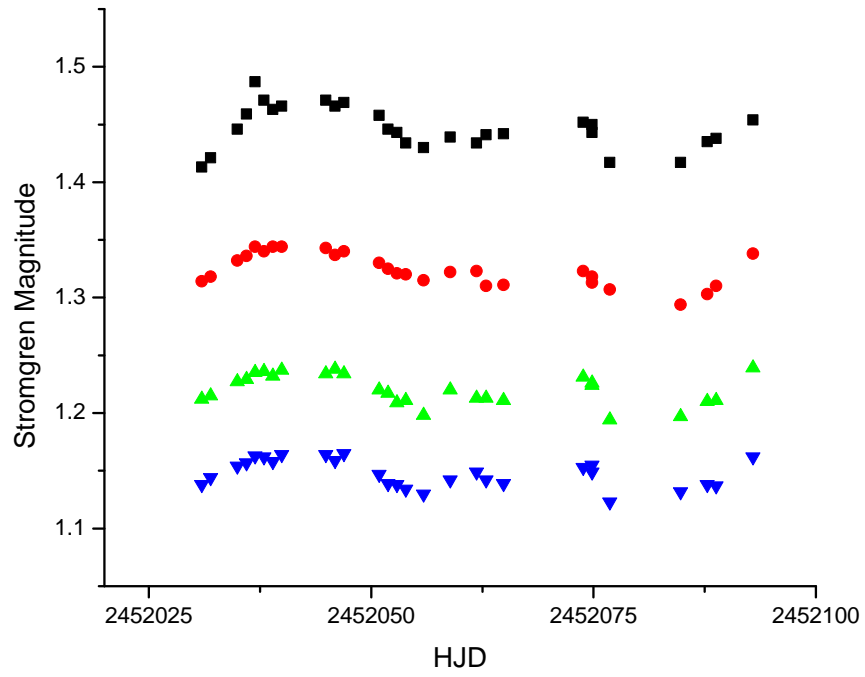


Figure D-7: Strömrgren photometry of Deneb for the spring of 2001. The values have been shifted to show detail in the light curve in the same manner as Figure 4-11.